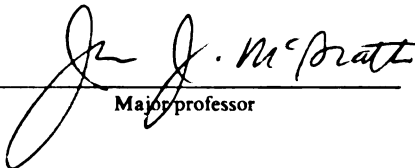This is to certify that the

dissertation entitled
Thermal and Chemical Modification
of Collagenous Tissues

presented by

Alptekin Aksan

has been accepted towards fulfillment
of the requirements for

Ph.D. degree in Engineering

_____
Major professor

Date 4/30/02

PLACE IN RETURN BOX to remove this checkout from your record.
TO AVOID FINES return on or before date due.
MAY BE RECALLED with earlier due date if requested.

DATE DUE	DATE DUE	DATE DUE
AUG 2 0 7 2004		

6/01 c:/CIRC/DateDue.p65-p.15

THERMAL AND CHEMICAL MODIFICATION OF COLLAGENOUS TISSUES

By

Alptekin Aksan

A DISSERTATION

Submitted to
Michigan State University
in partial fulfillment of the requirements
for the degree of

DOCTOR OF PHILOSOPHY

Department of Mechanical Engineering

2002

ABSTRACT

THERMAL AND CHEMICAL MODIFICATION OF COLLAGENOUS TISSUES

By

Alptekin Aksan

Over the last decade, *Sub-Ablative Thermotherapy* has found ever-increasing application in orthopaedic (in the treatment of the instabilities of the knee, ankle, hip and shoulder joints and in the elimination of the discogenic pain in spine) and ophthalmologic surgery (for the correction of near/farsightedness). Utilizing sub-ablative levels of heating, the therapy aims at altering the configuration of the strain-damaged, pathological or congenitally anomalous collagenous tissue (such as tendon, ligament, skin, joint capsule, cornea, etc.) in order to re-establish stability and function.

This thesis describes research directed towards understanding, modeling and controlling the heat-induced responses of collagenous tissues. The main aim of the research was to establish the scientific basis and develop the tools to increase the safety and efficacy of *Sub-Ablative Thermotherapy* procedures.

In-vitro thermomechanical experimentation with a model collagenous tissue (New Zealand white rabbit patellar tendon) is performed in order to determine the constitutive relationships between the accumulated thermal damage and the resultant mechanical response and the stress-state of the collagenous tissues. Finite Element Analysis-based simulation tools are also developed in order to quantify the differences among clinically applied heating modalities such as, monopolar/bipolar radiofrequency and Ho:YAG laser.

It is shown that there is a trade-off between the kinematical stability established by altering the configuration of the collagenous tissue and the mechanical stability compromised by the heat-induced degradation of its mechanical properties. For a homogeneously heated tendon tissue, existence of different shrinkage regimes and a mechanical optimum state in the heat-induced response is shown. Through Finite Element Analysis, thermal damage fields created by clinically applied heating modalities are established and the effects of clinically important parameters such as probe sweep speed, radiofrequency power and saline circulation are examined. A computer-based simulation tool is also developed in order to simulate the heat-induced mechanical behavior of the collagenous tissues.

To accurately simulate the heat-induced mechanical response of a collagenous tissue, future studies should extend the analyses established here to multi-dimensions and should take into consideration the non-homogeneous nature of the tissues. After these studies are completed, the next challenge would be to apply the technology developed to the clinical setting.

ACKNOWLEDGMENTS

ideas, directions. I always felt that he knew exactly what I would say even before I said it and he already had the answer. It was a great pleasure knowing him.

Through four and a half years of hard work, good and bad days, I enjoyed the help and support I received from my coworkers. Late nights washed with excessive amounts of coffee and enlightening discussions with Dr. Scott Morris enabled me to understand the meaning of "Quality" and the value of feeling passion for whatever one is doing. I consider myself to be very luck to be doing what I enjoy the most, and I believe I know at least one other person who feels the same way. It was great knowing you Scott!

I would also like to thank my dear friends Dr. Paul Hoke and Damien Fron for their endless support, help and friendship at all times. I also would like to thank Dave Nielobowich, Scott Dixon, Jessica Paskiewich and Rachel Tuttle for their hard work and the fun they brought into the lab.

I would like to thank my mom, dad and brother for being so understanding, supportive and loving, so much that they could even accept to be far away from me; so that I could pursue my dream. I can never be thankful enough for what these selfless, brave, wonderful people have done for me. My thanks are extended to my very good friends Can Murat Alpaslan and Dr. Selcuk Avci who always supported me and made me feel at home away from home and to my precious Istar, for eleven years of love, support and understanding me so well and helping me break down the walls I surrounded myself.

Last, but not least, I thank my second family, for never leaving me alone and always saving a place in their hearts and home for me: Thank you all so much McGraths.

TABLE OF CONTENTS

LIST OF TABLES

LIST OF FIGURES

CHAPTER 3:

APPENDIX C:

(Images in this dissertation are presented in color)

KEY TO SYMBOLS AND ABBREVIATIONS

A	Molecular collision frequency, [1/s]
A_o	Cross-sectional area [m^2]
c	specific heat [kJ/kg·K]
C_1	Coefficient in Equation 2.11
C_2	Coefficient in Equation 2.11
C_3	Coefficient in Equation 2.11
d_1	Instantaneous shrinkage, [mm]
d_2	Equilibrium shrinkage, [mm]
d_s	Laser spot diameter [mm]
e_1	Instantaneous strain
e_2	Equilibrium strain
E	Tensile Modulus [MPa]
E^*	Denaturation activation energy, [J/mol]
E_o	Peak surface irradiation for laser heating [W/m^2]
f	Laser pulse frequency [Hz]
F	Test load, [N]
g	Heat Generation [W/m^3]
ΔH	Enthalpy of denaturation, [J/mol]
h	Convection Coefficient [W/m^2·K]
I^*	Normalized fluorescence intensity
I	Fluorescence intensity
i	Centeroid x-coordinate of the REV
j	Centeroid y-coordinate of the REV
k	Thermal conductivity [W/m·K]
$k(T)$	Temperature dependent reaction rate constant, [1/s]
N	Number of collagen molecules at native state
P	Joule heat [W]
q''	Surface heat flux [W/m^2]

$\mathcal{R}$	Universal gas constant, [8.314 J/mol·K]
R	Recovery Ratio
r	Scanning (heating) rate, [1/min]
r_o	1/e radius of the Gaussian Profile [m]
t	Time, [s]
T	Temperature [K]
ΔT	Endotherm width at half height, [K]
T_{max}	Temperature when denaturation endotherm reaches its peak, [K]
V	Probe sweep speed [m/s]
$\mathcal{N}^*$	Subregion
$\mathcal{N}$	Region
x	x-coordinate [m]
x^*	Normalized tendon width
y	y-coordinate [m]

Greek:

$\Omega(t)$	Arrhenius damage integral
τ	Time to denaturation, [s]
ρ	density [kg/m^3]
ε	Strain
λ	Stretch Ratio
$\phi(t)$	Window function in Equation 3.4
μ_a	Absorption coefficient [1/m]
Λ	Latent Heat of Phase Change [kJ/kg]
δC_a	Perturbation in heat capacity, [J/mol·K]
Δt	Time increment [s]
Δl	Internode distance [m]
λ_s	Laser pulse width [s]
ω_o	Probe radius [m]
α	Thermal diffusivity [m^2/s]

$\underline{\sigma}_{i,j}$ Stress tensor for the REV

Subscripts:

a   Apparent

i   Initial

m   Midline

max   Maximum

o   Native state

set   Set value

th   Theoretical

x   x-component

xx   x-component

y   y-component

yy   y-component

∞   Far field conditions

Abbreviations:

BP   Bipolar

CV   Control Volume

DPPA   diphenylphosphorylazide

DSC   Differential scanning calorimetry

EDC   1-ethyl-3-(3-dimethylaminopropyl)-carbodiimide

FEA   Finite Element Analysis

GTA   Glutaraldehyde

HACS   Heat assisted capsular shift

HMDC   hexamethylene diisocyanate

IR   Infrared

MDSC   Modulated differential scanning calorimetry

MP   Monopolar

MRI   Magnetic resonance imaging

NXL   Non cross-linked

OCT   Optical coherence tomography

REV   Representative elementary volume

RF   Radiofrequency

UV   Ultraviolet

Chapter 1: Introduction

This dissertation describes research directed towards understanding, modeling and controlling the heat-induced responses of collagenous tissues. The main aim of the research was to establish the scientific basis and develop the tools to increase the safety and efficacy of *Sub-Ablative Thermotherapy* procedures applied to treat instabilities of the knee, ankle and shoulder joints and in the elimination of discogenic pain in the spine.

Arthroscopic thermotherapy in the form of Heat-Assisted Capsular Shift (HACS) procedures for shoulder instability-related diseases served as a focal problem. To date, over 70,000 patients have been treated with sub-ablative thermotherapy and this number is growing rapidly. By some estimates, as much as 8% of the US population suffers from shoulder joint instability. The number climbs to an estimated 35% of the population if knee and shoulder connective tissue diseases and injuries are included [Praemer, et al., 1999].

In the HACS procedure, mechanically deformed, lax collagenous tissues surrounding the shoulder joint (the shoulder capsule and the underlying ligaments [O'Brien, et al., 1990]) are thermally shrunk by means of laser or radiofrequency heating [Arnoczky & Aksan, 2001; Anderson, et al., 1999]. Even though the safety and long-term efficacy of these procedures are still being questioned [Perry & Higgins, 2000], in the year

2000 alone approximately 20,000 patients in the US underwent arthroscopic capsulorrhaphy operations [Praemer, et al., 1999].

1.1 Collagenous Tissue Structure: From Microscale to Macroscale

Dense, oriented collagenous tissue (such as tendon and ligament) structure follows a strict hierarchy [Figure 1.1]. The main structural element of soft tissues like tendon, joint capsule, ligament and skin is the Type I collagen molecule (approximate length is 300 nm). The collagen molecule is comprised of three polypeptide α-chains wound around each other in a helical pattern. Each α-chain is made up of approximately 1500 amino acid residues. Every third residue in this chain is glycine followed usually by proline or hydroxyproline. The structural stability of the collagen molecule is established by the inter-chain hydrogen bonds among the glycine residues of different α-chains and the intra-chain hydrogen-bonded water bridges between the proline and hydroxyproline residues within each α-chain. At a higher level of the hierarchy is the microfibril. The microfibril is made up of a parallel arrangement of five collagen molecules in a cylinder-like formation. Following similar assembly rules, moving further up in the hierarchical ladder the microfibrils form the fibrils and the fibrils form the fibers.

Fibrils are the smallest structures seen with transmitted light microscopy. In a dense, oriented soft tissue (tendon and ligament), the vast majority of the fibrils are aligned in the same direction whereas in other kinds of soft tissues (such as skin and joint capsule) there is a spatial variation in fibril orientation and density.

2

Hydrogen bonds are known to be responsible for the thermal and mechanical stability of the collagen molecule. The higher the hydroxyproline content, the higher the stability and the higher the denaturation temperature of the molecule [Nemethy, 1998]. This well-organized, hierarchical structure, which is enforced by the inter/intramolecular and inter/intrafibrillar chemical bonds (cross-links), determines the response of the tissue to various mechanical and thermal stimuli [Miles, et al., 1995; Olde Damink, et al., 1995; Wren & Carter, 1998].
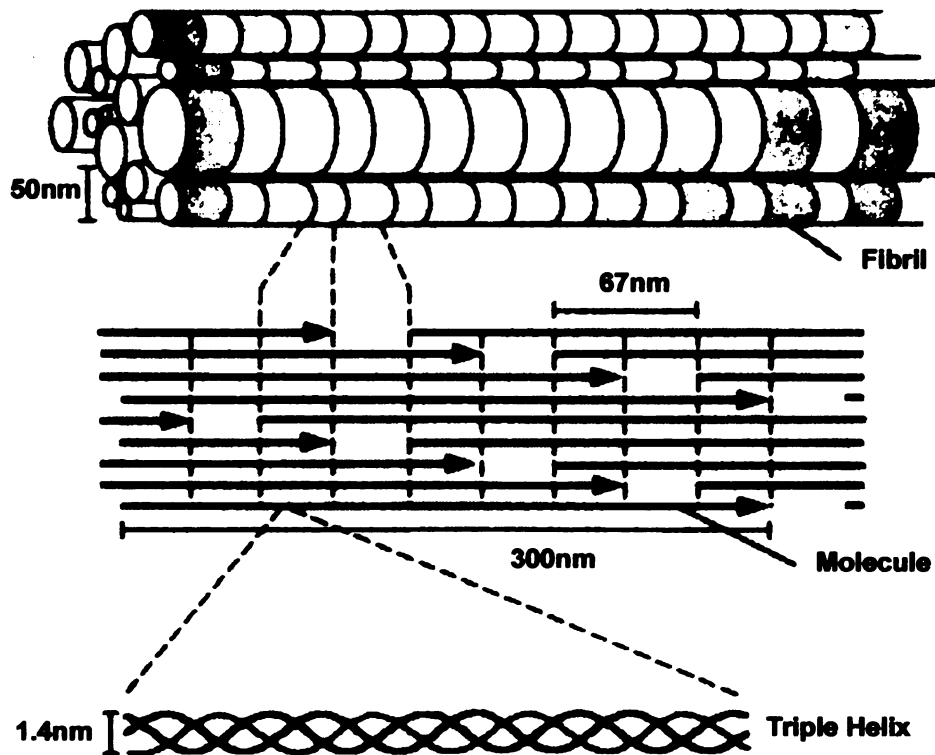
Figure 1.1: Collagenous Tissue Hierarchy [Hayashi, et al., 1996]. *(From Triple-Helical Collagen Molecule to Fibril Level)*

3

1.2 Shoulder Instability

In order to allow a wide range of motion, the shoulder (glenohumeral) joint lacks bony stability (Figure 1.2 A). The integrity of the joint is maintained mainly by the surrounding capsuloligamentous tissues (the shoulder capsule and its regional thickenings known as the glenohumeral ligaments [O'Brien, et al., 1990]) and the rotator cuff muscles and tendons (Figure 1.2 B, C). Low resilience of these surrounding structures contributes to the increased sensitivity to injury.

Kinematically, the shoulder instability may be defined as the inability to maintain the humeral head (the ball) centered in the glenoid (the socket) caused by the pathological redistribution of the forces that keep the joint in equilibrium. Redistribution of the forces is usually initiated by soft tissue problems. These can occur from a single acute event that deforms the capsule and causes capsular and ligamentous laxity (traumatic injury), recurrent micro-trauma that damages the biological microstructure of the joint capsule or by congenital disorders such as Ehlers-Danlos and Marfan's Syndrome.

In the case of traumatic injury, the problem is often initiated by joint dislocation (Figure 1.3). Subjected to lateral impact forces, the humeral head slips over the labrum (the protrusions around the glenoid fossa) and locks. In this locked position, the excessive tensile forces created may cause plastic deformation of the capsuloligamentous tissues. Even if the dislocated joint is reduced immediately, some irreversible laxity of the surrounding soft tissues remain. This is easily observed upon examination by the increased distance of the humeral head from the glenoid fossa [Baeyens, et al., 2001].

In the case of recurrent micro-trauma initiated instability, the possible mechanism of injury is the modification of the collagenous tissue structure due to microdamage created by interfibrillar slippage. Similar to the traumatic case, when subjected to repetitive high stresses, the tissue stretches beyond its anatomical length. This type of injury is usually seen in professional athletes (such as baseball pitchers, golfers and tennis players) performing overhead sports [Jobe, 1991].
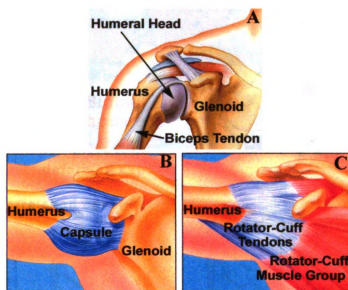
Figure 1.2: (**A**) Anatomy of the Glenohumeral (Shoulder) Joint, (**B**, **C**) Anatomy of the Glenohumeral (Shoulder) Capsule and Rotator-Cuff Muscle Group. *(http://scortho-docs.org/shoulder.html)*

It is estimated that at least 200,000 people in the US suffer from Marfan's Syndrome. In Ehlers-Danlos and Marfan's Syndrome, the triple helical structure of the collagen is altered causing hyperextensibility of the collagenous tissues. There has been no basic research on the feasibility of applying sub-ablative thermotherapy in persons suffering from such diseases resulting from a pathology of the collagen structure.

1.3 Treatment options for Shoulder Instability

Depending on the type (anterior, posterior or multidirectional) and severity of instability and the existence of complementary injuries such as capsule or rotator cuff muscle tears and fractures in the glenoid, different treatments are proposed. Currently applied therapies for the treatment of glenohumeral instability problems include closed, open and arthroscopic techniques.
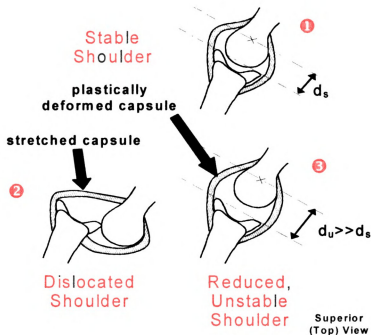
Figure 1.3: Shoulder Dislocation Causing Traumatic Shoulder Instability. (**1**) Stable Shoulder Joint, (**2**) Dislocated and Locked Joint, (**3**) Reduced, Unstable Joint

1.3.1 Conventional Methods

Closed Technique: This technique, based on exercise, depends on strengthening the muscle groups that surround the shoulder joint. In addition to a requirement for a very long treatment period (6-12 months), the high reoccurrence rate limits its application as a stand-alone method [Hayashi, et al., 1997]. While some success is achieved in the treatment of atraumatic subluxation cases (80-90%), only 16% success is obtained in the treatment of the traumatic ones [Burkhead, et al., 1992].

Open Techniques: Depending on the type of instability (anterior, posterior or multidirectional) approximately 300 different operative procedures have been applied for the surgical management of instability [Zayne, et al., 1995]. These operations aim at re-stretching the lax joint tissues, usually by folding the excess capsule beneath itself and stitching it by sutures or by tightening the capsule using surgical anchors attached to the glenoid. In addition to being technically difficult, these operations which are performed for the capsule shift or repair, are generally known to result in pain and have the potential to reduce range of motion and even cause loss of motion, nerve injury and osteoarthritis [Banas, et al., 1993; Bigliani, 1989; Jobe, 1989; Neer, 1990]. Only 30% of patients undergoing surgical operations appear to achieve their pre-injury function.

Arthroscopic Techniques: Although this technique has less risk of neuromuscular injury and requires a shorter rehabilitation period compared to open techniques, the reoccurrence rates observed (between 0% to 50%) show that this technique requires extreme technical expertise and is very much dependent on the skill of the surgeon. Long-

term follow-up studies indicate that the failure rate climbs in the case of generalized ligamentous laxity [Manta, et al., 1997].

1.3.2 Thermotherapy

Recently, arthroscopic thermotherapy (HACS) has been applied for the treatment of glenohumeral instability problems [Thabit, 1994]. This form of therapy aims to reduce the excessive capsular volume and laxity by heating the glenohumeral capsule and the surrounding ligaments (Figure 1.4 A). A Ho:YAG (Holmium:Yttrium-Aluminum-Garnet) laser or radio-frequency probe (Figure 1.4 B) is used by the surgeon to heat these soft tissues to sub-ablative levels (65-85°C). Heating to this level causes collagen denaturation resulting in overall tissue shrinkage. The amount of shrinkage obtained is, to a large extent, determined by the thermal protocol applied. Depending on the heating modality used during heating, in the literature the acronyms LACS (Laser-Assisted Capsular Shift) and ETAC (ElectroThermally-Assisted Capsulorrhaphy) are frequently used. For brevity, in this thesis the acronym HACS (Heat-Assisted Capsular Shift) will be used when referring to any one of them.

Although results of short-term follow-ups show that the therapy is promising and the side effects seem to be nearly nonexistent, questions about the long-term success remain unanswered [Savoie III & Field, 2000; Tyler, et al., 2000]. Improved range of motion of the repaired shoulder, accelerated patient healing as well as lower recurrence rates are the major advantages of this therapy.
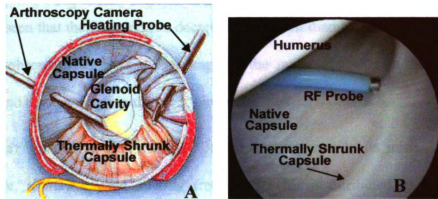
Figure 1.4: Arthroscopic Thermotherapy of the Shoulder (**A**) Schematic of HACS Procedure [Wolf, 1998], (**B**) Photograph Taken During HACS by an Arthroscopic Camera *(http://www.communityorthopedics.com/pages/thermal.htm)*

The disadvantages are the time-dependent decrease of tissue stiffness and strength and the trend for tissue recovery back to its untreated length. This kind of response is observed in research done on animal models [Chen & Humphrey, 1998; Chen, et al., 1998; Schaefer, et al., 1997], as well. Time-dependent changes in mechanical properties and behavior are thought to be the major reason for recurrence and failure of the therapy in the long run.

1.3.3 Mechanism of Thermotherapy (Heat-Assisted Capsular Shift)

Increased temperatures (higher than 60°C) cause a reaction at the tropocollagen level; the collagen molecules start to unwind due to breaking of the hydrogen bonds (Figure 1.5). This reaction causes weakening and shortening of the tropocollagen molecule. In a domino effect manner, these structural alterations in the microscale (as seen

9

in Figure 1.6) produce irreversible changes all the way up to the tissue level. At the fiber level, it is seen that the fiber lengths decrease while their diameters increase. At the tissue level, the observed response is shrinkage in the major direction of fiber orientation accompanied by a swelling in the other directions.

After heating, if the tissue is allowed to cool back to its initial, neutral state temperature, it may expand slightly (recovery). This is attributed to the partial re-naturation of the collagen structure. The magnitude of this recovery from shrinkage depends on the reversibility of the thermal-mechanical modification achieved.
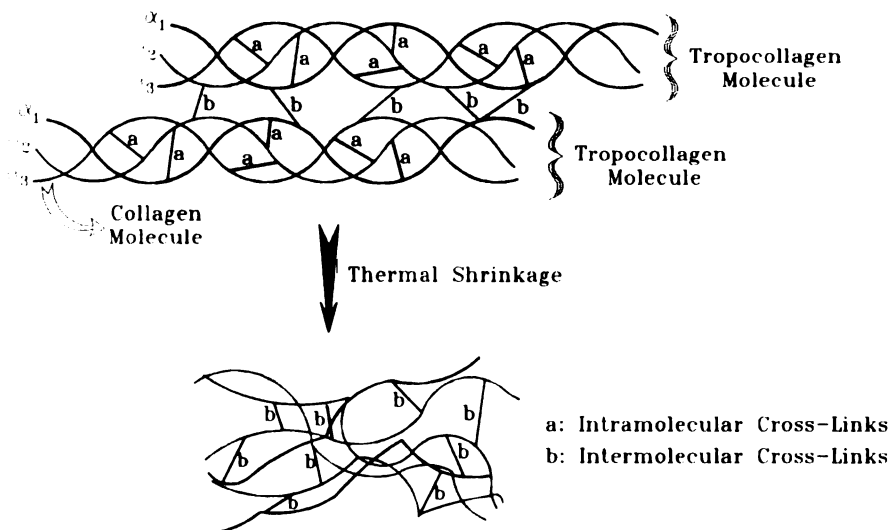
Figure 1.5: Heat-induced Collagen Denaturation [Arnoczky & Aksan, 2001]

A very effective method for the determination of denaturation at the micro scale is optical birefringence measurement [Pearce, et al., 1993]. The birefringence in collagenous tissues is due to the differences between the refractive indices of the ordered fibril structure and the surrounding ground substance [Sankaran, & Walsh, 1998]. Optical

measurement of the birefringence decay during the helix-to-coil transition of tropocollagen molecules (loss of ordered structure) has proved to be a very valuable nondestructive method to model thermal denaturation of various tissues [Maitland & Walsh, 1997]. This method is vital in understanding the relationships between the denaturation phenomena at the micro-scale and the bulk tissue shrinkage observed at the macro-scale.
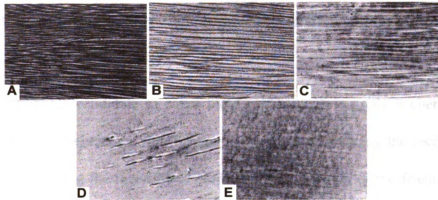
Figure 1.6: Loss of Fibrillar Structure with Heating. (*Inserts A Through E Show the Effect of Accumulating Thermal Damage on Fibrillar Structure*) [Wall, et al., 1999]

There are two important factors that accompany the denaturation-induced shrinkage of collagenous tissues. These are: the mechanical property degradation and the partial loss of shrinkage upon cooling back to lower temperatures (defined as recovery). Recovery is thought to be the result of re-naturation i.e., refolding of the partially unfolded tropocollagen molecules upon cessation of heat [Hormann & Schlebusch, 1971]. This is the main cause of ambiguity in measuring the exact amount of shrinkage produced by heating. This factor may be particularly important during HACS surgery where the

success of the operation is to a large extent dependent on the amount of shrinkage achieved.

The reduction in the tensile modulus and strength (up to 70-90% of the untreated tissue) of the collagenous tissue upon heating is reported in the literature [Vangness, et al., 1997; Schaefer, et al., 1997; Berend, et al., 1996; Hecht, et al., 1999]. This fact, coupled with the strain injury (microdamage yielding to plastic deformation) created in the glenohumeral capsular and ligamentous structures during subluxation or dislocation, indicates that immediately after the operation the tissue is excessively weak and vulnerable.

One possible candidate to solve these problems is to apply a chemical cross-linking method in conjunction with heating as a means of reducing the recovery of the tissue while enhancing the mechanical properties. Examination of the feasibility of this idea was the motive for preliminary research conducted as a part of this thesis (Chapter 5).

1.4 Research Objectives

The main aim of the research was to establish the scientific basis and develop the tools to increase the safety and efficacy of *Sub-Ablative Thermotherapy* procedures. To achieve this goal, the following objectives are established:

a) Modeling the thermal damage accumulation in collagenous tissues when they are subjected to clinically applied heating modalities. Research aimed at reaching this objective is presented in Chapter 3 of this thesis.

b) Determination of the constitutive relationships between the measured thermal and mechanical parameters (temperature, time, load) and the final state of the tissue (state-of-stress and mechanical properties). Chapter 2 of this thesis describes the experimental analysis performed with a model collagenous tissue (rabbit patellar tendon) in order to establish these relationships.

c) Modeling the thermomechanical responses of collagenous tissues in order to develop a simulation tool to be used for optimizing currently applied sub-ablative thermotherapy procedures (e.g. HACS, thermokeratoplasty, etc.). Chapter 4 of this thesis describes the thermomechanical response simulation algorithm developed for this purpose.

Additionally, the feasibility of applying chemical enhancement methods as a means of reducing the recovery of the tissue while enhancing the mechanical properties is examined in Chapter 5. Chapter 6 summarizes the results, presents the conclusions drawn from the research presented here and discusses important issues that are addressed by this research. Chapter 7 discusses the directions for future work.

Chapter 2: Heat-Induced Mechanical Response Analysis

2.1 Overview of Literature

Collagenous tissue denaturation and shrinkage in response to heating by laser, microwave, radio frequency devices and hydrothermy are extensively studied phenomena [Naseef III, 1997; Hayashi, 1996; Allain, 1980]. The amount and the extent of the irreversibility of tissue shrinkage (i.e., thermomechanical strain formation) depend on many factors. These factors include the maximum temperature reached and the exposure time [Miles, 1995; Cilesiz, 1997; Pearce, 1993; Le Lous, 1983] as well as the mechanical stress applied on the tissue during heating [Kang, 1995]. Other factors include the surrounding medium pH and electrolyte concentration [Privalov, 1982] as well as the type of collagen [Tang, 1997], its hydration level [Privalov, 1989], and the degree of the cross-linking [Olde Damink, 1995; Ruijgrok, 1994]. In other words, the amount and rate of heat deposition, coupled to the properties of the tissue and the surrounding medium govern the response at both the microscopic and macroscopic scales [Le Carpentier, 1993].

The heat-induced responses of a collagenous tissue for isothermal, stress-free and isotonic shrinkage conditions have been quantified recently for a bovine model [Chen, et al, 1997, 1998a,b,c] under hydrothermal heating conditions. These studies have revealed

that heat-induced denaturation of collagenous tissues (expressed in terms of thermal-mechanical strain formation) can be quantified by a single Arrhenius type of relationship. This relationship depends on the temperature, exposure time and mechanical stress applied to the tissue. This finding, together with the differentiation of various thermal-mechanical response regimes, may be considered the first attempt to establish a unique relationship which couples thermal and mechanical factors together in a model of the tissue thermal response.
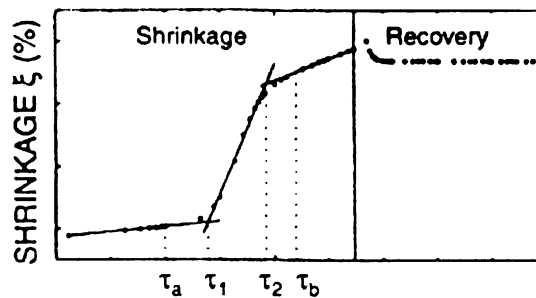
Figure 2.1: Isothermal Shrinkage of Bovine Chordae Tendineae [Chen, et al., 1998b]

Although the observation of shrinkage in response to various heating loads is well documented in the literature, a consensus regarding the magnitude and irreversibility of thermal-mechanical strain formation is far from being reached. Examination of the following examples chosen from the many in the literature, highlights this conclusion:

I.   Hydrothermal heating (where the tissue is completely immersed in a saline bath and the saline temperature is increased) of bovine calf knee capsule at 65°C for 60 seconds causes 50% shrinkage [Naseef III, 1997],

II. Hydrothermal heating of bovine chordae tendineae at 65°C for 100 seconds results in 20% shrinkage [Chen, et al., 1997],

III. Hydrothermal heating of cadaver glenohumeral capsule at 65°C for 600 seconds causes 11% shrinkage [Hayashi, et al., 1997],

IV. Ho:YAG laser ablation until tissue opacity changes at a dose of 300 J/cm^2 for rabbit patellar tendon results in 6.6% shrinkage [Schaefer, et al., 1997],

V. Ho:YAG laser ablation until tissue opacity changes at a dose of 300 J/cm^2 for canine patellar tendon results in 56% shrinkage [Berend, et al., 1996],

VI. Ho:YAG laser ablation until tissue opacity changes at a dose of 180 J/cm^2 for rabbit femoropatellar joint capsule causes 38% shrinkage [Hayashi, et al., 1995].

The inconsistencies and the contradictions of trends among the shrinkage values reported by different researchers are thought to result from the differences among the heating modalities and protocols applied. The differences in tissue composition in addition to the distribution of collagen types and variation of collagen fiber orientation inside the tissue also contribute [Olde Damink, 1995; Chvapil and Jensovsky, 1963; Horgan, et al., 1990]. The inconsistencies include the great difference in shrinkage values between examples *IV* and *V* for the same tendon tissue harvested from two different species but exposed to the same heating load. The contradictions include the decrease in observed shrinkage values with increase in exposure times in examples *I, II, III*, which is contrary to current knowledge. The differences between species, the age of the tissue sample, as well as the duration of heating and the maximum temperature reached are considered to be

major factors, which determine shrinkage [Olde Damink, 1995; Le Lous, et al., 1985; Allain, et al., 1980]. Additionally, there are some other parameters that have not been considered comprehensively in the literature. These are; *a)* the effects of the differences in thermal histories created by different energy deposition modalities, *b)* the correlation between the level of denaturation achieved at the micro scale and the thermomechanical response at the macro scale and *c)* the effects of stress and the chemical state of the tissue on thermal response characteristics. Examination of these parameters will be performed as part of this thesis.

2.2 Thermal Analysis (Collagen Denaturation Kinetics)

Traditionally, heat-induced denaturation of collagen has been modeled as a first-order reaction between its native and denatured states [Miles, 1993] or a second-order reaction (similarly between the native and denatured states) through an intermediary, activated state [Lyubarev & Kurganov, 1998]. The activated state corresponds to the partially unfolded configuration of the protein.

The first-order reaction theory [Miles, 1993] dictates that during denaturation phase change of the collagenous tissue, the decline in the number of molecules in the native state can be represented as a function of time, *t*, as follows:

$$\frac{dN}{dt} = -k(T)N.$$ **2.1**

In the equation above, N is the number of molecules in the native state and $k(T)$ is the temperature dependent reaction rate constant. Isothermal heating experiments are performed in order to determine how the reaction rate constant changes with temperature. In these experiments, the collagenous tissue is kept at the isothermal test temperature, and the time required for the completion of the chemical reaction (denaturation) is measured.

There are two major issues with the implementation of isothermal heating experiments. Firstly, the tissue temperature should instantly be increased to the isothermal test temperature and be constant throughout the test. Due to the thermal response characteristics of the experimental equipment used, this condition may be very hard to achieve. Secondly, a very accurate method is required to determine the completion of the chemical reaction. For heat-induced denaturation of collagenous tissues, the alternatives are optical (measurement of the variation of structural birefringence with denaturation [Pearce, et al., 1993]), chemical (determination of the number of hydrogen bonds broken [Usha & Ramasami, 1999]), mechanical (measurement of stress-relaxation during heating [Le Lous, et al., 1983]) and thermal (calorimetric analysis [Burdzhanadze, et al., 1997]) methods. Since thermal denaturation of collagen is intrinsically a heat-induced phenomenon, methods measuring the heat absorbed by the collagenous tissue during denaturation (i.e., calorimetric analysis) appear to be the natural choice.

2.2.1 Isothermal Heating Experiments

In order to determine the denaturation kinetics of the rabbit patellar tendon tissue (the tissue model used in the mechanical analysis), a model Q100 (TA Instruments, New

Castle, DE) Differential Scanning Calorimeter (DSC) was used. The cell temperature reading of the calorimeter was calibrated using Indium (melting point 156.6°C) as the standard.

A total of 18 isothermal heating experiments were performed with rabbit patellar tendon tissue samples excised from three different tendons. The frozen (kept at temperatures below -120°C), intact New Zealand White rabbit patellar tendon (RPT) tissues were thawed overnight at -5°C and kept in room temperature saline until testing. Before the experiment, small tissue samples, weighing between 5 and 25 mg were excised, weighed using a high precision scale (Sartorius 2842, Sartorius GMBH, Goettingen, Germany) and placed in aluminium heating pans. 10μl of saline was added to the sample pan to ensure proper hydration of the sample during the course of the experiment. The sample pan was then hermetically sealed and placed into the heating cell of the DSC together with a reference pan. The reference pan also contained 10μl of saline and was hermetically sealed. In the experiment, the sample was initially equilibrated at 25°C and then the sample temperature was increased to the test temperature at a rate of 200°C/min. (the maximum rate for the DSC used). The isothermal test temperature was set at half degree increments between 54°C and 56°C and kept constant for the duration of the experiment (maximum 3 hours). During the experiment, the heat flow to the sample pan, normalized with respect to that to the reference pan, was measured and recorded at 10 Hz. The onset of the denaturation phase change was marked by an increase in the rate of the heat flow to the sample. When the sample was fully denatured, the heat flow rate returned

to its baseline (pre-denaturation) value. The time between the onset and completion of denaturation was recorded for each experiment.

Nine out of the 18 experiments performed failed to produce dependable results due to high noise or sample pan movement during denaturation. It was observed that if the sample was small (less than 8 mg) the signal to noise ratio in the heat flow signal was very low and if the sample was big (weighing more than 10 mg), denaturation induced shape change of the sample caused sample pan movement. When the sample moved, the thermal contact resistance between the tissue sample and the sample pan and/or between the sample pan and the heating cell changed and very sharp, unnatural peaks were observed in the heat flow signal.

The results obtained from the remaining 9 experiments are presented below in Figure 2.2. Regression analysis performed on the data established an exponential correlation between the absolute value of the isothermal test temperature and the time required for full denaturation of the sample. The data showed that the reaction rate constant, $k(T)$, (which is equal to the mathematical inverse of the denaturation completion time) is a function of temperature as given by the well-known Arrhenius equation [Miles, 1993]:

$$k(T) = A \cdot e^{-\frac{E^*}{\Re \cdot T}}, \qquad\qquad 2.2$$

where A is defined as the molecular collision frequency, E^* is the denaturation activation energy, $\Re$ is the universal gas constant equal to 8.314 J/mol×K, and T is the absolute

temperature. For the data presented below in Figure 2.2, the constants were calculated as $E^*=4.045 \times 10^5$ J/mol and $A=6.311 \times 10^{61}$ 1/s.

There were two major problems identified with the isothermal heating experiments performed in this research. One apparent problem was the limitation imposed by the temperature response of the DSC used. In Figure 2.3, the temperature response of the DSC at a heating (scanning) rate of 200°C/min. is presented. As shown in this figure, it took approximately 3 minutes (the region between t=13 and t=16 minutes in Figure 2.3) to heat the sample to the set isothermal test temperature from the initial temperature (T_i=25°C).
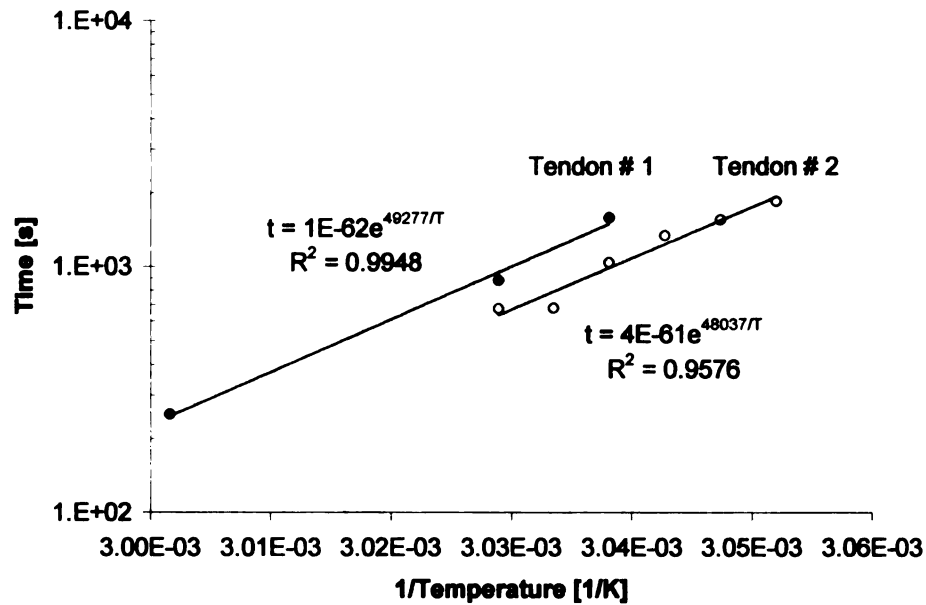
Figure 2.2: Isothermal Heating Experiments with Rabbit Patellar Tendon

This was far from satisfactory for the "instant heating" condition imposed by the experimental procedure. During this initial temperature transient, the heat flow signal for the sample experienced a transition as well. If in an experiment, the isothermal test

temperature was set to a high value where the reaction rate was high (i.e., denaturation reaction progressed fast), the denaturation phase change occured during this initial transition and was completed even before the isothermal test temperature was reached. In this thesis, this fact limited the higher end of the temperatures that could be experimented with to 56°C.

The lower temperature limit for the experiments was determined by the very long time required for the completion of the test. Since denaturation progressed very slowly, the heat flow signal was very weak and the signal to noise ratio decreased, making it impossible to determine the onset and completion of the phase change. Therefore, experimentation with test temperatures below 54°C did not yield any results. These factors limited the temperature range at which experiments could be performed to a very narrow range of 54-56°C.
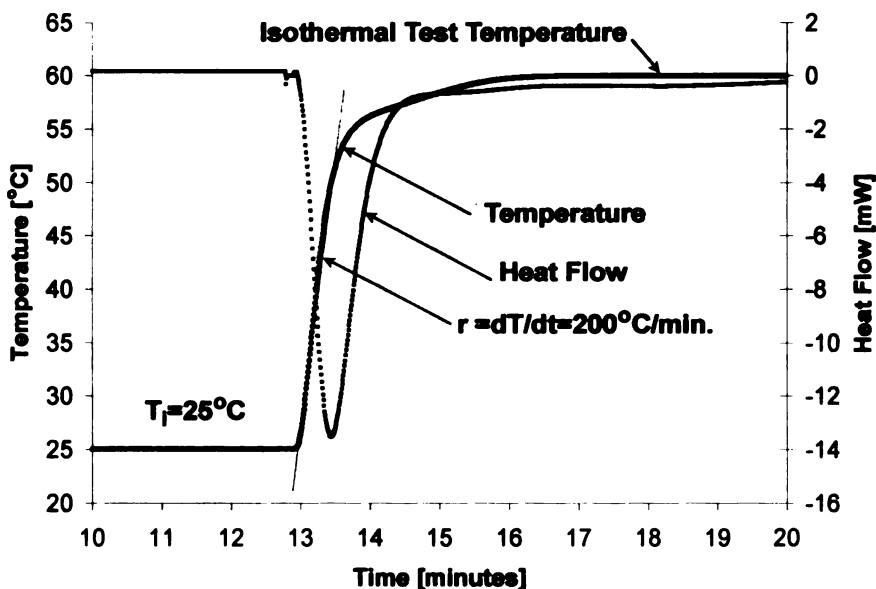
Figure 2.3: Q100 DSC Machine Response at 200°C/min. Heating (Scanning) Rate

Due to the reasons presented above, the results of isothermal heating experiments and the values for the coefficients of the Arrhenius rate equation (A, E^*) calculated from these experiments should be approached with extreme care. Validity of these constants at high isothermal test temperatures or for non-isothermal heating conditions (which are clinically relevant for the sub-ablative thermotherapy of collagenous tissues) could not be determined with this method. One method to check the validity of these coefficients is by examining the denaturation kinetics of the collagenous tissue by constant temperature increase tests. For this purpose, a method proposed by Miles, et al. [Miles, et al., 1995] was implemented and the details are presented in the following section.

2.2.2 Differential Scanning Calorimetry Experiments

Differential Scanning Calorimetry (DSC) has extensively been used to characterize the thermal behavior of acid soluble collagen [Tiktopulo and Kajava, 1998; Burdzhanadze, et al., 1997] and collagenous tissues [Miles, 1993; Miles, et al., 1995; Kampmeier, et al., 2000].

In the DSC method, the energy absorbed/released by the sample during ramp temperature increase is measured. The characteristic behavior of collagenous tissue in a DSC experiment is such that up to a certain temperature (denaturation temperature), the specific heat (the incremental amount of heat absorbed by the specimen during unit temperature rise) shows very little temperature dependence. As seen in Figure 2.4, denaturation is characterized by a sudden increase in the energy absorption endotherm (starting at approximately 55°C in Figure 2.4) in the neighborhood of the denaturation

temperature, T_{max}. With further heating, the endotherm reaches its maximum value (at approximately 67°C in Figure 2.4) and then decreases and finally returns back to its baseline value (at approximately 80°C in Figure 2.4). It is reported in the literature that the denaturation endotherm characteristics are heating (scanning) rate dependent. Burdzhanadze [Burdzhanadze, et al., 1997] reports that with dilute solutions of collagen, an increase in denaturation enthalpy and denaturation temperature (endotherm maximum) is seen with increasing scan rates while the half width of denaturation remains unaltered. He explains that these "unexpected" results are due to the temperature dependent negative enthalpy created by "disturbing hydrophobic interactions".

Miles, et al. [Miles, et al., 1995] show that the location and the shape of the denaturation endotherm changes with scanning rate but the enthalpy of denaturation remains constant. They also show that the constants, (A, E^*), calculated from isothermal heating tests performed on rat tail tendon samples can be used to predict the characteristics of the denaturation endotherm (such as its shape and position) at different heating (scanning) rates during a DSC test.

If during the an experiment, the temperature is increased linearly (as would be the case in a Differential Scanning Calorimetry (DSC) experiment) as a function of time as,

$$T = T_i + rt, \qquad\qquad 2.3$$

where T_i and r are the initial temperature and the heating (scanning) rate, respectively and if the temperature dependence of the reaction rate constant, $k(T)$, is given by the Arrhenius equation (Equation 2.2), the location (the temperature at which it reaches its maximum

(peak) value, T_{max}) and the shape of the denaturation endotherm can be predicted using the following equations [Miles, 1993]:

$$\frac{rE^*}{ART_{max}^2} = e^{\left[-\frac{E^*}{RT_{max}}\right]} \qquad\qquad 2.4$$

$$\Delta T = 2.446\frac{RT_{max}^2}{E^*} \qquad\qquad 2.5$$

$$\left(\frac{\delta C_a}{\Delta H}\right)_{T_{max}} = \frac{E^*}{eRT_{max}^2} \qquad\qquad 2.6$$

where r, T_{max}, ΔT, δC_a, ΔH are the scanning rate, the temperature when the endotherm reaches its denaturation peak (determines the endotherm location), the peak width at half height, perturbation in heat capacity and the enthalpy of denaturation, respectively (see Figure 2.4 for details).

Once the Arrhenius equation rate constants (A, E^*) are calculated from isothermal heating experiments, the location of the denaturation endotherm, T_{max}, can be determined as a function of the scanning rate, r (from Equation 2.4). When the value of T_{max} is determined, it is possible to calculate ΔT from Equation 2.5, and $\delta C_a/\Delta H$ from Equation 2.6. These two variables determine the shape (the flatness or sharpness) of the denaturation endotherm.
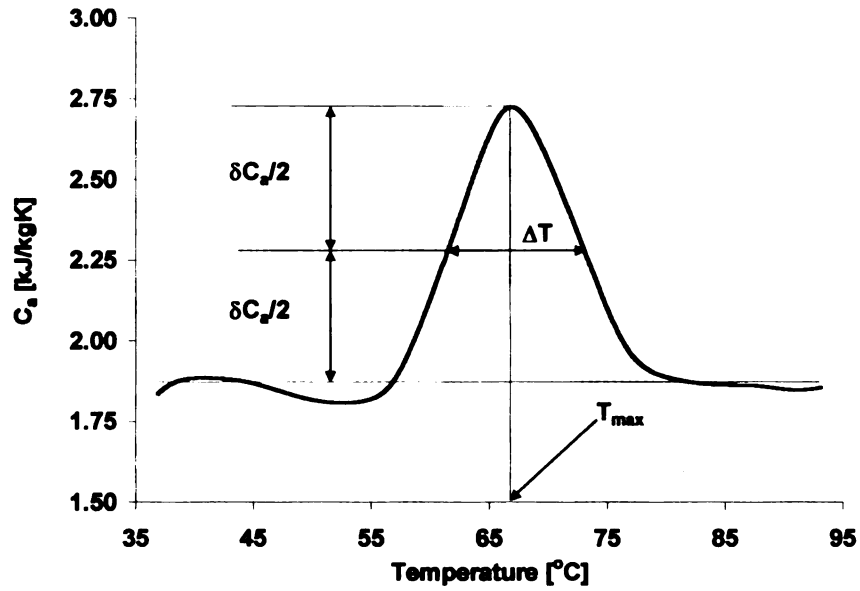
Figure 2.4: Characteristic DSC Experimental Data Collected from one RPT Sample

A series of conventional (DSC) and modulated differential scanning calorimetry
(MDSC) tests were performed using a calorimeter (Q100, TA Instruments, New Castle,
DE). Similar to the procedure followed in the isothermal heating tests (described in the
previous section), the cell temperature reading of the calorimeter was calibrated using
Indium and the absolute specific heat measurement was calibrated using Sapphire as the
standard.

A total of 43 rabbit patellar tendon specimens were subjected to ramp heating
experiments (at a rate of either 1, 5 or 10°C/min.) in the range of 25°C to 90°C and their
heat absorption were measured and recorded over the course of the experiments. Samples
were prepared in the same way as the samples used in the isothermal heating tests

26

described in the previous section. The differential scanning calorimetry test was comprised of these following steps:

1. The temperature of the sample was increased to 25.00 $^{\circ}$C.

2. Sample was equilibrated at 25.00 $^{\circ}$C.

3. Sample was kept at 25.00 $^{\circ}$C for 2 minutes.

4. Temperature was modulated by 1.00 $^{\circ}$C every 60 seconds (this step was included only in MDSC experiments).

5. Sample was kept at 25.00 $^{\circ}$C until it reached thermal equilibrium.

6. The temperature was increased to 90.00 $^{\circ}$C at a predetermined scanning (heating) rate (r = 1, 5 or 10°C/minute).

7. The sample was kept at 90°C for 2 minutes.

8. Sample was cooled back to 25.00 $^{\circ}$C.

After the experiment was completed, the samples were weighed again and their post-experimental weights were compared to their pre-experimental weights to ensure that there was no change (i.e., saline has not leaked from the sealed pans). Measurements showed that none of the samples tested has leaked during the experiments.

Table 2.1: RPT Collagen Denaturation Endotherm Characteristics

Scanning Rate, r [°C/min.]	Method	Endotherm Peak Temperature, T_{max} [°C]	Student's T-test Two-tailed P value	Endotherm Width at Half Peak, ΔT [°C]	Student's T-test Two-tailed P value
1 (n=4)	DSC	61.477 ± 0.581	0.0682	3.187 ± 0.320	0.2182
5 (n=6)	DSC	63.347 ± 0.824	0.0433	6.485 ± 0.361	0.0886
10 (n=6)	DSC	67.427 ± 0.442	0.3527	13.438 ± 1.413	0.0002
1 (n=3)	MDSC	60.397 ± 0.397	-	2.458 ± 0.656	-
5 (n=2)	MDSC	64.615 ± 0.389	-	3.820 ± 0.485	-
10 (n=4)	MDSC	66.608 ± 1.449	-	5.518 ± 1.498	-

The data collected during the experiment were analyzed using the Universal Analysis software (Universal Analysis, V3.4C, TA Instruments, New Castle, DE). Out of the 43 experiments, 18 failed due to pan movement during denaturation of the collagen sample inside the pan. These data were discarded.

The parameters that were determined with data analysis were, the denaturation peak width at half height, ΔT, the temperature when the endotherm reached its denaturation peak (the denaturation temperature), T_{max}, the perturbation in heat capacity, δC_a, and the enthalpy of denaturation, ΔH (see Figure 2.4 for details). Except for the case of r = 5°C/min., the difference between the T_{max} values obtained from DSC and MDSC experiments for the same heating rates were not statistically significant (see Table 2.1 on page 28).
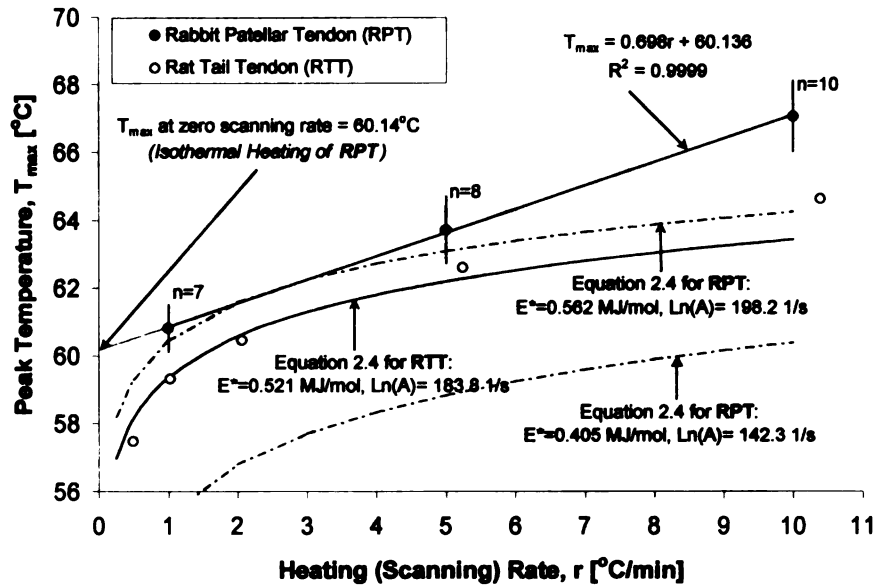
Figure 2.5: Transition Peak Temperature, T_{max}, as a Function of Heating (Scanning) Rate, *r*. *(Data for Rat Tail Tendon (RTT) is from Miles, et al. [Miles, et al., 1995])*

The data showed that irrespective of the method used (DSC or MDSC) the transition peak temperature, T_{max}, increased linearly ($R^2=0.9999$) with the scanning rate, *r* (Figure 2.5; filled circles). T_{max} changed approximately 6°C over a change of an order of magnitude in the scanning rate, *r*. A similar increasing trend in transition peak temperature with scanning rate is also observed by Miles, et al. [Miles, et al. 1995] in experiments performed with rat tail tendon (RTT) specimens but the increase is established as logarithmic rather than linear (Figure 2.5; solid line connecting the open circles).

The difference between the RTT data and the RPT data (in the scanning rate range examined) were within 2°C, therefore, it is believed that the exact form of the

mathematical relationships established were not of great significance when the experimental error and the limitations of the calorimeters were considered.

Table 2.2: Enthalpy of RPT Collagen Denaturation

Scanning Rate, r [°C/min.]	Denaturation Enthalpy, ΔH [J/g]	$(\delta C_q/\Delta H)$ at T_{max} [1/K]
1 (n=7)	7.296 ± 1.469	0.139 ± 0.054
5 (n=8)	8.664 ± 3.931	0.218 ± 0.050
10 (n=10)	10.486 ± 3.798	0.283 ± 0.025

Transition half width, ΔT, values found with DSC and MDSC experiments however, were significantly different for the same heating rate with the exception of the values calculated at r=1°C/min. (Figure 2.6). The results from MDSC experiments showed higher ΔT values. This may be explained by the variation (modulation) of the temperature during MDSC experiments which slowed the denaturation behavior and that the model proposed by Miles, et al., is based on DSC measurements with constant temperature increase (given by Equation 2.5). In MDSC, even though the mean temperature of the sample increased linearly with time, there was a superimposed sinusoidally varying component (modulation). Both DSC and MDSC data showed exponential dependence of ΔT on the scanning rate (R^2>0.98 for DSC and R^2>0.99 for MDSC) (see Figure 2.6). For rat tail tendon and porcine lens capsule the method proposed by Miles et al. [Miles, et al., 1995; Miles, 1993] predicts a linear relationship (see the

curve for RTT in Figure 2.6) but nevertheless their measured values (see the RTT and PLC data in Figure 2.6) are very close to the values measured with DSC for RPT.
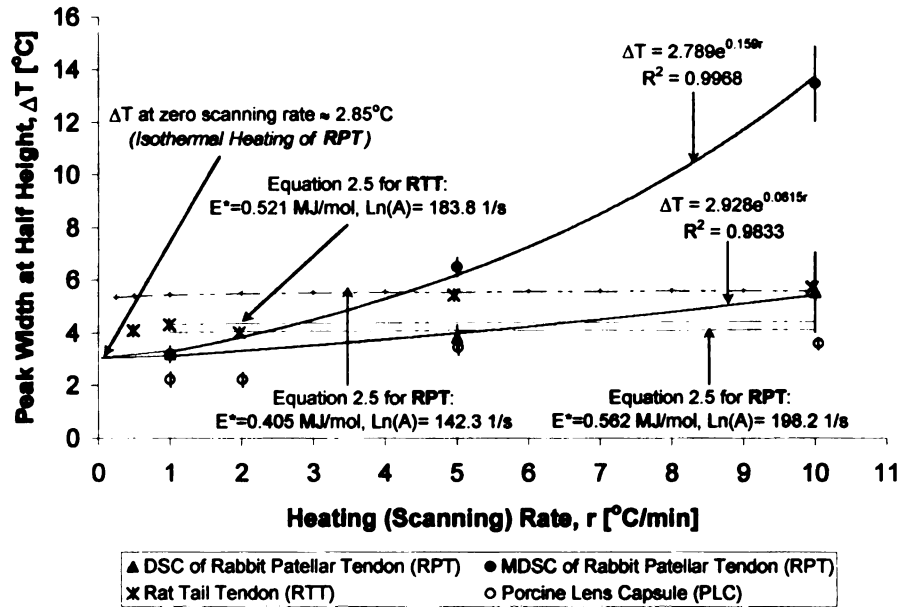
Figure 2.6: Peak Width at Half Height, ΔT, as a Function of Heating (Scanning) Rate, r. (Data for Rat Tail Tendon (RTT) is from Miles, et al. [Miles, et al., 1995], data for Porcine Lens Capsule (PLC) is from Miles [Miles, 1993].)

The change in denaturation enthalpy, ΔH, with scanning rate, calculated by integrating the area under the endotherm over time was found to be insignificant (P=0.41), however the standard deviations of these measurements were extremely large (see Table 2.2 on page 30).

When the Arrhenius equation coefficients calculated from isothermal heating experiments ($E^* = 4.045 \times 10^5$ J/mol and $A = 6.311 \times 10^{61}$ 1/s) are used in Equations 2.4 and 2.5 to determine the variation of T_{max} and ΔT with heating (scanning) rate, it was seen that

the predicted values were significantly lower than the measured values. This is demonstrated in Figure 2.5 for T_{max} by comparing the measured values of T_{max} for RPT to the predictions (lower dash-dot line in Figure 2.5 for E^* =0.405 MJ/mol and *Ln(A)* =142.3 1/s) and in Figure 2.6 for ΔT by comparing the measured values of ΔT for RPT to the predictions (higher dash-dot line in Figure 2.6 for E^* =0.405 MJ/mol and *Ln(A)* =142.3 1/s). This difference was attributed to the problems inherent to isothermal heating experiments (please see the previous section for a detailed discussion).

Through least-squares analysis of Equations 2.4 and 2.5, it was determined that in the scanning rate range experimented, E^*=5.623x10^5 J/mol and A=1.136x10^{86} s^{-1} yielded the best predictions when compared to the measured values. Additionally, the difference between the predictions and measurements vanished in the neighborhood of r =2°C/min. (which also corresponded to the temperature change recorded in the hydrothermy bath during mechanical testing; see Section 2.4 for details). These values were also well within the range reported in literature for similar biological materials (for example, A=6.6577x10^{79} s^{-1} and E^*=5.21x10^5 J/mol for rat-tail tendon specimens [Miles, et al., 1995]) [Pearce & Thomsen, 1995; Pearce, et al., 1993]. Therefore, these values (E^*=5.623x10^5 J/mol and A=1.136x10^{86} s^{-1}) were used for the remainder of this thesis instead of the values calculated by isothermal heating experiments (E^*=4.045x10^5 J/mol and A=6.311x10^{61} 1/s).

2.3 Arrhenius Damage Integral

The Arrhenius damage integral is frequently used in order to characterize the combined effects of temperature and exposure time on protein denaturation [Kampmeier, et al., 2000] and collagen birefringence loss [Pearce, et al., 1993]. The Arrhenius damage integral is given as [Henriques & Moritz, 1947]:

$$\Omega(\tau) = \int_0^\tau A \cdot e^{-\frac{E^*}{\Re \cdot T(t)}} dt. \qquad\qquad 2.7$$

In this formulation, $\Omega(\tau)$ is the thermal damage accumulated up to time, τ. A is the molecular collision frequency, E^* is the denaturation activation energy, $\Re$ is the universal gas constant equal to 8.314 J/mol×K, and T is the absolute temperature. The values for A and E^* are specific for each kind of tissue and phenomenon examined. These constants govern the kinetics of thermal denaturation and establish the dependence of the rate constant of the reaction, $k(T) = d\Omega/dt$, to the temperature, T, at which the reaction takes place.

In order to determine how the rate constant of the reaction changes with temperature, (and therefore to calculate the corresponding activation energy, E^*, and the collision frequency, A, isothermal heating experiments were performed. However, it has been shown in this research that due to the errors encountered in isothermal heating tests, DSC experimentation was to be used to determine these constants. It was therefore possible (through integration as seen in Equation 2.7) to determine the state of a chemical reaction (here in this research, the heat induced denaturation of collagenous tissue) when it

experienced an arbitrary thermal history (not necessarily isothermal) through the use of

the Arrhenius damage integral concept (Equation 2.7). As explained in the previous

sections, the constants for New Zealand white rabbit patellar tendon were chosen as

$A=1.136 \times 10^{86}$ s^{-1} and $E^* = 5.623 \times 10^5$ J/mol in this research.
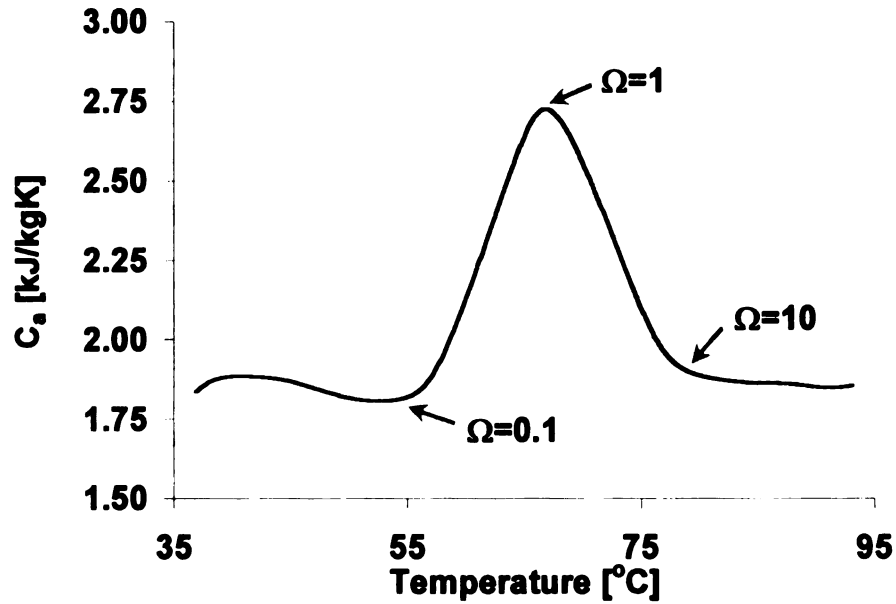
Figure 2.7: Variation of Rabbit Patellar Tendon Collagen Apparent Specific Heat with Accumulating Thermal Damage

When these constants were used in the calculation of the Arrhenius damage

integral during a constant heating rate test, for a stress-free patellar tendon tissue $\Omega=1$

corresponded to the peak of the apparent specific heat curve and $\Omega=10$ corresponded to

the completion of denaturation transition where no further change in apparent specific

heat was recorded (Figure 2.7).

Utilization of the simple Arrhenius thermal damage integral representation would not be possible for a stressed tissue if the load applied on the tissue were to change the denaturation enthalpy. Based upon the evidence presented above, it was reasonable to assume that when normalized with respect to the effect of the stress-state (which changes the phase transition entropy [Miles & Ghelashvili, 1999]), the thermal response of collagenous tissues could be represented as a function of the Arrhenius damage integral calculated at the stress-free (reference) state.

2.4 Mechanical Analysis (Heat-Induced Mechanical Response)

In this chapter of the thesis, one-dimensional, heat-induced response of collagenous tissues has been characterized experimentally using a New Zealand white rabbit patellar tendon model. The tissue model chosen for this research is suitable to quantify the one-dimensional behavior since the great majority of fibers in the patellar tendon are oriented in one direction (along the axis connecting the patella and the tibia).

2.4.1 Specimen Preparation

Patellar tendon samples were harvested from the hind legs of the New Zealand White rabbits supplied from other researchers at Michigan State University (Dr. Steven Arnoczky of the College of Veterinary Medicine and Dr. Hangboa Ma of the College of Human Medicine). None of the animals had undergone experimentation that would affect their musculoskeletal tissues. Patellar tendon complexes (patella-patellar tendon-tibia)

were harvested immediately after sacrifice and were stored in a cryogenic freezer at -120°C until testing. Prior to testing, the samples were thawed overnight at -5°C followed by 1-2 hour immersion in room temperature saline solution. It has been reported for tendons and ligaments stored at -70°C that there is no significant variation in the mechanical properties due to the freezing [Bechtold, et al., 1994; Woo, S.L.-Y., et al., 1986]. Additionally, all of the specimens included in this study were exposed to the same freezing and thawing protocol. It is therefore reasonable to assume that even if there may have been some changes in the mechanical properties of the frozen-stored specimens (when compared to those of the fresh tissues), among the specimens tested, mechanical property variation due to the specific freeze/thaw protocol applied was not significant.
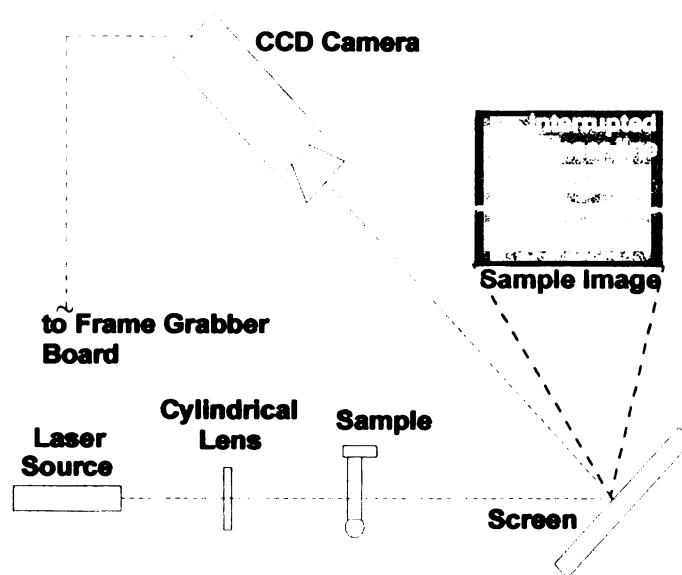
Figure 2.8: Laser Shadowgraph System for Dimension Measurements

The cross-sectional dimensions and the length of the patellar tendon were measured optically by a custom-made, non-contact laser shadowgraph system (Figure

2.8). In this method, a laser sheet was formed by passing a low intensity laser light through a cylindrical lens. The laser light was then projected on the patellar tendon specimen and the part of the light that was not blocked by the specimen was projected on a screen. With a CCD camera (connected to a frame-grabber board in a PC) focused on the screen, the image of the interrupted laser line (see insert in Figure 2.8) was captured and the length of the laser light blocked by the specimen was compared to that from an image of a cylinder of known diameter (placed at the same location as the sample).

By this non-nontact method, the width and thickness of the tendon specimen was measured at multiple locations along its length. After these measurements were completed, the tibia was potted in an aluminum tube by an inert glue and was then secured using two steel pins inserted in the holes drilled through the tubing and the bone (Figure 2.9).

2.4.2 Experimental Setup

The aluminum tube was then clamped to the base of a materials testing machine (DDL Inc., Eden Prairie, MN) using a custom made, adjustable angle, horizontal offset compensation grip (Figure 2.11). The upper grip of the materials testing machine enclosing the patellar bone was connected to a 50-lb. load-cell (MFG Inc., Scottsdale, AZ).

A hydrothermy cabin, which was connected to two circulation pumps (one for hot (70-80°C) saline circulation and the other for room temperature (22-24°C) saline circulation) enclosed the grips and the tendon sample (Figure 2.12).
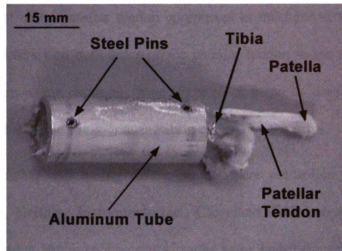
Figure 2.9: Patellar Tendon Specimen
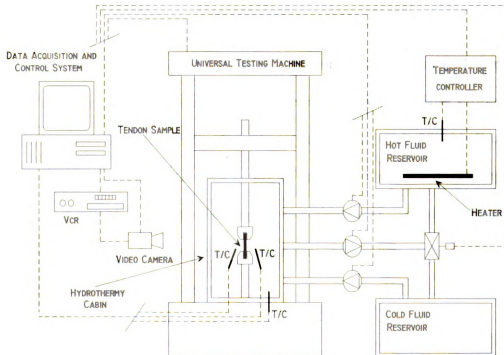
Figure 2.10: Schematic of the Experimental Setup

The objective of this setup was to apply a tensile load on the patellar tendon specimen along its anatomical axis when the tendon was immersed in saline solution. One major advantage of using patellar tendon complexes in mechanical testing was that the bones (patella and tibia) on both sides of the patellar tendon tissue facilitated gripping. This eliminated any error resulting from slippage in grips or damage created on the tendon specimen due to the stress concentration created by the grips.

The sequencing and timing of the pumps were controlled with a D/A board (DAS1802ST-DA, Keithley Instruments Inc., Cleveland, OH) connected to a PC. The load and displacement data were also routed to the same board from the materials testing machine, sampled and recorded at 8 Hz. The temperature of the saline solution was measured at 8 Hz using three T-type thermocouples connected to a thermocouple data acquisition board (DAS/TC-B, Keithley Instruments Inc., Cleveland, OH). The thermocouples were immersed into the saline circulating inside the hydrothermy cabin and were placed very close (~0.5mm) to the surface of the tendon sample at various points along the specimen's diaphysis. Finite element analysis [Aksan, et al., 2001] indicated that the temperature difference between the center of the tendon and the circulating saline solution did not exceed 4K any time during the experiments. It was therefore concluded that the thermocouple readings represented the actual temperature of the tendon sample quite well for the purpose of this research.
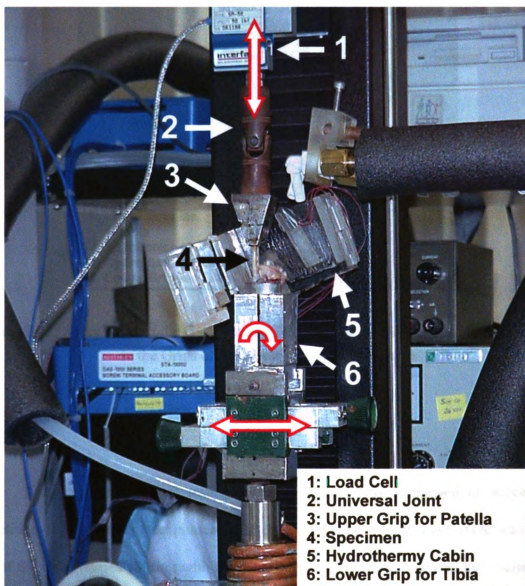
Figure 2.11: Photograph of Experimental System

One shortcoming of the experimental setup being used was that the temperatures during high temperature saline circulation increased slightly due to the non-optimum response of the temperature controller. During the course of heated saline circulation (30-50s), the temperature of the bath increased 2-2.5°C.
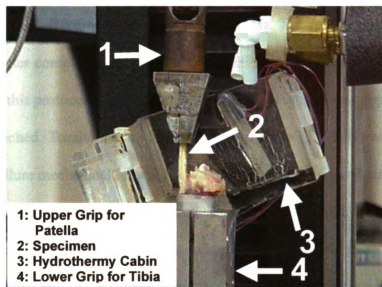
Figure 2.12: Zoom View of the Hydrothermy Bath and the Patellar Tendon Sample Fixed
to the Grips of the Materials Testing Machine

2.4.3 Experimental Protocol

The thermomechanical testing protocol applied was comprised of successive repetition of three distinct test phases, which made up one test cycle. Each cycle contained all of the three phases starting with mechanical preconditioning followed by mechanical testing and ending with thermal testing. Mechanical preconditioning was applied to minimize the viscoelastic response of the tissue [Fung, 1993; Humphrey, 2002]. Figure 2.13 shows the load history of the tendon specimen recorded during one cycle and Figure 2.14 shows the elongation/shrinkage response of the same sample during the same cycle. Therefore, the mechanical test performed in any cycle reflected the effects of the thermal and mechanical history that the specimen experienced in the previous cycles.

During the mechanical preconditioning phase, the tendon sample was subjected to sinusoidal excitations (10 times) at a frequency of 0.1 Hz. The amplitude of the excitations was 0.8 mm. After completion of sinusoidal stretching, the tendon was kept at 1.5N for 20s. Following this protocol, tensile testing at a rate of 0.05mm/s was applied until a load of 20N was reached. Tensile testing in this low load range (1.5-20N) was performed to eliminate subfailure mechanical injury. This range was considered safe since three control tendons undergoing 30 cycles of continuous experimentation did not exhibit signs of subfailure injury. Additionally, there is evidence in literature that this range (the corresponding stress and strain values) is safe for rabbit anterior cruciate ligaments, which are of similar composition [Panjabi, et al., 1996].
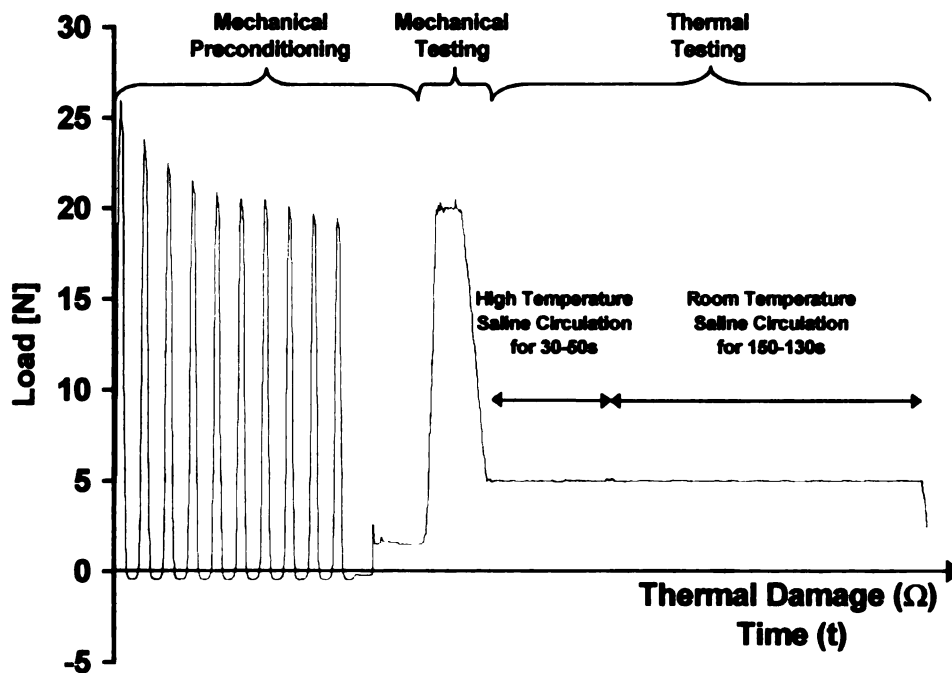
Figure 2.13: Patellar Tendon Load History in One Heating Cycle Comprised of Three Testing Phases (Mechanical Preconditioning, Mechanical Testing and Thermal Testing). *(Data is taken from Cycle #1 in Figure 2.15)*

After tensile testing was completed, the tendon was kept at 20N for 10s and then unloaded (at a rate of 0.05mm/s) to the predetermined test load (F = 2.5, 5.0, 7.5, 10.0 N). These test loads were chosen to simulate physiological loading conditions. Once the test load was reached, heated saline solution was circulated in the hydrothermy cabin for 30, 40 or 50s depending on the heating protocol applied.
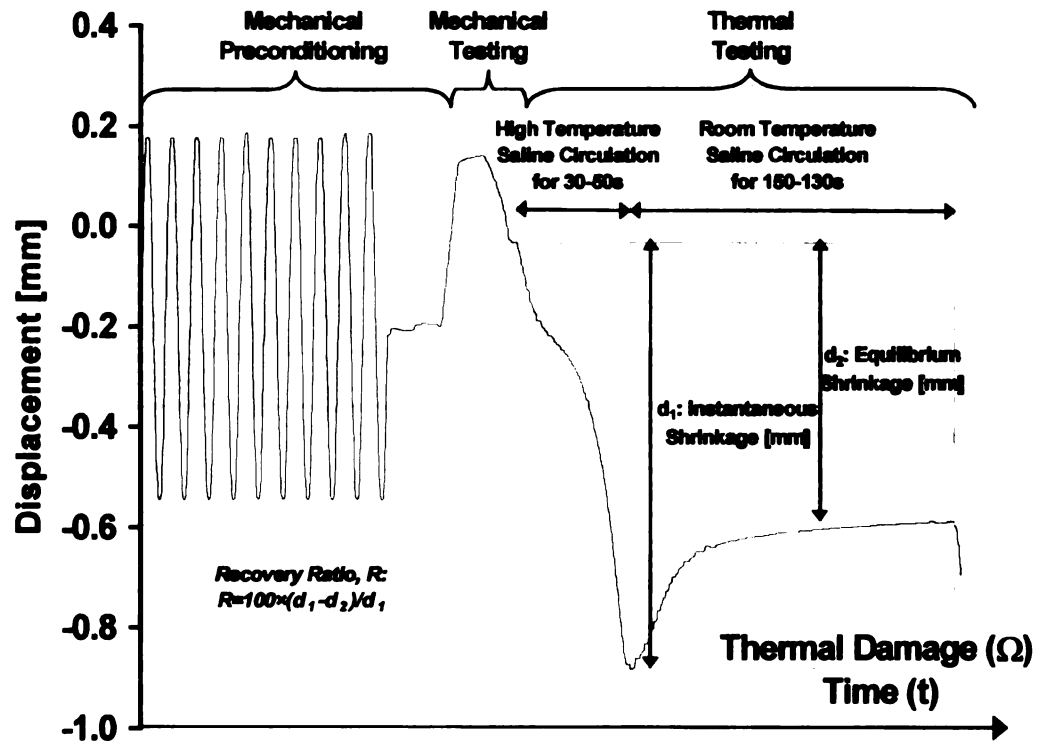
Figure 2.14: Patellar Tendon Elongation/Shrinkage History in One Heating Cycle Comprised of Three Testing Phases (Mechanical Preconditioning, Mechanical Testing and Thermal Testing). *(Data is taken from Cycle #1 in Figure 2.16)*

The total duration of the heating and cooling phases was set at 180s. During that time, the materials testing machine kept the sample at a constant load (see the load data

during thermal testing phase in Figure 2.13), and recorded the length of the sample (see the displacement data during thermal testing phase in Figure 2.14).
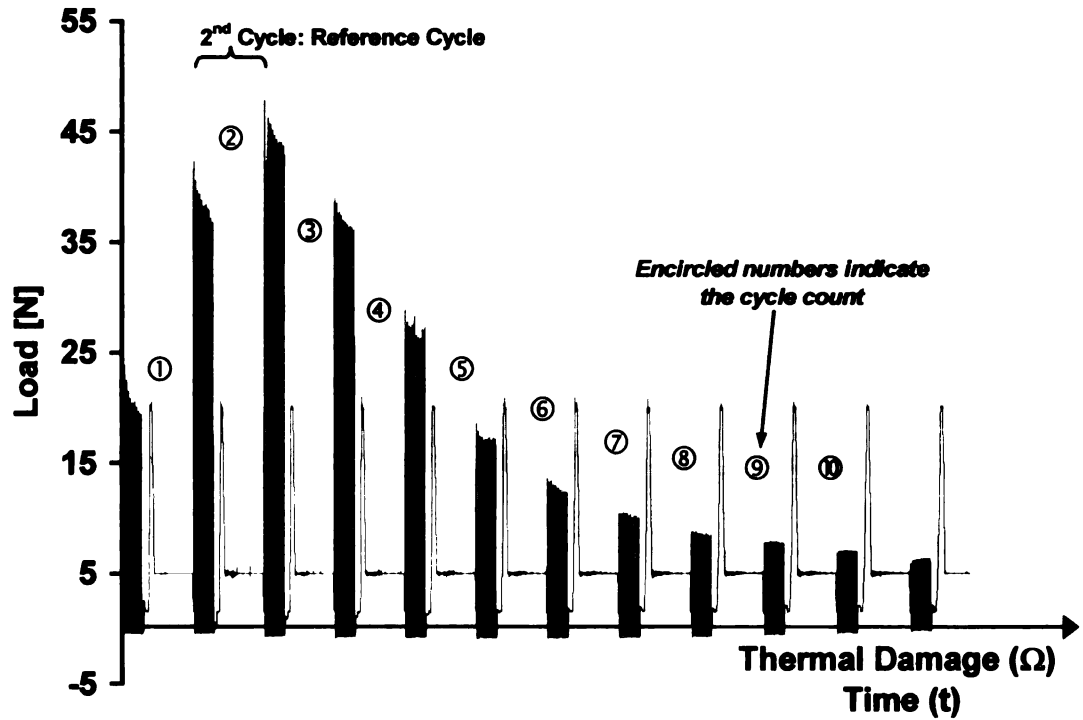
Figure 2.15: Load History of a Patellar Tendon Specimen Subjected to Successive Heating Cycles

2.4.4 Analysis Parameters

The maximum displacement recorded during the heating phase is called the instantaneous shrinkage, d_1 (Figure 2.14). After the completion of the heating phase, room temperature saline solution (22-24°C) was circulated around the specimen for (150, 140 or 130s). It was observed that during cooling, the tendon recovered slightly from its shrunken length. This is caused by re-naturation, which is due to re-winding of the partially un-

wound tropocollagen molecules [Hormann & Schlebusc, 1971]. The plateau shrinkage value reached at room temperature is called the equilibrium shrinkage, d_2 (Figure 2.14). Another important parameter defined here is the recovery ratio, R, defined as the percentage of instantaneous shrinkage recovered upon cessation of thermal stimulus. Each sample has been subjected to a number of cycles (between 20 and 30) until no change in specimen length or material properties was observed. The total number of cycles required to reach this point depended on the severity of the thermal protocol applied. The higher the saline temperature and the longer the exposure time, the fewer the number of cycles required. Finally, the test was stopped and the tendon sample was removed from the test setup, its dimensions were measured and the specimen was discarded.
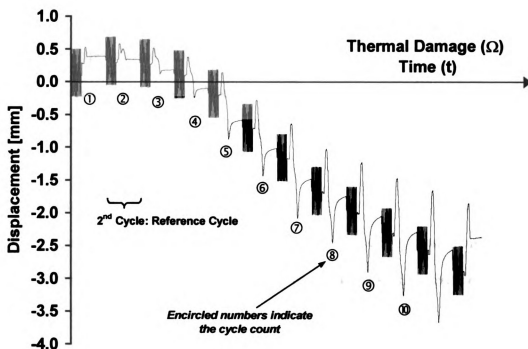
Figure 2.16: Shrinkage History of a Patellar Tendon Specimen Subjected to Successive Heating Cycles.

The tendons in the control group experienced the same mechanical history as the experimental groups but without any thermal loading. Therefore, for control experiments, at each cycle the thermal testing phase was skipped.

During the mechanical preconditioning phase, in response to sinusoidal excitation, all of the three tendons tested in the control group experienced stress relaxation. This phenomenon is revealed by the progressive decrease in the peak load measured (approximately 25% decrease between the first and the tenth peaks). This was attributed to the viscoelastic nature of the tissue (possibly due to interfibrillar slippage and displacement of unbound water within the fibers) [Woo, et al., 1981; Hubbard & Chun, 1988]. Additionally, with increasing number of cycles an increase in the average peak load measured at each cycle was detected. The cycle-to-cycle increase was significant between the first and the second cycles but then diminished.

For the experimental groups, in order to minimize viscoelastic contributions and to isolate the heat-induced response of the specimen, the experimental protocol was designed such that in the first cycle no thermal testing was applied. In Figure 2.15, the load history recorded during the course of a representative experiment (only the first 10 cycles is shown) is presented. The shrinkage/elongation response recorded during the same experiment is also given in Figure 2.16. The values for tissue length and tensile modulus obtained at the beginning of the second cycle were taken as the reference values (see Figure 2.15 and Figure 2.16).

2.5 Mechanical Response to Accumulating Thermal Damage

For the experimental groups each cycle was made up of three phases; mechanical preconditioning, tensile testing and thermal testing. It was imperative to distinguish between the two viscoelastic phenomena observed: *a)* the successive decrease in the peak load within each cycle and *b)* the cycle-to-cycle increase in the average peak loads in consecutive cycles. Adaptation of the above-mentioned experimental protocol helped minimize the effects of the latter (cycle-to-cycle variation) while the former (in-cycle variation) was still observed in the experiment data. However, with increasing thermal damage this response disappeared as well. This indicated that heat-induced denaturation inhibited the viscoelastic character of the tissue and that for the resultant amorphous state (gelatinous form), the tissue mechanical response was elastic (though still not linear). The same behavior was observed in thermomechanical analysis as well; with the accumulation of thermal damage (with increasing number of cycles), the recovery ratio, R, converged towards its plateau value of 100% ($d_1 \neq 0$ but $d_2 = 0$). This showed that for the resultant amorphous state the tissue behavior was thermoelastic; the tissue returned to its previous mechanical state upon cessation of thermal stimulus without further permanent shrinkage or change in its mechanical properties.

For all of the samples tested, the resultant effect of the thermal damage accumulation was shrinkage in the dominant direction of fiber orientation (along the length of the tendon). However, each specimen went through distinct shrinkage (accumulated d_2) regimes before reaching its respective final state. The final state was reached quickly if the thermal damage accumulation in each cycle was accelerated by

either increasing the temperature of the circulated saline solution or the exposure time. On the contrary, if the thermal damage accumulation in each cycle was kept to a minimum by decreasing the temperature of the saline solution or decreasing the exposure time, an interesting regime in tendon response (one not easily observed in accelerated denaturation experiments) became apparent (Figure 2.17).
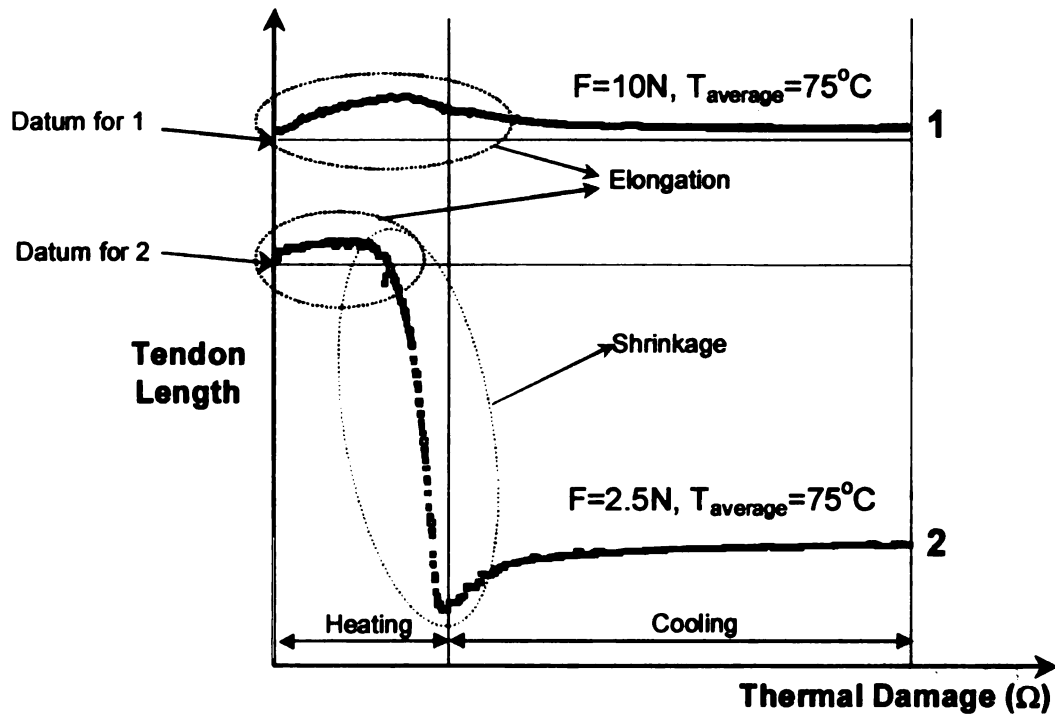
Figure 2.17: Heat-Induced Elongation and Shrinkage *(Effect of Test Load on Heat-Induced Response)*

This regime corresponded to an initial elongation response just before the onset of shrinkage and was characterized by a gradual increase in sample length corresponding to approximately 0.5% strain (Tendon Sample 1 (F=10N) in Figure 2.17). This was accompanied by a significant increase in tensile modulus (up to 125% that of the native tendon). The tensile modulus was determined from the slope of the stress-strain curve at

σ=1MPa (when the tensile moduli was determined at different stress values and normalized with respect to the values at the native state, similar trends were observed). The elongation response observed in this regime was purely heat-induced and irreversible. Once a certain amount of energy was absorbed, the specimen would start to shrink with further heating (Tendon Sample 2 (F=2.5N) in Figure 2.17). Even if the experiment was paused after the elongation stopped and the tendon was returned back to rest in room temperature saline solution (tests done for up to 1 hour), and then reheated, it continued to shrink with further heating without elongating further. Note that the temperatures and the exposure times (therefore the Arrhenius damage integral values) were identical for both of the specimens even though the test load was different.
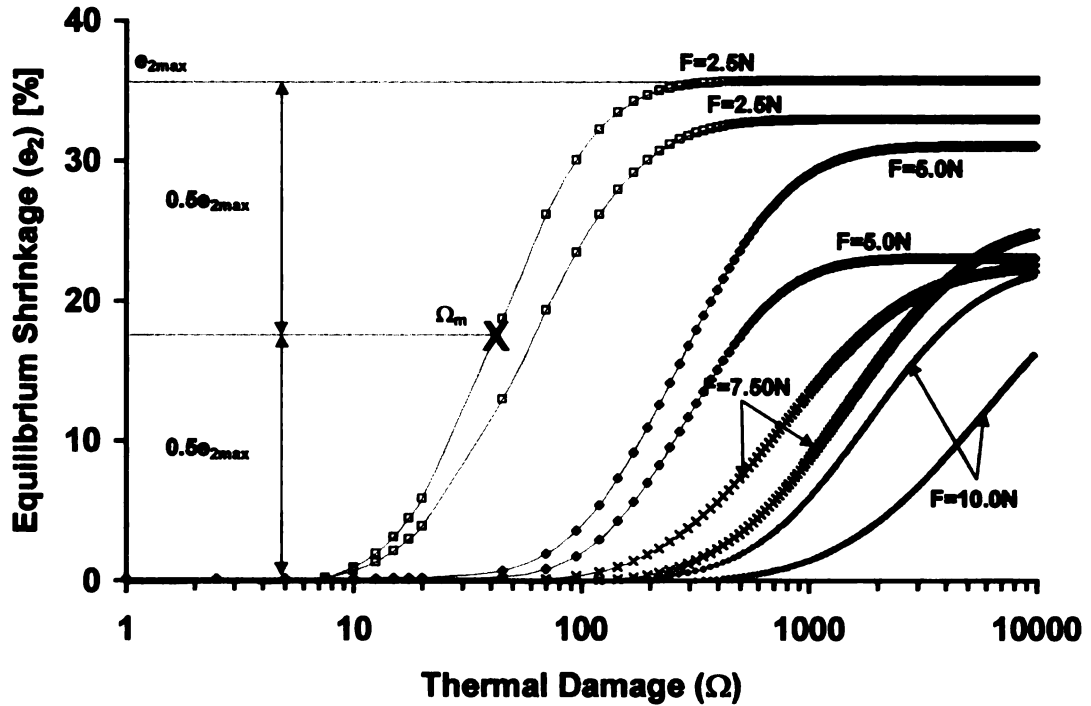
Figure 2.18: Progression of Equilibrium Shrinkage (e_2) with Accumulated Thermal Damage (Ω) at Different Test Loads (F).

Once the initial elongation regime was completed, the overall instantaneous shrinkage (calculated by summing the d_1 values measured at consecutive cycles) of every specimen increased exponentially with accumulated thermal damage. However, after a rapid increase, the recovery ratio converged to its plateau value of 100%. Irrespective of the test load applied, the overall equilibrium shrinkage varied in a sigmoidal fashion with increasing thermal damage (Figure 2.18).

The permanent (equilibrium) shrinkage of the tendon did not increase indefinitely but was bounded. Briefly, the heat-induced thermomechanical response of the patellar tendon composed of three distinct regimes determined by the changes in its length and tensile modulus (examined in the next section). These regimes were:

1. Irreversible Elongation: Elongation up to 0.5% strain accompanied by an increase in tensile modulus (E ~ 125% of the native tendon calculated at the reference state).

2. Irreversible Shrinkage: Decrease in the overall length of the sample in the dominant direction of fiber orientation accompanied by an exponential decrease in tensile modulus (with respect to the native value) and disappearance of viscoelastic response.

3. Reversible Shrinkage: Defined by thermoelastic response where shrinkage was completely reversible. Upon returning to room temperature, the tissue regained its pre-heating length (which was the length at the beginning of the cycle, not the experiment) as also shown by *R*, converging to 100% with increasing thermal damage, Ω In this regime, There was no decrease in tensile modulus with further heating.

2.6 Empirical Correlations

2.6.1 Equilibrium Shrinkage (e_2) and Thermal Damage (Ω)

The mechanical load plays a very important role in determining the denaturation kinetics and the final state of the tissue. Experimental results revealed that increased test load *delayed* the shrinkage of the tendon sample, as indicated below in Figure 2.19. With increasing load, the sigmoidal equilibrium shrinkage curve shifted towards higher thermal damage. Ω_m is defined as the thermal damage accumulated in the tendon specimen where 50% equilibrium shrinkage is reached. When the variation of Ω_m with stress, σ, is plotted (for all of the samples tested, n=9) it was observed that there was a direct correlation between the stress applied on the tissue and the denaturation midpoint (Figure 2.19). An exponential curve fit (R^2=0.9593) gives this correlation as:

$$\Omega_m = 5.7027e^{7.9899\sigma} \qquad \qquad \textbf{2.8}$$

As discussed previously in the *Introduction* part of this thesis, for a stress-free patellar tendon specimen the denaturation rate was maximum at Ω=1 and the tissue was completely denatured at Ω=10. The intercept of the function given in Equation 2.8 with σ=0, gives Ω_m=5.7027, which was well within the limits determined by the DSC studies given above. The reason for transition retardation is a decrease in the activation entropy of denaturation [Miles & Ghelashvili, 1999].
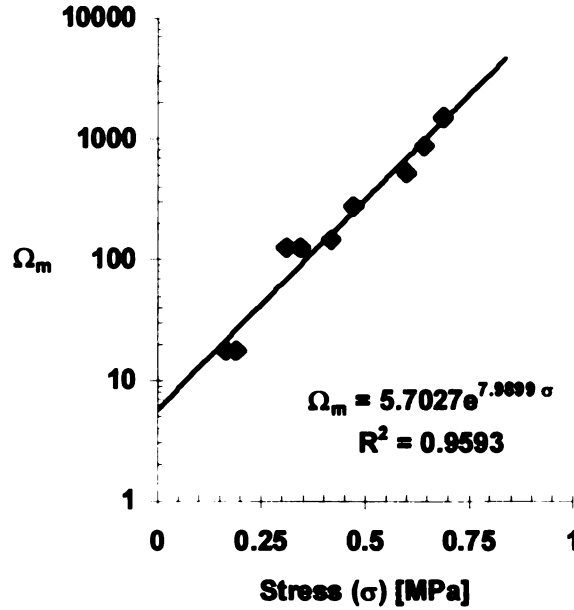
Figure 2.19: Variation of Ω_m as a Function of Test Stress, σ, $(\sigma = F/A^*)$.

Another question that needs to be answered is whether the applied stress has an effect on the amount of final shrinkage achieved. When the maximum shrinkage each specimen experienced when it was fully denatured was plotted as a function of the test stress applied on the tissue during denaturation (Figure 2.20), a significant reduction with increasing test load was observed (n=9). The larger the stress on the tissue during heating, the less the final shrinkage. This relationship was given as:

$$e_{2max} = -10.728 \cdot \ln\sigma + 15.752 . \qquad\qquad 2.9$$

To explain this behavior, the following hypotheses are offered: when tropocollagen molecules unwind by heat-induced denaturation, they exert tensile forces on the

neighboring molecules through heat resistant intermolecular cross-links (this is the mechanism of gross tissue shrinkage). Meanwhile, the strength of the molecules also decreases (due to losing intramolecular heat-labile bonds). When the point is reached where the local thermomechanical stress is greater than the yield stress (or tensile strength) of the weakened molecule, the molecule plastically deforms (or ruptures). The elastic energy of the molecule dissipates and the overall thermal stress decreases causing a lower overall shrinkage. This hypothesis also explains the degradation of the mechanical properties (decrease in the resistance to deformation).
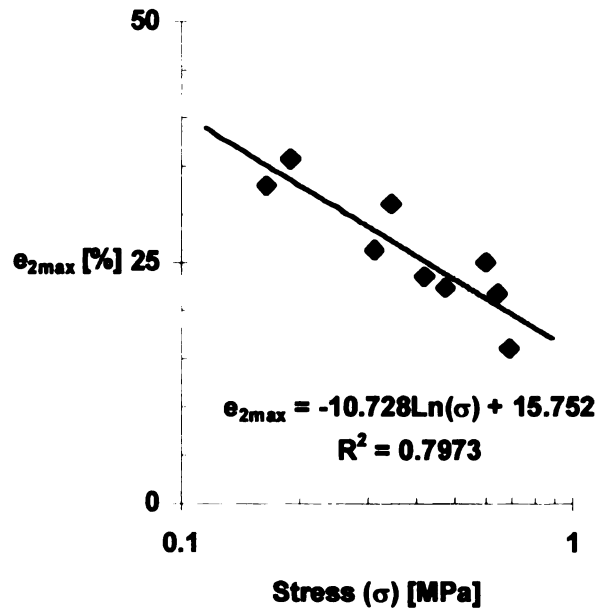
Figure 2.20: Variation of Maximum Equilibrium Shrinkage (e_{2max}) as a Function of Test Stress, σ, ($\sigma = F/A_0$).

When the data presented in Figure 2.18 were modified by dividing the equilibrium shrinkage by the shrinkage plateau value, (e_2/e_{2max}) and the accumulated thermal damage

was normalized (Ω/Ω_m), all of the heating protocols converge on the same master shrinkage curve (Figure 2.21). The correlation between the damage parameter (Ω/Ω_m) and the resultant nondimensional shrinkage may be represented by a dose response ($R^2=0.9875$) given by:

$$\frac{e_2}{e_{2max}} = -0.005 + \frac{0.9965}{1 + \left[\dfrac{\Omega/\Omega_m}{2.24}\right]^{-1.97}}$$

2.10

As seen in Figure 2.21, irrespective of the stress-state of the tissue, once it starts, shrinkage progresses rapidly and then converges to a final value.
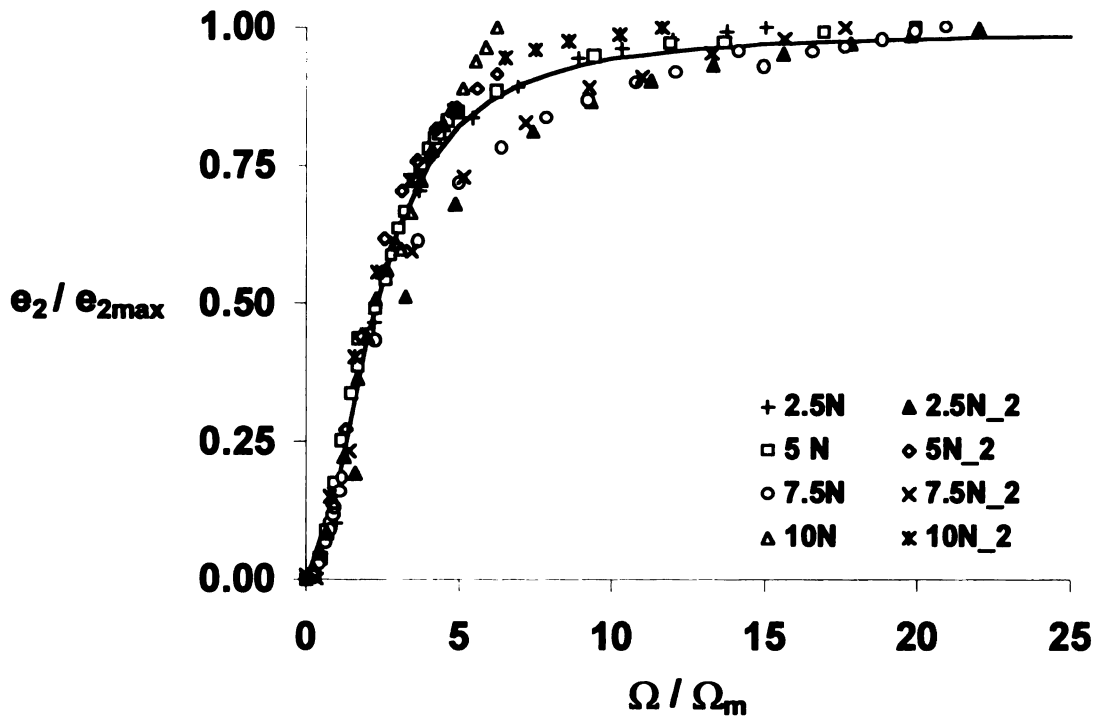
Figure 2.21: Master Curve for Heat-Induced Shrinkage of Rabbit Patellar Tendon (for $2.5 \leq F \leq 10.0N$)

2.6.2 Normalized Tensile Modulus (E/E_0) and Thermal Damage (Ω)

Irrespective of the thermal and mechanical history of the specimen, during tensile testing (in the load range the test was performed: 1.5-20N) the mechanical stress, σ, varied exponentially ($R^2 > 0.999$) with the applied strain, ε:

$$\sigma = C_1 + C_2 e^{C_3/\varepsilon}$$

2.11

In the equation above, C_1, C_2 and C_3 are functions of the thermal damage, Ω accumulated before the onset of the particular tensile test. In Figure 2.22 the effect of accumulating thermal damage on the tensile behavior of a representative tendon specimen is given. As shown, the tendon became more compliant with accumulated thermal damage.
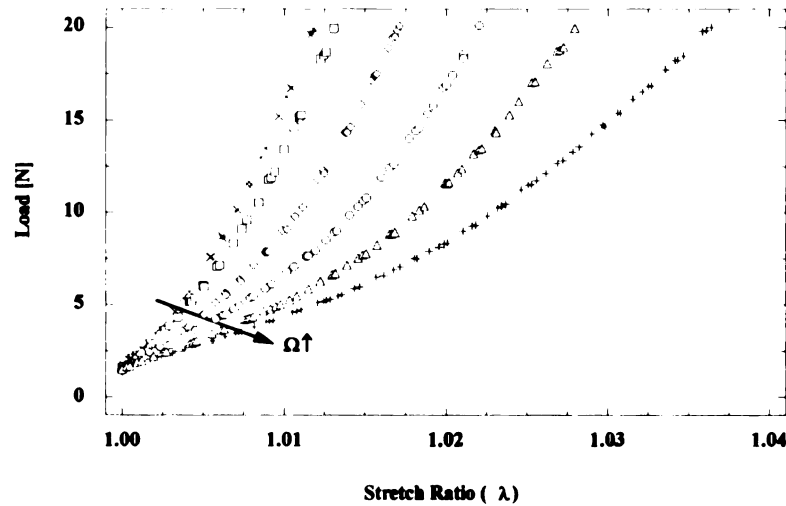
Figure 2.22: Effect of the Accumulating Thermal Damage, Ω on the Stretch-Load Response of a Representative Tendon Specimen. *(Test Load=5N, Bath Temperature=75°C, Exposure Increment=30s)*

The three distinct regimes observed in the shrinkage analysis reflected on the mechanical properties as well. The irreversible elongation regime corresponded to an increase in tangent modulus (up to 125% of the reference state). During the irreversible shrinkage regime, with each additional heating cycle, a progressively lower stress value corresponded to the imposed strain, indicating a decrease in tangent modulus. In the reversible shrinkage regime, a plateau value for tangent modulus was reached. The one-to-one correspondence between the shrinkage behavior and mechanical state indicated that the mechanism responsible for shrinkage and mechanical property degradation was the same.
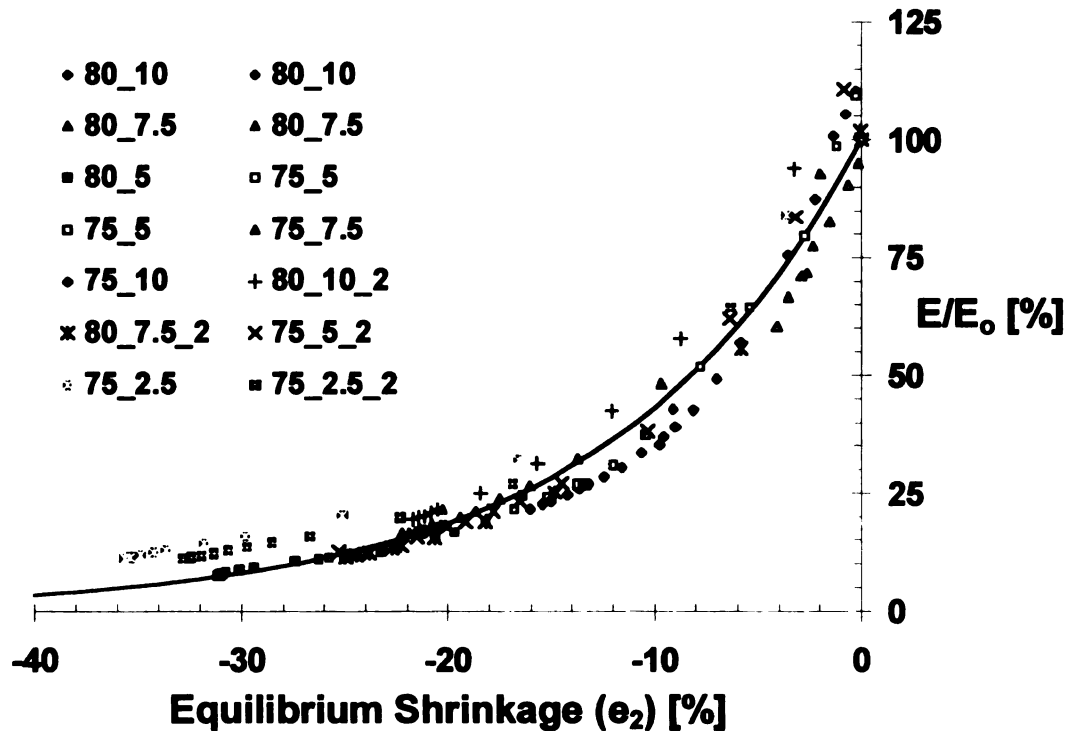
Figure 2.23: Master Curve for the Variation of Normalized Tensile Modulus (E/E_0) with Equilibrium Shrinkage (e_2). (Both E and E_0 are the Tangent Moduli Calculated at 1MPa)

The variation of tangent modulus, E, with thermal damage at different stress values ($\sigma=0$, 0.5, 1 MPa) was calculated and the same trend was observed. In Figure 2.23, the tangent modulus calculated at 1MPa is plotted as a function of equilibrium shrinkage achieved.

One very important observation made here was that the mechanical properties of the tissue degraded exponentially with shrinkage. Behavior similar to that for shrinkage was observed if the decrease of the tensile modulus at any given stress was plotted for each test load as a function of the thermal history of the specimen. Such a representation revealed that the decrease in the tensile modulus at a higher test stress was more prominent with each incremental heating. Once shrinkage started, the variation of normalized tensile modulus as a function of equilibrium shrinkage could be represented as ($R^2=0.975$):

$$\frac{E}{E_o} = 100.01 e^{e_2/11.893}$$ **2.12**

Briefly, the equilibrium shrinkage increased with the accumulated thermal damage while the tensile modulus decreased. As mentioned before, these observations pointed to the existance of a mechanical optimum in terms of the thermal stress formed in the tissue. It was reasonable to choose the thermal stress as the parameter to be maximized during heating since it was the main driving force determining the final configuration and state of the heat-treated tissue. As a first order approximation, the tissue response was assumed to be governed by the Hooke's Law, and that the thermal stress, σ_{th}, formed in the uniformly

heated tissue, as a result of sub-ablative heating, was determined by the product of the equilibrium shrinkage and the tensile modulus.

Below, the variation of the thermal stress with the achieved equilibrium shrinkage is presented (Figure 2.24). From a purely mechanistic standpoint, there was an optimum final state (corresponding to approximately 12% shrinkage where the thermal stress formed in the tissue was maximum) that can be reached. Beyond this point, the thermal stress started to decrease since the material became excessively compliant with additional heating and therefore, the mechanical stability reduced. At the point where the thermal stress reached its maximum, the uniformly heated tissue was at its optimum state; both mechanically and kinematically stable.
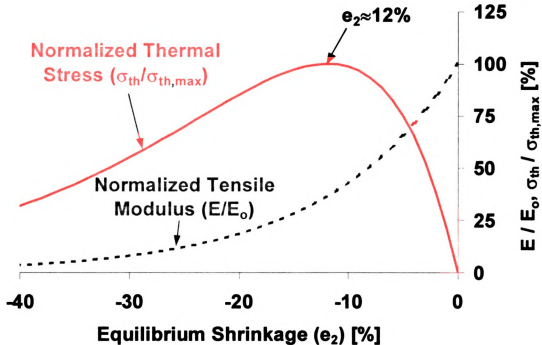
Figure 2.24: Variation of Thermal Stress with Equilibrium Shrinkage

Chapter 3: Thermal Exposure Simulations for Thermotherapy

A sub-ablative level of thermal damage produced in collagenous tissues is known to be the result of micro-scale structural changes driven by the helix-coil transition of the collagen molecules. When heat is applied, this highly oriented parallel structure transforms to an amorphous, randomly coiled state (denaturation) since the tropocollagen molecules lose the harness of their heat-labile intramolecular bonds. The effect of denaturation in the macro scale is tissue shrinkage. For tendon collagen, this phenomenon is observed at temperatures in excess of 62°C. In the sub-ablative heating levels, the non-thermal effects of the heating modalities are insignificant. It is hypothesized here that different heating modalities (laser, monopolar and bipolar radiofrequency), owing to the variations in their modes of action, create significantly different temperature distributions and thermal histories within the tissue. It is felt that this fact alone contributes prominently to the variations in the results reported in the literature related to the outcome of the therapy. Therefore, an effort has been made here to simulate the various heating conditions in a virtual environment to examine the effects of different clinical parameters of interest. These parameters are: heating modality, heating probe power setting, probe sweep speed and the influence of arthroscopic fluid circulation.

A finite element method-based simulation tool was therefore utilized to predict the temperature distributions and thermal damage gradients for different heating conditions.

3.1 Modeling the Temperature Distributions Created by Thermotherapy

The conservation of energy equation in a two-dimensional, Cartesian coordinate system (x, y) for a homogeneous, isotropic material is:

$$k\frac{\partial}{\partial x}T(x, y, t) + k\frac{\partial}{\partial y}T(x, y, t) + g(x, y, t) = \rho c\frac{\partial}{\partial t}T(x, y, t) \qquad \textbf{3.1}$$

T, t, k, g, ρ, c are the temperature, time, thermal conductivity, spatially varying volumetric heat generation, mass density and specific heat, respectively. If the material is also undergoing phase change, the thermal inertia term on the right hand side of Eqn. 3.1 should be modified to account for the latent heat effects. Introducing the definition of apparent specific heat, c_a,

$$c_a = c + \frac{\partial \Lambda}{\partial T} \qquad \textbf{3.2}$$

in terms of the latent heat of phase change, Λ, it can be shown that Equation 3.1 can be written as,

$$k\frac{\partial}{\partial x}T(x, y, t) + k\frac{\partial}{\partial y}T(x, y, t) + g(x, y, t) = \rho c_a\frac{\partial}{\partial t}T(x, y, t) \qquad \textbf{3.3}$$

where the effect of collagen denaturation, modeled as a solid-to-solid phase change (helix-to-coil transition) is incorporated in the specific heat term.

The solution to the governing equations for each heating modality was obtained using commercial finite element analysis (FEA) software (MSC.Marc Mentat®, MSC Software Corporation, Los Angeles, CA) on a UNIX® platform using a Sun Enterprise 250 compute server with two 296 MHz UltraSPARC-II processors (Sun Microsystems, Inc., Palo Alto, CA). Two user subroutines were incorporated into the main FEA code (see Appendix C for details). One of the subroutines was used to impose spatially and temporally varying heat flux and generation and the other one was used to calculate the thermal damage accumulation.

The control volume (CV) used in these simulations was two-dimensional Cartesian, homogeneous and isotropic (Figure 3.1). The dimensions were, 10 mm in the horizontal direction, x, and 2 mm in the vertical direction, y. The CV was uniformly divided into 50000 rectangular elements with an internode distance of 20μm.
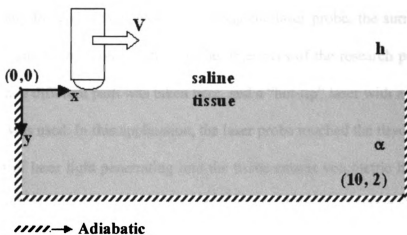
Figure 3.1: The Control Volume for FEA

61

3.1.1 Overview of Clinically Applied Heating Modalities

The heating modalities are discussed below.

3.1.1.1 Ho:YAG Laser Heating

In the simulations of laser heating, the photon energy deposition on the surface was assumed to be a Gaussian pattern with an exponential decay into the tissue following Beer's absorption law [Welch, 1985]. "Cold-tip" lasers are used frequently to shrink collagenous tissues without causing ablation [Schaefer et al., 1997] (Figure 3.2, Probe #3). The term "cold-tip" refers to an application where the laser probe is kept 1-2 mm away from the surface of the target tissue. Owing to the short penetration depth of the Ho:YAG laser (~300 μm), and the practice of keeping the laser tip 1-2 mm away from the surface, it is reasonable to assume that in this application, the laser has no direct thermal effect on the tissue other than heating the surrounding fluid.

Modeling the complex interactions among the laser probe, the surrounding fluid and the tissue was far too complicated for the objectives of the research presented here. For this reason, a different path was taken here, and a "hot-tip" laser with a slightly lower power setting was used. In this application, the laser probe touched the tissue surface. The thermal effect of laser light penetrating into the tissue causes volumetric heat generation [Welch, 1985]. If the light is assumed to be absorbed by the tissue without scattering, then the volumetric heat generation is expressed as:

$$g(x, y) = \phi(t) \cdot \mu_a E_o \cdot e^{(-(2x^2)/r_o^2)} \cdot e^{(-\mu_a y)} \qquad\qquad 3.4$$

where, $\phi(t)$ is a window function used to represent the pulsating nature of the laser. This function gives the value of one during a pulse and zero elsewhere. E_o, μ_a and r_o are the peak irradiance on the surface, absorption coefficient and (1/e) radius of the Gaussian beam profile, respectively. The motion of the probe on the surface at constant velocity, V, was established by replacing the variable x with the transformed variable (x-Vt). The boundary condition at the free surface was expressed as:

$$\frac{\partial}{\partial y}T(x, y, t)\Big|_{y=0} + \frac{h}{k}(x, y, t)\Big|_{y=0} = \frac{h}{k}T_\infty \qquad\qquad 3.5$$

whereas all the other boundaries were assumed to be adiabatic. The validity of the adiabatic boundary assumption was checked against the results later. T_∞ is the surrounding arthroscopic fluid temperature and is assumed to be constant at 37°C~310 K at all times. It is also assumed that before heating starts, the tissue is also at the deep core body temperature of 310K. Therefore the initial condition was established as:

$$T(x, y, t)\Big|_{t=0} = T_i = 310K \qquad\qquad 3.6$$

3.1.1.2 Bipolar Radiofrequency Heating

The bipolar radiofrequency method uses a saline-based arthroscopic cooling solution to establish electrical contact between the active and the passive electrodes placed on the body of the heating probe [Nath et al., 1994] (Figure 3.2, Insert 2).

1: Bipolar Radiofrequency Probe:
   Arthrocare Arthrowand, 3mm CAPSure

2: Monopolar Radiofrequency Probe:
   Oratec Vulcan TAC-S Electrothermal Probe

3: Ho:YAG Laser Probe:
   Trimedyne OmniTip Model 20474-HP

4: Ground Plate for Monopolar Radiofrequency
   Probe: (sized for in-vitro experimentation)
   Oratec
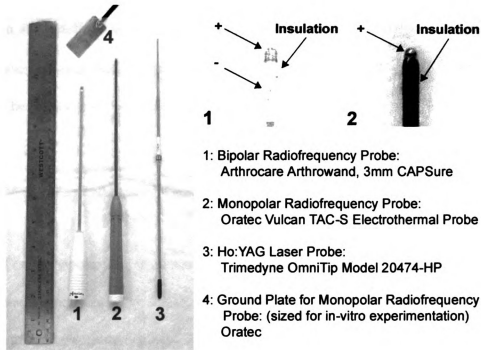
Figure 3.2: Probes used in HACS procedures

The mode of action of this method is that of heating the arthroscopic liquid in the immediate vicinity of the tissue instead of directly heating the tissue itself. Therefore, it was hypothesized that tissue heating with a bipolar probe was mainly a surface heat transfer phenomenon that could be modeled as a Gaussian surface flux on the upper boundary of the CV as:

$$\frac{\partial}{\partial y} T(x, y, t)\big|_{y=0} = \frac{q''}{k} e^{-(2x^2)/r_o^2} \text{ where } (|x| \leq r_o) \qquad 3.7$$

$$\frac{\partial}{\partial y} T(x, y, t)\big|_{y=0} + \frac{h}{k} T(x, y, t)\big|_{y=0} = \frac{h}{k} T_\infty \text{ where } (|x| > r_o) \qquad 3.8$$

such that there was no volumetric heat generation within the tissue. The heat flux, q'', in Equation 3.7 is defined as the magnitude of the surface heat flux and r_o is the $(1/e)$ radius of the Gaussian distribution. The other boundary conditions and the initial condition were taken to be identical to those of the laser heating case.

3.1.1.3 Monopolar Radiofrequency Heating

For monopolar radiofrequency heating, frequencies between 300kHz and 1MHz are applied through an active electrode [Penascu et al., 1995] (Figure 3.2, Insert #2). The passive, ground electrode is placed on the skin surface (Figure 3.2, Number 4). The tissue in the vicinity of the active probe is heated volumetrically by the Joule effect [Shitzer, 1985]:

$$g(x, y) = \frac{P \cdot r_o}{4\pi(x^2 + y^2)^2} \text{ for } \sqrt{(x^2 + y^2)} \geq r_o \qquad \textbf{3.9}$$

$$\frac{\partial}{\partial y}T(x, y, t)\big|_{y=0} + \frac{h}{k}T(x, y, t)\big|_{y=0} = \frac{h}{k}T_\infty \qquad \textbf{3.10}$$

where P is the Joule heat produced by the electrical current passing through the tissue and r_o is the probe diameter. In modeling this heating modality, the interactions between the probe and the surrounding liquid were neglected. The other boundary conditions and the initial condition were taken to be identical to those of the laser heating case.

3.1.2 Hydrothermy

During hydrothermal heating, the tissue was completely immersed in a saline bath and the saline temperature was increased. Even though this method is not suitable for clinical applications, it is the method of choice in most in-vitro experiments because of the simplicity of its application. The surface heat transfer phenomena is governed by:

$$\frac{\partial}{\partial y}T(x, y, t)\Big|_{y=0} + \frac{h}{k}T(x, y, t)\Big|_{y=0} = \frac{h}{k}T_{\infty} \qquad \textbf{3.11}$$

where the circulating saline temperature, T_{∞}, took a constant value for each simulation in the range from 62 to 90°C.

3.1.3 Finite Element Analysis

The control volume (CV) used in these simulations is shown in Figure 3.1. For the radiofrequency heating cases, a constant time increment of 0.05s was used. For laser heating cases an adaptive variable scheme utilizing a time increment of 0.00005s during the pulses and 0.01995s between the pulses was employed. This was done to ensure that the temperature change between consecutive time increments was not more than 0.25K. The stability of the solutions was ensured by checking the time increment and mesh size values used against the stability criteria established by the software publisher. The singularity ratio of the mass matrix was recorded at each time increment and checked against the dependability range given by the software manufacturer. The sensitivity of the

66

solution to mesh size was also analyzed and the same optimum mesh was used throughout the simulations.

In this analysis, all of the material properties except the apparent specific heat were assumed to be isotropic and temperature independent. The cases simulated included stationary and moving probes as well as different energy deposition magnitudes.

The mesh for the rectangular control volume was created automatically using the mesh generation interface of the FEA software utilized. For this geometry, rectangular elements of equal size were generated. Control simulations utilizing triangular elements were performed and compared to rectangular element simulations. No difference in the results was observed. Due to the finite difference approximation used when calculating the time increments, in the transient heat transfer analysis algorithm, stability and convergence of the solution became issues. In order to ensure convergence of the solution, the following condition should be satisfied:

$$\Delta t \geq \frac{\rho c}{6k}(\Delta l)^2 \qquad\qquad 3.12$$

where Δt, Δl, ρ, c, k are the time increment, internode distance where the higest temperature gradients are expected, mass density, specific heat and thermal conductivity, respectively.

Depending on the heating modality simulated, the solutions for 2-D simulations took approximately 2-8 hours (8 hours was for the laser heating case) on a Sun Enterprise 250 compute server with two 296 MHz UltraSPARC-II processors. For each one of the 3-D simulations however, ther run time was approximately 10 days.

3.2 Temperature Distribution Results

3.2.1 Temperature Field on the Surface of the Control Volume

The temperature distributions predicted in each simulation were closely monitored and attention was focused on choosing low enough values for the power settings such that a temperature of 100°C was not exceeded either on the surface or inside the control volume. This was done to ensure that latent heat effects from water evaporation or tissue ablation were not significant when compared to the collagen phase change energy levels.

Table 3.1: Values Used in Simulations

Variable	Explanation	Value Range
E_o [W/m^2]	Laser Peak Irradiance	0.75×10^6-1.75×10^6
r_o [m]	1/e Radius of Gaussian Profile	0.5×10^{-3}-2.0×10^{-3}
V [m/s]	Probe Sweep Speed	$0, 2 \times 10^{-3}, 4 \times 10^{-3}$
q'' [W/m^2]	Surface Heat Flux (Bipolar)	0.75×10^5-1.5×10^5
P [W]	Joule Heat (Monopolar)	5.0-12.5
f [Hz]	Laser Pulse Frequency	5
μ_a [1/m]	Absorption Coefficient	1×10^4
h [W/m^{2}K]	Convection Coefficient	$5 \times 10^1, 5 \times 10^2$
λ_s [ms]	Laser Pulse Width	200

Simulations for four different heating modalities namely, Ho:YAG laser, bipolar and monopolar radiofrequency and hydrothermy were considered. Temperature and thermal damage distributions created with each heating modality were determined for two

ve

me

dec

sig

by

different convection coefficients, two different velocities and a stationary case. The values used in the simulations were taken from the literature for the clinical application of respective modalities (Table 3.1 on page 68). Depending on the modality 4-5 different power settings were simulated.

The graph shows temperature T [K] on the y-axis (ranging from 300 to 380) versus x [m] on the x-axis (ranging from 0.0E+00 to 3.5E-03). The legend indicates:

- $q''\text{max} = 1.0E+05$
- $q''\text{max} = 7.5E+04$
- $q''\text{max} = 5.0E+04$
- $P = 7.5E+00$
- $P = 5.0E+00$
- $P = 6.125E+00$
- $E_{omax} = 5.0E+05$
- $E_{omax} = 2.5E+05$
- $E_{omax} = 7.5E+05$
- $E_{omax} = 1.0E+06$

with $h = 50 \ W/m^2 K$ and $V = 0$.
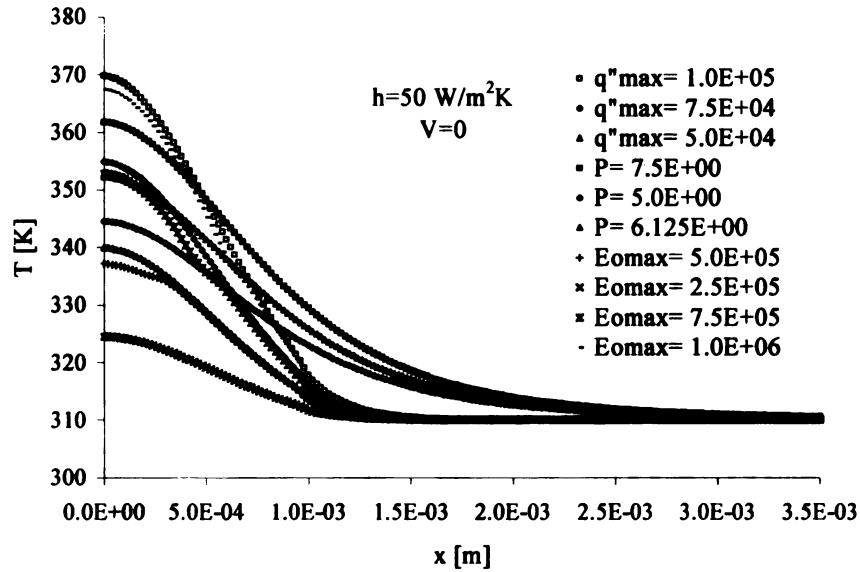
Figure 3.3: The Temperature Distribution Created on the Surface of the CV by a Stationary Heating Probe (V=0). *(Convection Coefficient, h=50W/m²K).*

From the predictions obtained, it was observed that with increasing probe sweep velocity, the temperature field tended to get narrower. Additionally, when the probe was moved, for the same power settings, the maximum temperatures reached in the tissue decreased significantly. Owing to the differences among their modes of action, there were significant differences among the temperature profiles created at the surface of the tissue by the different heating modalities. This is demonstrated in Figure 3.3 for the case of

h=50W/m^{2}K when the heating probes were kept stationary at the origin. In Figures 3.4 and 3.5, the surface temperature distributions created by moving probes (at V=2mm/s and V=4mm/s, respectively) are shown for the three different modalities. In each case, the probe was swept from left to right and the temperature distribution inside the CV at t=4 seconds were simulated. For both cases, the convection coefficient, h, was taken as 50W/m^{2}K.
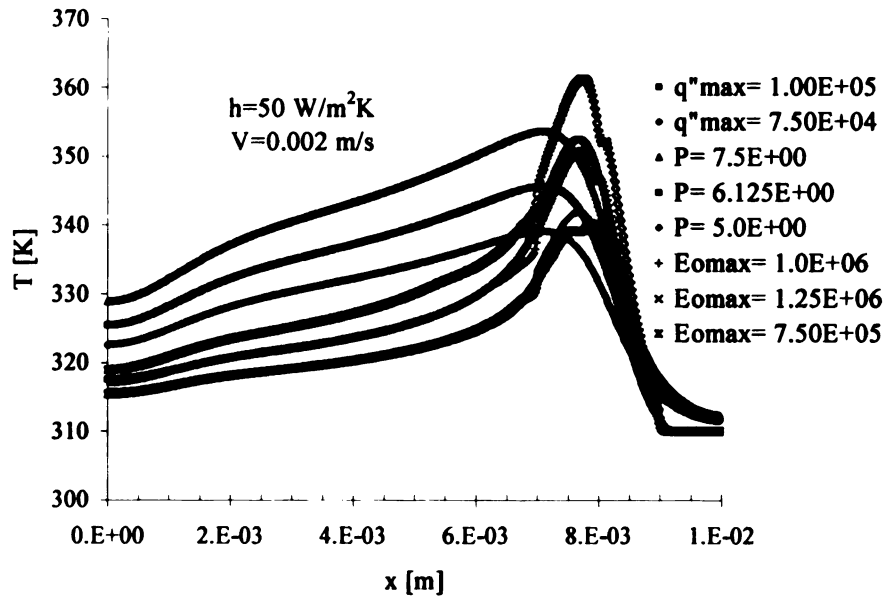
Figure 3.4: The Temperature Distribution Created on the Surface of the CV by a Moving Probe (V=0.002m/s). *(Convection Coefficient, h=50W/m^{2}K). (The probe was located at x=8.0E-03 m and moved to the right at a speed of 2mm/s).*
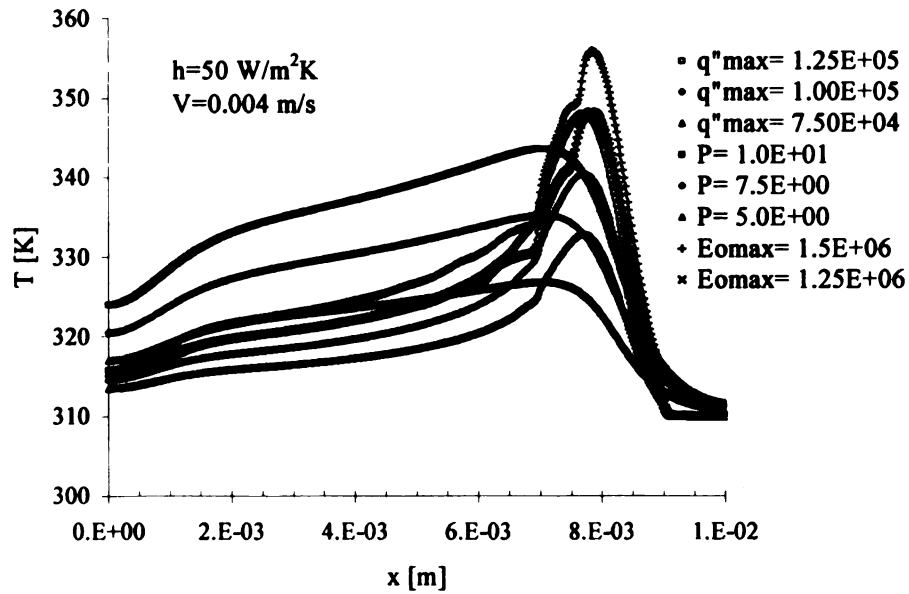
Figure 3.5: The Temperature Distribution Created on the Surface of the CV by a Moving Probe (V=0.004m/s). *(Convection Coefficient, h=50W/m²K). (The probe was located at x=8.0E-03 m and moved to the right at a speed of 4mm/s).*

3.2.2 Temperature Field within the Control Volume

In the simulations presented below (Figure 3.6), the temperature scales are taken to be identical. It was observed that the temperature distributions created by bipolar and laser heating were distinctly different from that of the monopolar heating. Upon inspection of the temperature distributions near the surface, it was detected that the temperature gradients produced by the laser heating were steeper than those of the bipolar heating Also, because of the pulsating behavior of the laser, a series of hot spots were observed near the surface.

310 K (37°C)   360 K (87°C)   Bipolar
                                                $q"_{max}$ = 1.25E+5 W/m^2
                                                ω = 1 mm

310 K (37°C)   360 K (87°C)   Ho:YAG Laser
                                                E_{omax} = 1.25E+6 W/m^2
                                                ω = 1 mm, f = 5Hz

310 K (37°C)   360 K (87°C)   Monopolar
                                                P = 10 W/m^3
                                                r_o = 1 mm
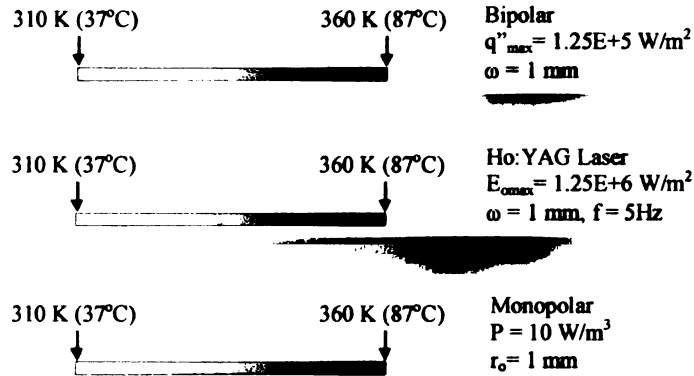
Figure 3.6: Temperature Distributions at t=4s

Among the three modalities examined, the monopolar radiofrequency heating

created the most uniform heating patterns. It is also important to note that the thermal

penetration of this modality is very high when compared to others (see Figures 3.7, 3.8

and 3.9). Since it is mainly a surface phenomenon, bipolar heating created a heated region

near the surface, similar to that of laser. On the other hand the temperatures decreased

gradually from the surface into the tissue. The gradients created were not as sharp as the

ones created by the laser. The temperature distributions predicted and the observations

made from the simulations were in agreement with the published reports [Glen, et al.,

1996].
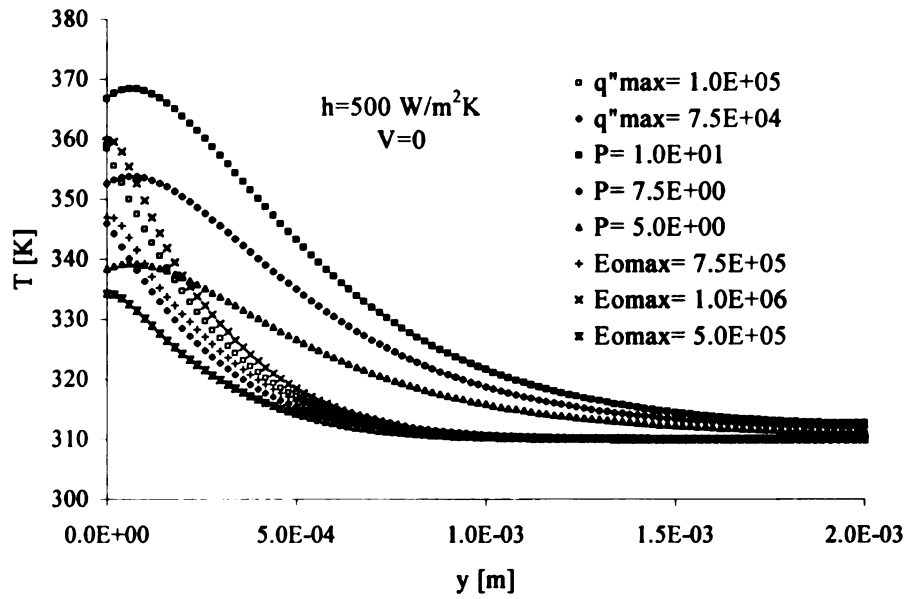
Figure 3.7: The Temperature Distribution Created within the CV by a Stationary Heating Probe (V=0). *(Convection Coefficient, h=500W/m²K)*
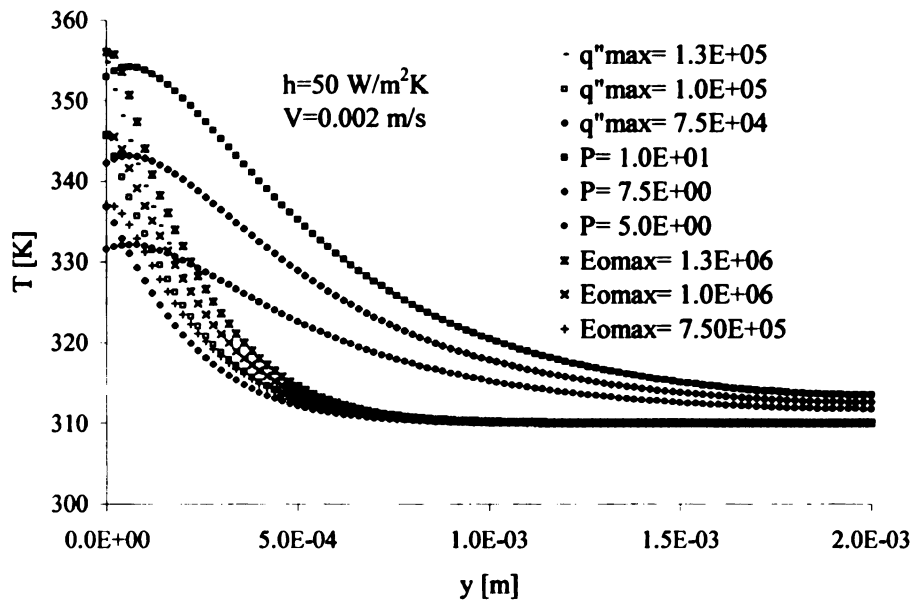
Figure 3.8: The Temperature Distribution Created within the CV by a Moving Probe (V=0.002m/s). *(Convection Coefficient, h=500W/m²K). (The probe was located at x=8.0E-03 m and moved to the right at a speed of 2mm/s).*
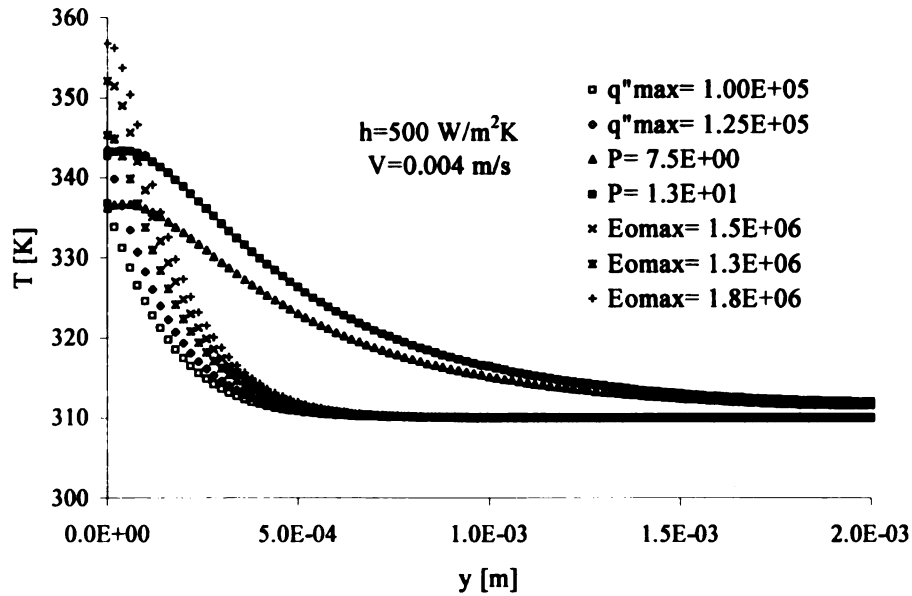
Figure 3.9: The Temperature Distribution Created within the CV by a Moving Probe (V=0.004m/s). *(Convection Coefficient, h=500W/m²K). (The probe is located at x=8.0E-03 m and moving to the right at a speed of 2mm/s).*

3.2.3 Model Verification

For the case of a 2 mm wide probe with uniform heat flux moving on the surface of the rectangular CV, the exact solution to the surface temperature given by Rosenthal [Rosenthal, 1946] was compared to the FEA predictions (Figure 3.10). For both 2 mm/s and 4 mm/s probe sweep speeds, the results showed very good agreement (within 1K). Thus the numerical simulations were considered acceptably accurate to extend to other cases of interest.
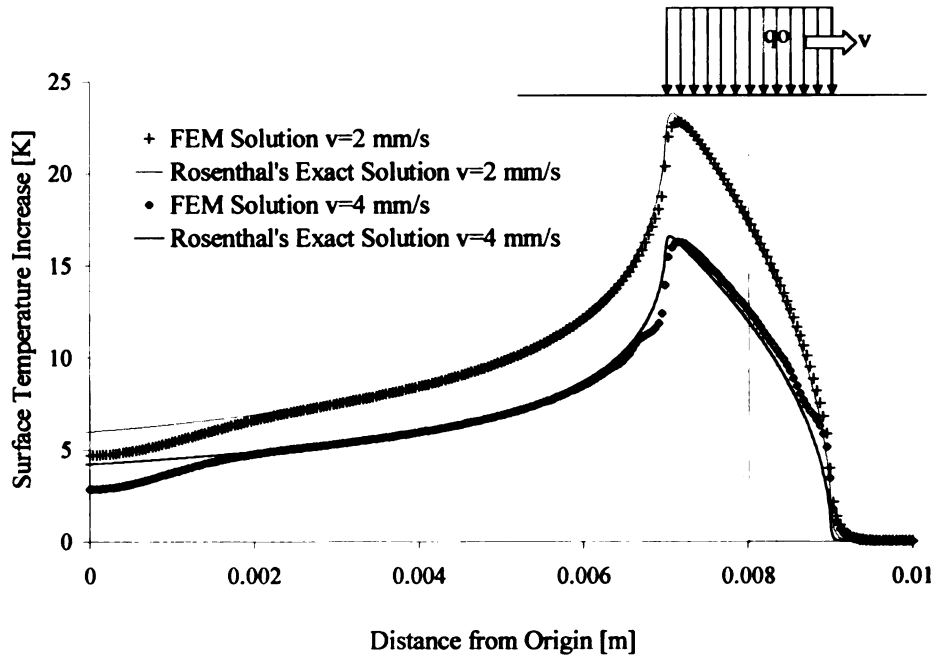
Figure 3.10: Comparison of FEA Results with the Exact Solution

3.3 Modeling the Thermal Damage Accumulated During Thermotherapy

In order to quantify the accumulation of thermal damage by the three different heating modalities, an Arrhenius formulation of a damage integral was utilized. The details are presented in Sections 2.2.1 and 2.2.2 of this thesis.

It has been shown by various researchers and by the results from our laboratory [Aksan & McGrath, 2001] that collagenous tissue denaturation phenomena is not only a function of the maximum temperature reached but also the exposure time, the mechanical load applied and the chemical state of the tissue.

Using a user subroutine and the built-in functions of MARC, thermal damage accumulation was also calculated for each simulation. In Figure 3.11 the results for thermal damage accumulation are shown for the same cases presented in Figure 3.6. This information was very important in determining the final mechanical and structural state of the tissue and its corresponding shrinkage behavior. It was observed that even though the maximum temperatures created by different heating modalities were similar, the thermal damage accumulated within the tissue was drastically different (Ω=7, 240 and 6000). Additionally, it is important to stress the fact that it is not the temperature distributions but the accumulated thermal damage that governs the heat-induced response of the collagenous tissues.

Ω=0 Ω=240   Bipolar
                                          q''_{max}= 1.25E+5 W/m^2
                                          ω = 1 mm

Ω=0 Ω=7   Ho:YAG Laser
                                          E_{omax}= 1.25E+6 W/m^2
                                          ω = 1 mm, f = 5Hz

Ω=0 Ω=6000   Monopolar
                                          P = 10 W/m^3
                                          r_o= 1 mm
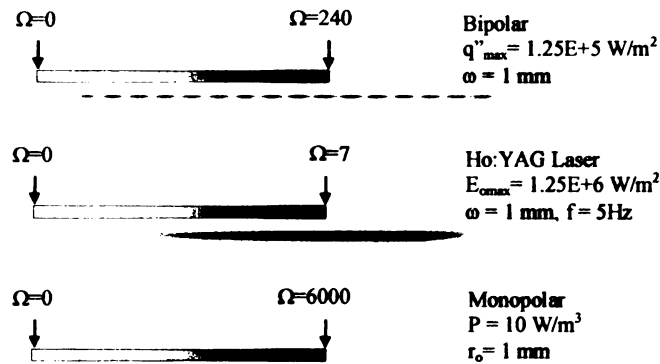
Figure 3.11: Thermal Damage Accumulation at t=4s

In Figure 3.11, the thermal damage penetration into the tissue is given for the three different modalities. Examination of the laser heating simulations (Figures 3.11, 3.12 and 3.14) showed that for this modality, thermal damage was superficial and was composed of small high damage spots surrounded by low damage regions. This was caused by the

pulsed application of the laser energy when it was swept on the tissue surface. The main reason for utilizing pulses rather than a continuous exposure is to give tissue some time to uniformly distribute the thermal energy and to reduce overheated regions within the tissue.

The damage profiles created by the bipolar radiofrequency probe were similar to those created by laser in terms of the penetration depth but the magnitude of the damage created was greater. The main difference was that these profiles were more uniform due to the continuous application of energy as opposed to the pulsed application of laser. If, on the other hand, a temperature-controlled bipolar probe were used (it automatically turns off when a certain temperature at the probe tip is reached) damage profiles more similar to those of laser would be observed.

The monopolar case depicted in Figure 3.11 shows a very interesting characteristic. This picture shows an isolated high damage zone deep in the tissue with surrounding regions of very low or no-damage. It should be noted that these simulations were performed with a rather high convection coefficient (h=500W/m^{2}K). The cooling effect of the surrounding fluid was therefore very significant and the thermal damage was confined to the regions deep within the tissue. This is a very important finding, especially from the clinical point of view. In the operating room setting, the visual perception of the surgeon is the only tool available to quantify the extent of the thermal damage established.
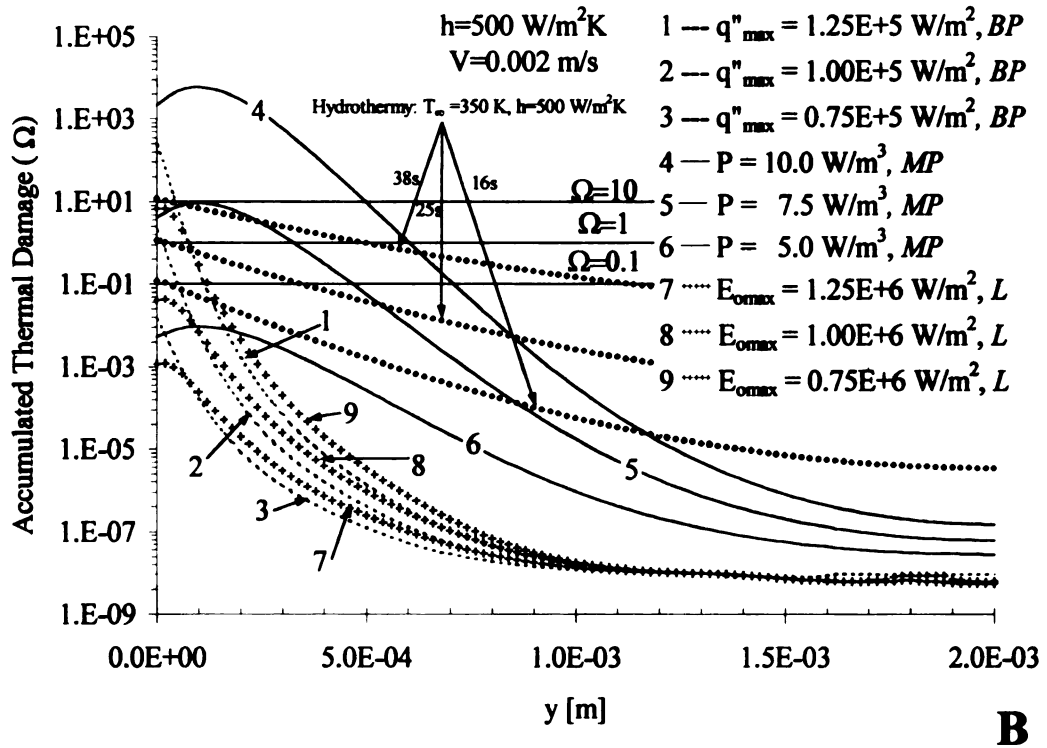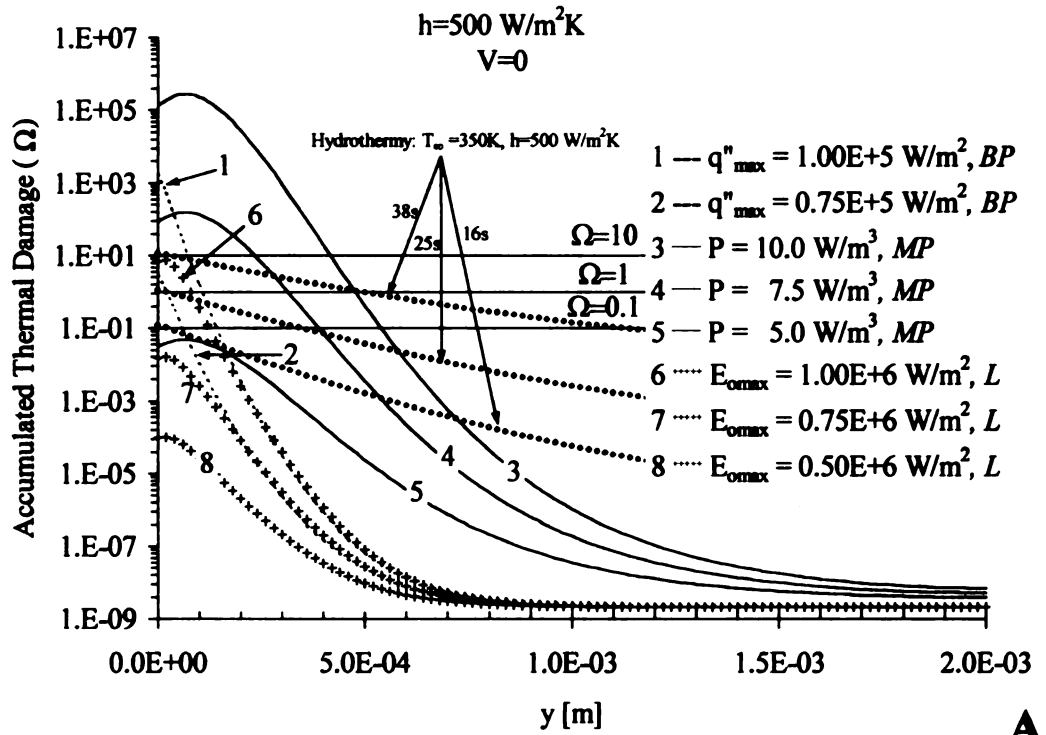
Figure 3.12: Thermal Damage Accumulation in the Tissue *A)* *h*=500W/m²K, *ω=r₀*=0.001m, *V*=0; *B)* *h*=500W/m²K, *ω=r₀*=0.001 m, *V*=0.002 m/s;

h=500 W/m²K
V=0.004 m/s

Ω=10

Ω=1

Hydrothermy: T_o=350 K, h=500 W/m²K

Ω=0.1

38s

25s

16s

$1 — q''_{max} = 1.25E+5$ W/m², *BP*

$2 — q''_{max} = 1.00E+5$ W/m², *BP*

$3 — P = 12.5$ W/m³, *MP*

$4 — P = 7.5$ W/m³, *MP*

$5 \cdots E_{omax} = 1.75E+6$ W/m², *L*

$6 \cdots E_{omax} = 1.50E+6$ W/m², *L*

$7 \cdots E_{omax} = 1.25E+6$ W/m², *L*

Accumulated Thermal Damage (Ω)

1.E+02
1.E+01
1.E+00
1.E-01
1.E-02
1.E-03
1.E-04
1.E-05
1.E-06
1.E-07
1.E-08
1.E-09

0.0E+00   5.0E-04   1.0E-03   1.5E-03   2.0E-03

y [m]

C
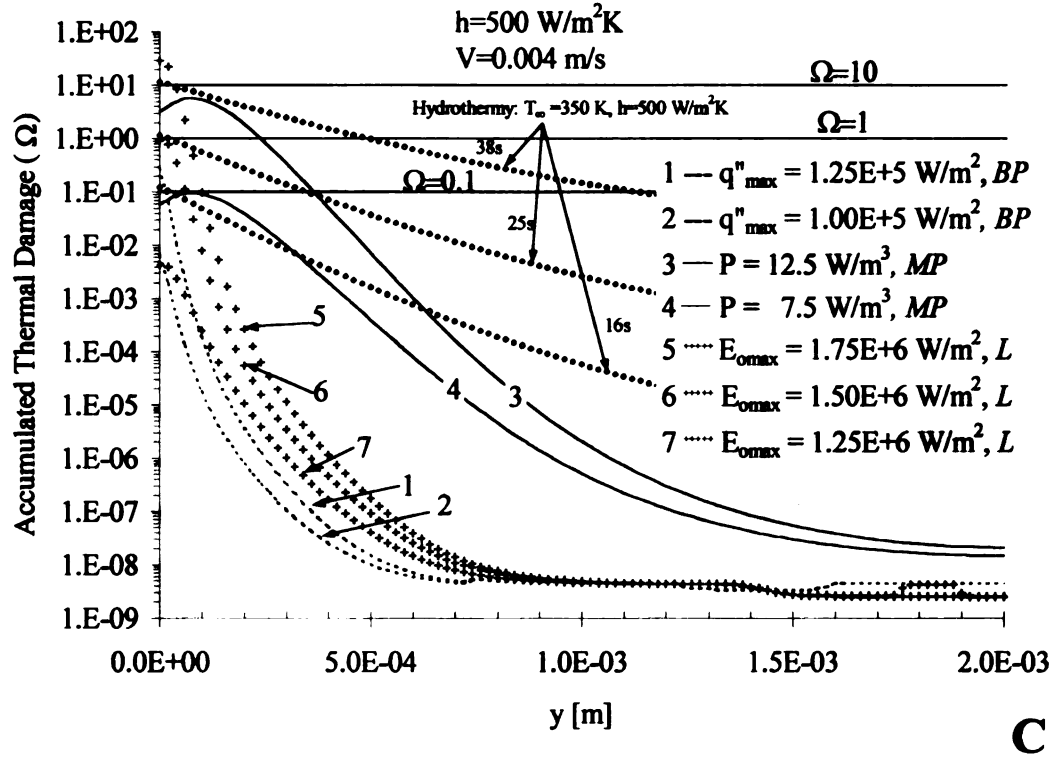
Figure 3.12. (Continued): *C)* h=500W/m²K, $\omega=r_o$=0.001 m, *V*=0.004 mm/s. (E_o: Laser (L) Surface Heat Flux [W/m²], q'': Bipolar (BP) Surface Heat Flux [W/m²], *P*: Monopolar (MP) Joule Heating [W]).

The undamaged, unheated zone on the surface of the tissue may easily act as a visual barrier by hiding the damaged zone, which is deep inside the tissue. In response, the surgeon thinking that he/she has not heated the tissue yet, more than likely would go over the same region repeatedly, creating significant damage deep within the tissue. This may also cause extreme necrosis of the untargeted surrounding tissues and weakening of the targeted collagenous tissue. This fact becomes increasingly important and obvious by close inspection of the damage penetration curves of the different cases as given in Figure 3.12 and Figure 3.13. In the close proximity of the surface, accumulated damage

79

decreased with increasing convection coefficient. When the arthroscopic fluid circulation rate was increased, the convection coefficient also increased. While irrigation of the target tissue surface is essential for decreasing the hot spots on the surface and cleaning the debris, too much of it can result in underestimation of the thermal damage generated. The horizontal black lines in Figures 3.12-3.14 are the threshold damage lines. These lines indicate the progress of the phase change process.

When the damage penetration depths in Figures 3.11 and 3.12 are examined, it is seen that the convection coefficient as well as the power output of the heating probe, regardless of the heating modality, plays a very important role in determining the extent of damage. In all the cases examined, the monopolar radiofrequency probe was found to cause the highest damage penetration with lower surface temperatures. The negative aspects of this modality may be the damage created in the underlying, untargeted tissues and the fact that the maximum damage zone is deep inside the tissue where it is hidden from the surgeon.

Another observation from these figures is that for the same power setting, the damage accumulated in the tissue decreases with increasing probe sweep velocity (Figures 3.12-3.14). The stagnant probe simulations (Figures 3.12A, 3.13A and 3.14A) indicate severe damage even after very brief exposure.

Figure 3.14 shows the distribution of the accumulated thermal damage on the surface of the tissue. One major observation is the undulations created by the laser probe. These are the same hot spots seen in the 2-D pictures (Figure 3.11). After the probe starts its motion at $x=0$, there is a transient region, followed by a steady damage region. The length of the transient region is a function of the probe sweep velocity.
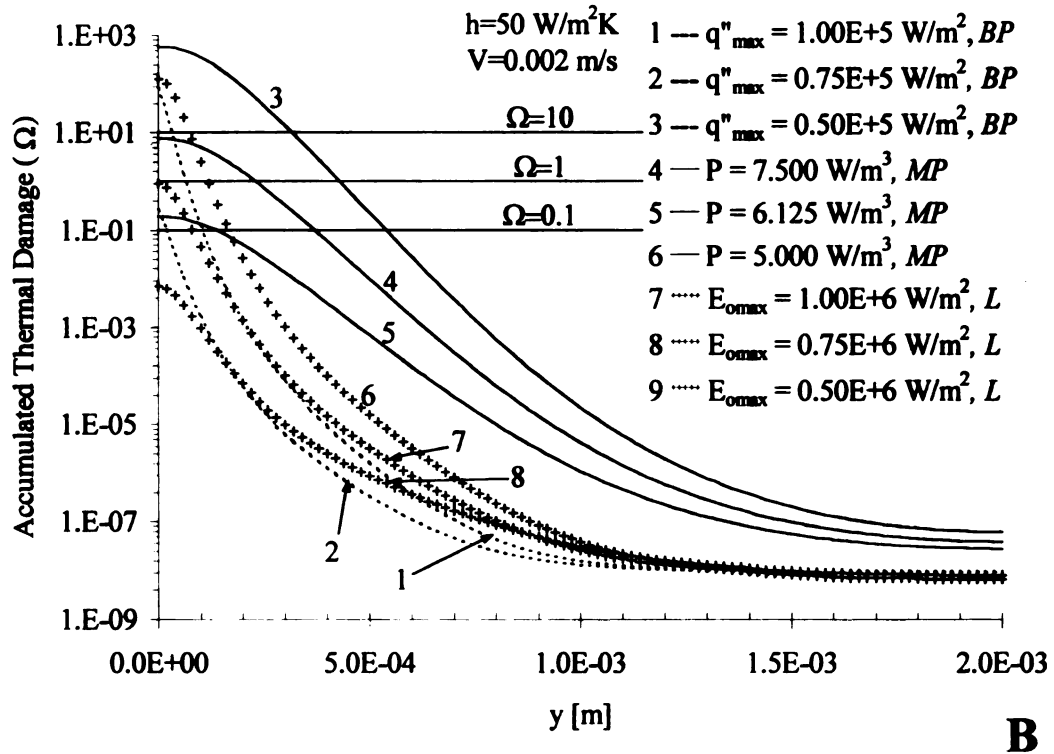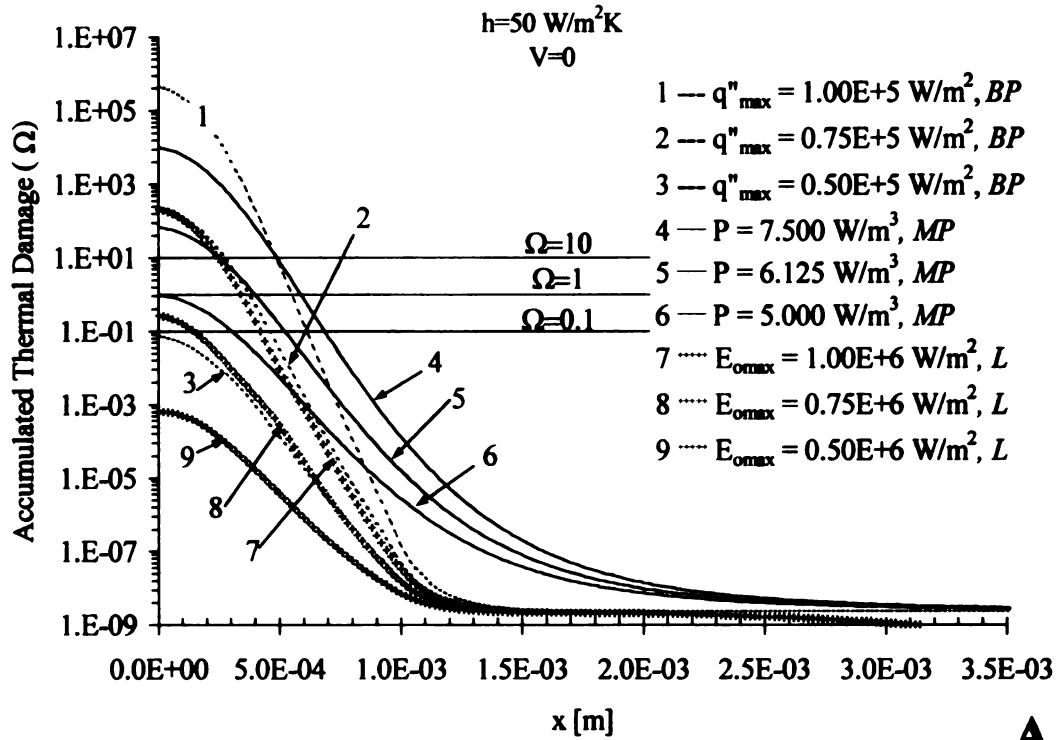
Figure 3.13: Thermal Damage Accumulation in the Tissue *A)* *h*=50W/m²K,

ω=r_0=0.001m, *V*=0; *B)* *h*=50W/m²K, ω=r_0=0.001m, *V*=0.002m/s; *C)* *h*=50W/m²K,
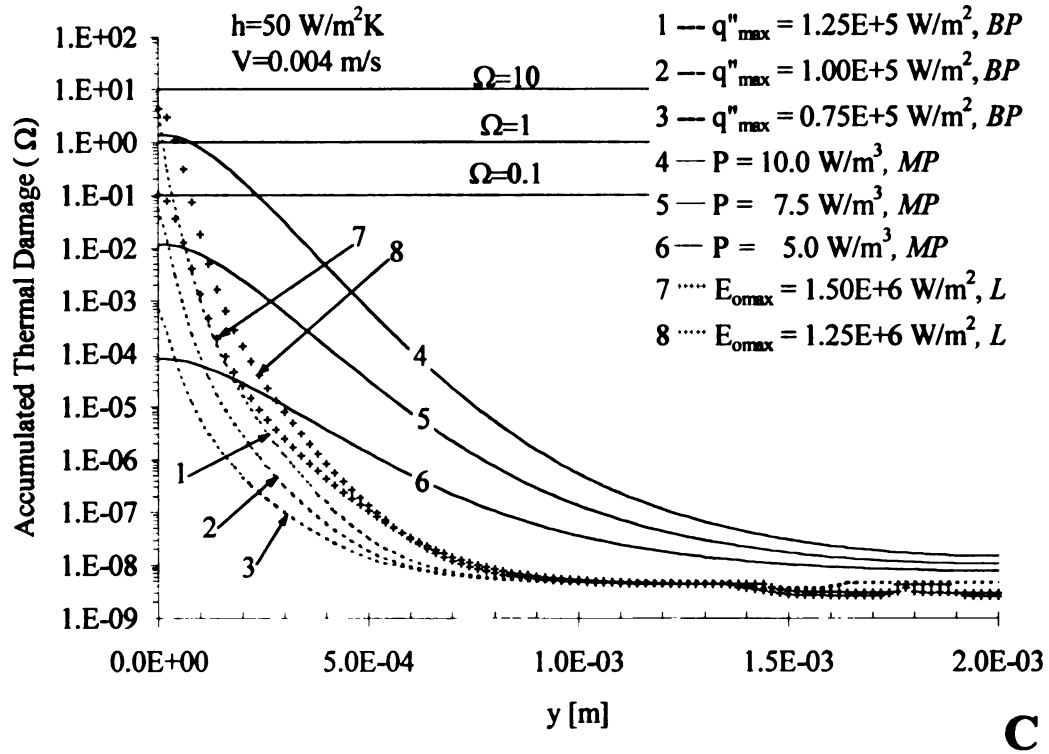
Figure 3.13 (Continued): *C)* h=50W/m²K, $\omega=r_o$=0.001 m, V=0.004 mm/s. (E_o: Laser (L) Surface Heat Flux [W/m²], q'': Bipolar (BP) Surface Heat Flux [W/m²], P: Monopolar (MP) Joule Heating [W]).

The changes in the temperature distributions and the thermal damage profiles after multiple sweeps with a heating probe as well as the effects of the changes in the material properties with denaturation, and the geometrical effects were not included in this resrearch but deserve attention in future work.

The dependence of collagen shrinkage on various factors like temperature, exposure time and mechanical load is well established. Mechanical property degradation of the tissue is also documented as a function of the severeness of the thermal protocol applied.

The main purpose of the research presented here was to quantify the differences among clinically utilized heat deposition modalities namely, laser, bipolar and monopolar radiofrequency. The initial results of the collagenous tissue heating simulations performed using a commercial finite element analysis software (MARC.Mentat) were presented. It was shown that there were significant differences in terms of the temperature distributions and thermal damage produced within the virtual tissue. Specifically, it was concluded that the thermal effects of the laser and the bipolar probe were very superficial when compared to monopolar heating. This could be observed by comparing the penetration depths of various modalities into the tissue, as shown by (Figures 3.12 and 3.13). On the other hand, it was observed that the thermal damage accumulated by the pulsating Ho:YAG laser was not spatially uniform, but rather created high damage "islands" surrounded by low damage regions.

Temperature distribution simulations performed showed that the phase change energy levels of collagen denaturation were significant and that if realistic models to quantify the thermal-mechanical behavior of collagenous tissues are to be constructed, this factor should be taken into consideration. Other clinically important parameters examined here include the convection coefficient and the probe sweep velocity. The convection coefficient is a function of the flowrate of the irrigation solution circulated around the target tissue during heating. It was concluded that the increased probe sweep velocity and irrigation solution circulation tend to smooth the thermal gradients created, yielding a more uniform thermal damage within the tissue.
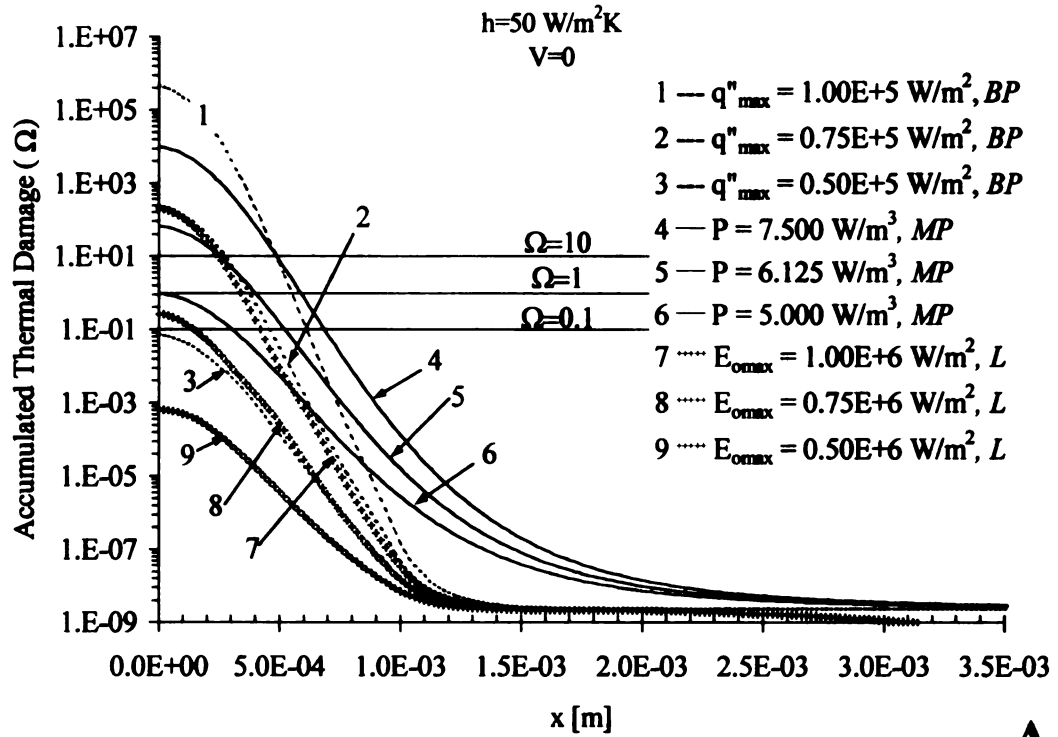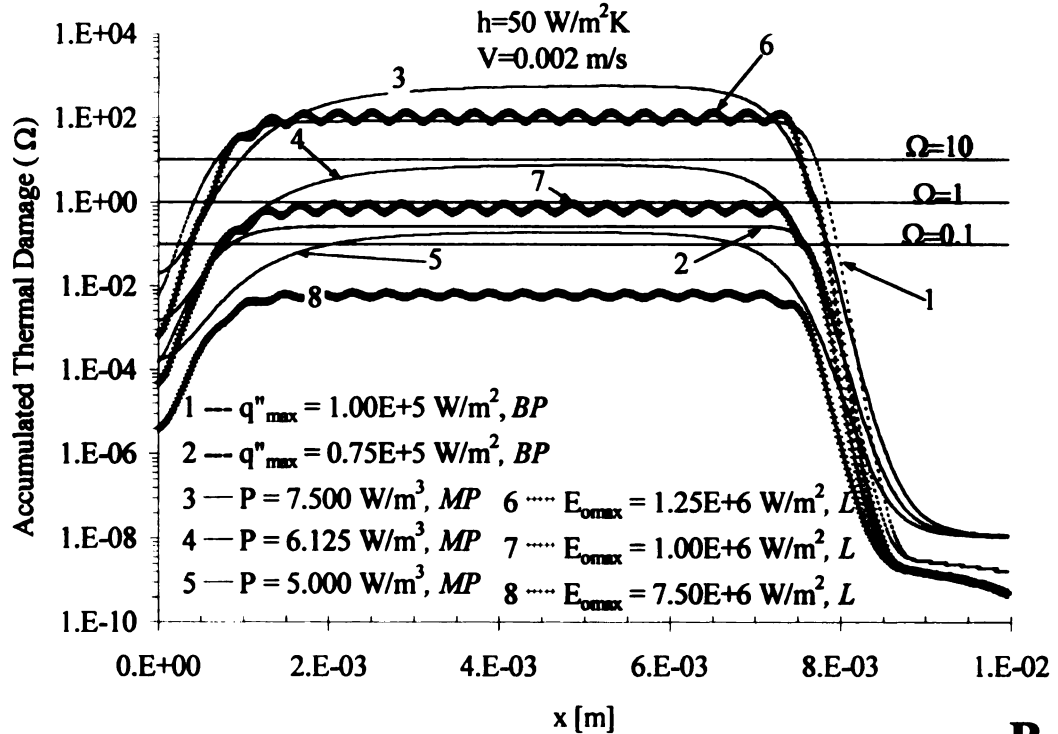
Figure 3.14: Thermal Damage Accumulation on the Tissue Surface *A)* h=50W/m²K, ω=r_0=0.001m, V=0; *B)* h=50W/m²K, ω=r_0=0.001m, V=0.002m/s;

h=50 W/m²K
V=0.004 m/s

Ω=10
Ω=1
Ω=0.1

Accumulated Thermal Damage (Ω)

1.E+02
1.E+01
1.E+00
1.E-01
1.E-02
1.E-03
1.E-04
1.E-05
1.E-06
1.E-07
1.E-08
1.E-09
1.E-10
1.E-11

$1 — q''_{max} = 1.25E+5$ W/m², BP

$2 — q''_{max} = 1.00E+5$ W/m², BP

$3 — q''_{max} = 0.75E+5$ W/m², BP   6 — P = 5.0 W/m³, MP

$4 — P = 10.0$ W/m³, MP $7 \cdots E_{omax} = 1.50E+6$ W/m², L

$5 — P = 7.5$ W/m³, MP $8 \cdots E_{omax} = 1.25E+6$ W/m², L

0.E+00   2.E-03   4.E-03   6.E-03   8.E-03   1.E-02

x [m]

C
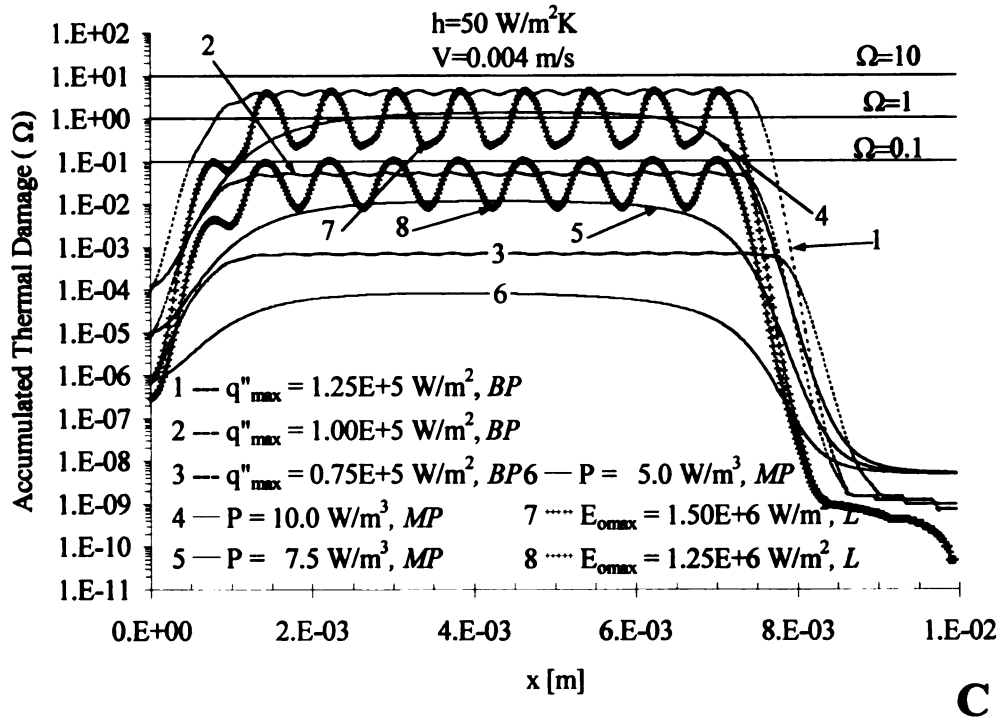
Figure 3.14 (Continued): *C)* h=50W/m²K, $\omega=r_o$=0.001 m, V=0.004 mm/s. (E_o: Laser (L) Surface Heat Flux [W/m²], q'': Bipolar (BP) Surface Heat Flux [W/m²], P: Monopolar (MP) Joule Heating [W]).

The heating pattern created by the laser heating may be preferred if one wishes to boost the healing response of the tissue since the migration of the cells from the surrounding regions would be facilitated. Additionally, this characteristic may be useful if only superficial tissue damage is desired as in the case of skin resurfacing or as in cases when underlying nerve damage is an issue. One other point that should be stressed here is that the simulations presented are for the Ho:YAG laser (2.1mm) which has a very small penetration distance (~300 mm). Light at this wavelength is mainly absorbed by the bound water in the superficial layers of the tissue. In order to increase thermal penetration and

minimize hot spots, pulsating the laser light, increasing the arthroscopic fluid circulation around the treated region and low power settings were used. If, for instance, an Nd:YAG laser (1064 nm) with a penetration depth of approximately 1400 mm was used instead, deeper and more uniform thermal damage might be expected. On the down side, the undulations created on the surface by the laser may create a composite medium where the high damage "islands" act as stress concentration zones that may have adverse effects, especially on the tensile properties of the soft tissue.

The advantage of having irrigation circulation, from a thermal point of view, is to smooth the temperature gradients within the tissue. The disadvantage of having very high circulation around the target tissue, especially when modalities with volumetric heat generation effects (such as monopolar radiofrequency) are used is that the damage created deep inside the tissue may be underestimated. This may result in repetitive heating of the same region of the tissue causing overexposure and significant decrease in the mechanical properties of the tissue. The effect of an increase in sweep velocity is similar to that of increased irrigation circulation. The sweeping action tends to smooth the thermal gradients within the tissue. Keeping the probe stagnant over the tissue for even a few seconds was shown to cause extreme thermal damage.

The simulations presented in this thesis did not take into account the nonhomogeneity and anisotropic character of the tissue. They did not consider the interaction between the probe and the surrounding fluid, variations in probe geometry and the probe design by different manufacturers. Therefore, these simulations should be taken as first approximations until further detailed studies are performed.

The main objective of this research was to prove that the temperature profiles and the accumulated thermal damage profiles created by the clinically applied heating modalities are considerably different. Performing 2-D simulations served this purpose in a very fast and efficient way. In a 3-D analysis, additional information would be available concerning the accumulation of thermal damage in the third direction. This would help examine other parameters such as the distance between consecutive probe sweep paths.

The next step in this research was to combine the thermal model with a mechanical model. The mechanical model predicted the final mechanical state of the tissue subjected to various thermal loads. The transition between these two models (thermal and mechanical) was achieved through in-vitro experimentation, which determined the variation of mechanical and thermal properties with damage accumulation.

3.4 Temperature Controlled Monopolar Heating Probe Experiments & Simulations

In order to verify the results of the FEA simulations, in-vitro experimental analysis with rabbit patellar tendons was performed. A custom-made, computer controlled stepper-motor driven carriage was immersed in 37°C saline solution.

A rabbit patellar tendon sample was placed on the carriage and secured using two clamps on each end of the carriage (Figure 3.15). A temperature controlled monopolar heating probe (Oratec, Vulcan TAC-S Electrothermal Probe, Oratec Interventions Inc., Menlo Park, CA) set to operate at a temperature of 75°C and a power setting of 30W was used to heat the tendon specimen.
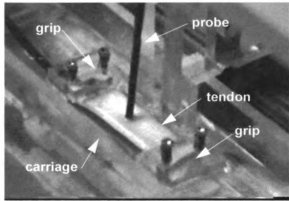
Figure 3.15: Photograph of the Motor Driven Carriage

The return (ground) electrode was placed underneath the specimen (Figure 3.16). During the experiment, initially, the heating probe was kept stationary for 1s and then was swept along the major axis of the tendon at a predetermined speed. The sample was then frozen prior to Optical Coherence Tomography (OCT) and Magnetic Resonance Imaging (MRI) experiments in order to determine the extent of thermal denaturation within the tissue.

In order to simulate the temperature control of the monopolar radiofrequency probe, the Fortran subroutine used in the simulations presented in the previous sections was modified. In the modified version, the node temperature corresponding to the location of the probe (stationary or moving) was checked against the set temperature value (T_{set}=75°C) at each time increment. An hysterysis temperature was utilized in order to eliminate excessive hunting of the on/off controller simulation. Through the use of the hysterysis temperature, if the node temperature was within 2.5K of the set value, the heat flux was turned off for the following time increment.
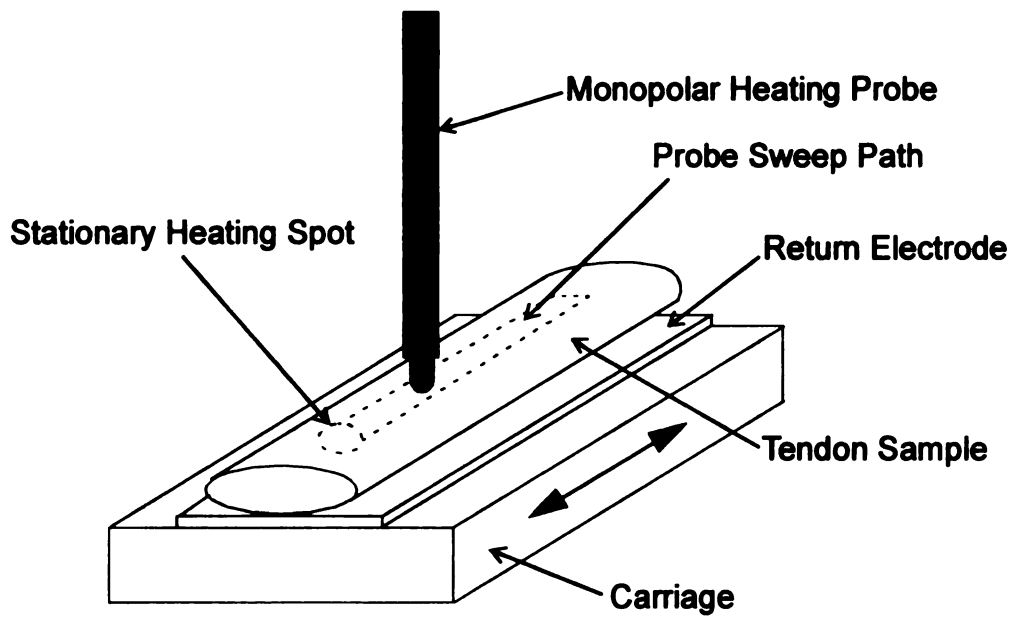
Figure 3.16: Experimental Setup for the Verification of FEA Simulations
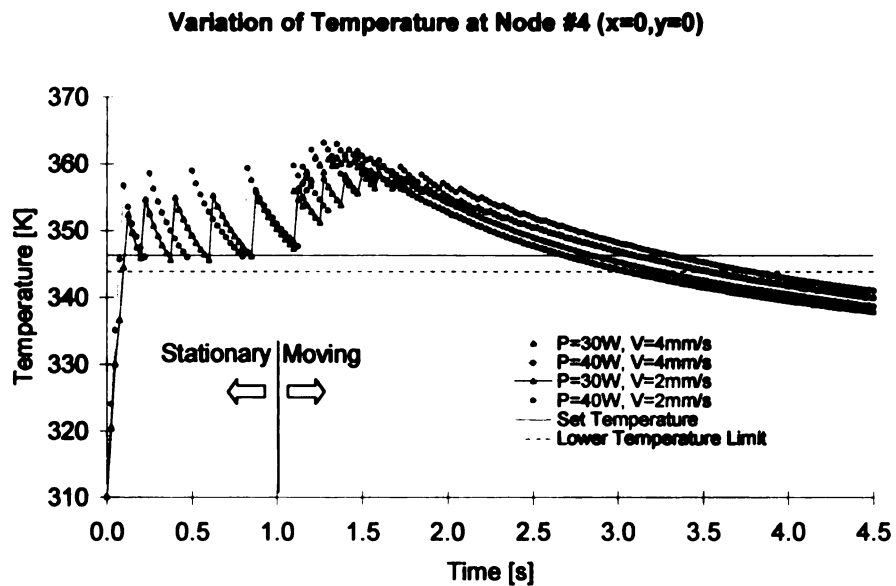
Figure 3.17: Temperature at the Origin During Stationary and Moving Heating
Simulations with a Temperature Controlled Monopolar Radiofrequency Probe

In two-dimensional heating simulations, the temperature history for node #4 located at the origin is presented below during stationary and moving heating (Figure 3.17). As long as the probe was stationary, the tip temperature of the probe and therefore the corresponding tissue temperature where the tip was located could be controlled within certain limits. The interesting finding here was the increase in the tissue temperature at the origin after the onset of probe motion. Since at any instant, the temperature of the tissue where the probe tip was located was the main criterion for the control system and since with the sweeping motion the probe moved to a new location which was considerably cooler than the previous location, the heat was turned on. However, the heat flux distribution was Gaussian in the x-direction, not only the tip of the probe, but also the surrounding tissue (including the downstream location which is already at a high temperature) was heated. This caused overheating of downstream locations (Figure 3.19). This phenomenon may be characterized by the Peclet number, which is here of the order of unity, meaning that the axial conduction in the tissue is as important as the heat convected by the motion of the probe (not to be confused with the uniform convection heat transfer on the surface of the tissue caused by the circulation of saline). In order to solve this problem, one alternative would be to decrease the diameter of the probe or to sweep the probe faster. However, faster probe speeds cause new problems, such as limited thermal damage penetration. Below in Figure 3.18, the penetration of thermal damage into the tissue, predicted by the FEA simulation is presented for different power settings (P=30, 40W) and probe sweep speeds (V=2, 4 mm/s). As seen below, there is not a significant difference between the simulations. The onset of denaturation is shown to be located at approximately 900µm below the tissue surface. The same simulations predicted

that in a band ($0 \leq y \leq 600 \mu m$), the tissue was completely denatured.
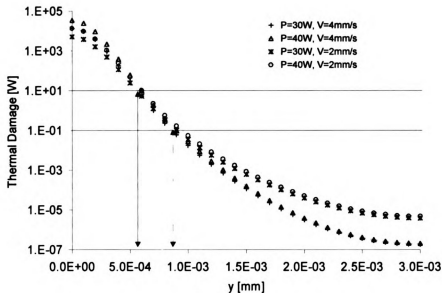
Figure 3.18: Penetration of Thermal Damage, Ω Predicted at the Origin
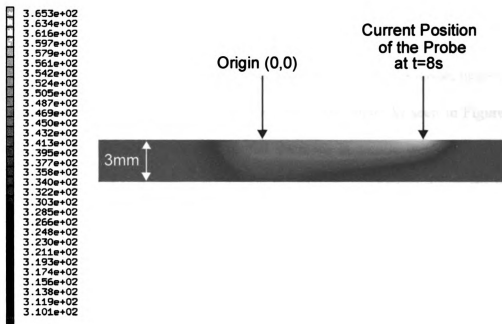
Figure 3.19: Temperature Distribution at t=8s Within the Tissue Subjected to a Moving, Temperature Controlled Monopolar Radiofrequency Heating Probe

Chapter 4: Collagenous Tissue Thermomechanics

As long as it is properly hydrated, the post-denaturation mechanical state of a collagenous tissue is defined mainly by its thermal and mechanical histories [Chen, et al., 1998, Aksan & McGrath, 2002]. These two parameters determine the heat-induced deformation (as shown in Figure 2.20 by the decrease in the maximum equilibrium shrinkage as a function of the load applied on the tissue during heating) and the mechanical properties of the tissue (as seen in Figure 2.23 by the decreasing trend of the normalized tensile modulus with increasing shrinkage and hence with accumulated thermal damage).

It was shown in Chapter 2 of this thesis that, in a collagenous tissue, heat-induced deformation and mechanical properties are inversely correlated. As seen in Figure 2.23, heat-induced shrinkage causes an exponential decrease in tensile modulus. When this observation is extended to the clinic (to the application of sub-ablative thermotherapy for treatment of joint instability) it is transformed into the trade-off between the kinematic and mechanical stabilities of the joint. Kinematic stability of the joint is achieved by the heat-induced shrinkage of the lax tissue while the mechanical stability is compromised by the heat-induced degradation of the mechanical properties of the tissue. Hence, there is a very close relationship between the success of sub-ablative thermotherapy and the mechanical

state of the joint tissue. At this point, the usefulness of a thermomechanical model representing the heat-induced behavior of collagenous tissues becomes obvious. This model is crucial for analyzing the parameters mentioned above in terms of their individual and synergistic contributions to the outcome of sub-ablative thermotherapy and for establishing guidelines for optimum treatment protocols. Other important clinical parameters that can be analyzed using this model are the efficacies of different heating modalities, techniques and patterns.

In clinical practice of sub-ablative thermotherapy, there is not yet a well-defined recipe to follow to achieve successful therapeutic outcome. Such a recipe could not yet be established partly due to the different heating modalities (Ho:YAG laser, monopolar/ bipolar radiofrequency) utilized and partly due to the variety of heating techniques (e.g. continuous or repetitive heating) and patterns applied. Some surgeons prefer paintbrush patterns, uniformly heating the overall capsule surface while others prefer creating grid patterns or parallel lines of denatured regions (Figure 4.1).

Due to the variations in clinical application and the problems in defining optimum treatment protocols, it is not surprising to see controversial reports on the outcome of the HACS procedures. The patient-to-patient variations in the anatomy and histology of the joint [Obrien, et al., 1990] and the pathology (variations in the tissue microstructure due to repetitive microdamage or congenital disorders such as Ehlers-Danlos and Marfan's Syndromes) of the targeted tissue introduce additional challenges.
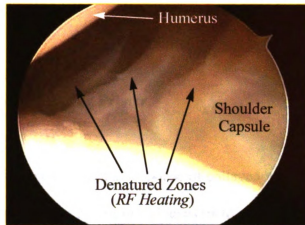
Figure 4.1: Arthroscopic View Showing the Parallel Zones of Denaturation Created on the Shoulder Capsule by Monopolar Radiofrequency Heating *(http:// www.communityorthopedics.com/pages/thermal.htm)*

4.1 Characteristics of Thermal Stresses

Thermal stresses are created in the collagenous tissue due to the heat-induced structural transition (denaturation) of the collagen network. Denaturation causes considerable dimensional change mainly in the direction of the collagen fiber orientation. Accompanying this response are the strains formed in the transverse directions. Tissue volume may also increase due to water influx [Wiederhorn & Reardon, 1952]. If an isotropic and homogeneous tissue is uniformly heated, and it is at an otherwise uniform (or zero) stress state, the thermal stresses formed cause it to deform uniformly. However, if any of the following conditions apply then the thermal stresses formed will be nonuniform resulting in a nonuniform and complex stress/strain field: *a)* the tissue is structurally inhomogeneous, *b)* the tissue has an initial (prior to heating) nonuniform stress distribution due to traction boundary conditions, *c)* its deformation is confined due to

displacement boundary conditions, *d)* there are thermal gradients within the tissue (due to localized heating).

4.2 Thermomechanical Modeling Primer

To model the thermomechanical response of collagenous tissues, the conventional approach is either to perform an experimental analysis to establish empirical relationships between the measured parameters (temperature, time, load, elongation, tissue hydration, etc.) and the final state (defined by its state-of-stress (or deformation) and mechanical properties) of the tissue or to solve the coupled thermoelasticity equations [Nowacki, 1986] that govern the thermomechanical phenomena in a continuum.

The former approach is species and tissue specific, requires tremendous effort and a very large number of specimens. In the latter case, when solution of the thermoelasticity equations are considered, two major problems arise: *a)* a solution to these equations can only be obtained for very simple tissue geometries if very radical simplifying assumptions are made, and *b)* these equations do not carry phase change or history information (these models assume that upon cessation of heating, when the material is returned back to its initial temperature, no permanent effect remains). In the case when denaturation causes a phase change of the collagen however, the effect of heating is irreversible beyond a certain temperature (for a stress-free tendon tissue the threshold temperature for irreversible transition is approximately 60°C. Yet, there is evidence that even at 40°C there are certain irreversible changes in the microstructure [Hormann & Schlebusch, 1971]). During

transition, in addition to formation of permanent thermal stresses (yielding to permanent thermal deformations), the physical properties of the tissue change irreversibly as well.

Hypothetically, it is also possible to model the heat-induced gross tissue response based on the configurational and structural transformations of the collagen molecule. If all the mechanical interactions between the consecutive structural levels of the tissue hierarchy could be established, it would be possible to extrapolate the microstructural response to the macroscale tissue behavior. As a first step in understanding the microscale mechanics of tissues, some studies focused on measuring the mechanical properties of a single collagen fiber using conventional biomechanical experimentation techniques [Svendsen & Thomson, 1984] and of a single tropocollagen molecule using laser tweezers and optical strain measurement techniques [Luo, et al., 1997]. Due to inherent technical challenges in establishing the complex interactions among the tissue structures at different hierarchical levels, there are as yet no reported studies focusing on the thermomechanical behavior of these microscopic structures.

In this research, in order to model and simulate the heat-induced collagenous tissue response, a radically different approach is taken. It is proposed that the thermomechanical response of a collagenous tissue to local heating (such as by laser or radiofrequency) can be modeled based on the thermomechanical response of a dense, oriented tissue to a uniform heating modality (such as by hydrothermy for very high Biot numbers) by a combination of experimental and numerical analysis. Details of this new approach are presented in the following section.

4.3 Thermomechanical Response Simulation Algorithm

In this part of the thesis the computer-based simulation tool that has been developed in order to model the thermomechanical responses of collagenous tissues will be described. As a first step in the development of the software, a two-dimensional analysis in simple geometries has been performed. Later in the development stage, the analyses have been extended to three dimensions.

The virtual tissue (the Control Volume (CV) used in the Finite Element Analysis (FEA)) was hypothetically divided into small, representative elementary volumes (REVs) at the same hierarchical level. It was assumed that each REV is large enough to be considered a continuum. A REV was also considered to be structurally homogeneous, thermally lumped and to be in mechanical interaction with the surrounding REVs. The heat-induced thermomechanical behavior of each REV was assumed to be identical to that of a dense, oriented collagenous tissue when it was subjected to uniform heating (i.e., when there were no thermal gradients in the tissue except at the boundaries).

The schematic representation of the algorithm used for collagenous tissue thermomechanical response simulation is shown in Figure 4.2. Basically, there are three main routes:

1) Heat Transfer Analysis by which the temperature distributions and thermal damages created in a collagenous tissue by clinically used heating methods (Ho:YAG laser, Monopolar or bipolar radiofrequency) can be modeled using finite element analysis (see Chapter 2 of this thesis for details).

2) In-vitro Experimentation with a dense, oriented collagenous tissue model (rabbit patellar tendon) in order to establish empirical correlations between the mechanical and thermal histories and the final state of the tissue. Details of this research are presented in Chapter 3 of this thesis.

3) Mechanical Analysis, which allows the prediction of the pre-heating mechanical stress fields within the control volume and the mechanical history of the tissue.
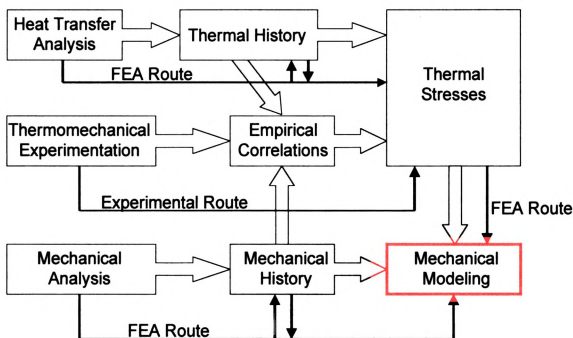
Figure 4.2: Collagenous Tissue Thermomechanical Response Simulation Algorithm

The information collected though these analysis routes was used to model the thermal stresses formed in the virtual tissue (the CV) and the resultant state of the tissue. Details of each step are presented below.

For a given problem the thermomechanical response simulation began with the solution of the heat transfer problem through finite element analysis (FEA) following the procedures established in Chapter 2 of this thesis. Through this analysis, the temperature distributions created in the tissue by clinically applied heating modalities and the thermal damage accumulation (calculated by the Arrhenius damage integral) were determined. These values were calculated and recorded for each node in the finite element mesh comprising the CV. For each REV (which is equivalent to an element in the FEA), a single representative thermal damage value, Ω was calculated by averaging the thermal damage accumulated at each node of the element. In Figure 4.3A, the thermal damage accumulated inside a two-dimensional control volume is shown. In this figure, the blue color indicates undamaged zones and the yellow color shows highly damaged regions. The white squares in Figure 4.3A are the REVs covering the CV (some space is left between REVs for visual clarity). Figure 4.3B shows the Arrhenius damage integral value corresponding to each REV. It is shown that the REVs in columns 1 and 5 and in the third row are not damaged and therefore not assigned any value. The black line in each REV shows the primary direction of fiber orientation that can be assigned for each REV.

For the same geometry, a static mechanical analysis was performed in order to determine the state of stress of each REV prior to heating. Consequently, through these two analyses, for every REV (each element in the mesh) represented by its respective center coordinates (i,j), the corresponding representative thermal damage (a scalar quantity), Ω_{ij}, and the state of stress (a tensor), $\underline{\sigma}_{ij}$, were determined.

In collagenous tissues collagen fiber orientation may vary spatially (except in dense, oriented soft tissues such as tendon). However, it was reasonable to assume that the

direction of collagen fiber orientation in a REV coincides with the axis of the maximum principal stress. The rationale behind this assumption is that in collagenous tissues, collagen fibers align themselves in the direction of the maximum load. Once the state of stress is known, the maximum principal stress for any $REV_{i,j}$, σ^*_{ij}, can be easily calculated from σ_{ij} as follows:

$$\sigma^*_{ij} = \frac{\sigma_{x,ij} + \sigma_{y,ij}}{2} + \sqrt{\left[\frac{\sigma_{x,ij} - \sigma_{y,ij}}{2}\right]^2 + (\tau_{xy,ij})^2} \qquad \textbf{4.1}$$

In Equation 4.1 $\sigma_{x,ij}$, $\sigma_{y,ij}$ and $\tau_{xy,ij}$ are the normal stress in the x-direction, the normal stress in the y-direction and the shear stress in the x-y plane for REV_{ij}, respectively. In order to account for the *delay* in transition (as seen in Figure 2.18, with increasing load, equilibrium shrinkage curves shift towards higher thermal damage values) with increased stress, the midpoint thermal damage, $\Omega_{m,ij}$, corresponding to the maximum principal stress, σ^*_{ij}, for the same REV was determined using Equation 2.8 (also shown in Figure 2.19). Increase in stress also effects the maximum equilibrium shrinkage (see Figure 2.20). Therefore, maximum equilibrium shrinkage, $e_{2max,ij}$, corresponding to the maximum principal stress, σ^*_{ij}, was calculated from Equation 2.9. These values were inserted into Equation 2.10, which in turn was solved for the equilibrium shrinkage, e_2, REV_{ij} undergoes when it was subjected to a thermal damage, Ω_{ij}, and when wat is at an initial state of stress represented by $\underline{\sigma}_{ij}$.

The calculated equilibrium shrinkage, e_2, would be equal to the resultant shrinkage if REV_{ij} was completely isolated from its surroundings (Figure 4.3C). In Figure 4.3C, the

deformation of each REV (REVs A through F) are shown as if they were completely isolated from their surroundings (i.e., not in mechanical interaction with surrounding REVs). However, this is not the case since the surrounding interacting REVs are also undergoing denaturation at different levels and are exerting additional stress on their surroundings (and on REV$_{ij}$, as well). In order to account for the interactions among all of the REVs in the CV (including the native REVs as well as the thermally damaged ones) a procedure utilizing transient mechanical analysis by means of FEA was developed.
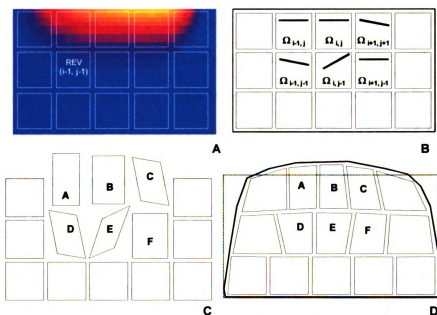
Figure 4.3: REV Approach and Schema of Thermomechanical Coupling

Following the same rationale used to develop Eshelby's Method [Eshelby, 1957], it is assumed that the global effects of the transformation stresses (such as the stresses due to the denaturation of collagen) created in a sub-region, N^*, enclosed by a region N can be calculated from the stress-free transformations of the sub-region N^* when it is completely

isolated (see Appendix A for details). Therefore, the stress-free transformation (equilibrium) strain, e_2, calculated for each REV was converted to a resultant potential stress, σ_2, using Hooke's Law. The material constants were taken at the transformed state as a function of equilibrium shrinkage (see Figure 2.23). The stress calculated for each REV was assumed to be acting at the boundary of the respective REV at its undeformed (pre-heating) configuration. This was analogous to an initial value problem, where there is an initial stress distribution (at $t=0$) over a volume and through transient analysis, the final deformations of the system were calculated. Using this analogy the problem was converted into an initial value problem and was solved using FEA (as seen in Figure 4.3D). The solid lines around the REVs show the final deformed state of the CV and the dashed lines show its shape at the initial (reference) configuration prior to heating. Note the difference in the shape of the REVs between (Figure 4.3C and Figure 4.3D).

The applicability of the algorithm presented here is tested for a two-dimensional geometry and the analysis is presented below.

4.4 Two-Dimensional Simulations

A two dimensional control volume (2mm x 20mm) representing a rabbit patellar tendon specimen was heated by a Ho:YAG laser on one face (Figure 4.4). The top surface of the control volume was assumed to be immobile simulating a suspended specimen. In the single spot heating simulations, the laser beam was focused on the center of the right face of the CV. In the multiple spot heatings, heating was symmetric about the same center point.

Thermal stresses were calculated for each REV (in this case a square element in the mesh with the dimensions 20μm x 20μm) and assigned as initial stresses distributed over the heated region. Following the methodology established below, mechanical response to six different heating conditions with an Nd:YAG laser (1064nm) were simulated. The following table (Table 1) lists those conditions:

Simulation Number	Laser Spot Size (1/e Diameter) [mm]	Number of Spots	Distance Between Spots [mm]
1	0.25	1	N/A
2	0.50	1	N/A
3	0.75	1	N/A
4	0.50	3	0.5
5	0.50	5	0.5
6	0.50	3	1.0

Table 4.1: Mechanical Response Simulations Performed

The results of the heat-induced mechanical response simulations performed are presented below in Figure 4.4. In this figure the white rectangle represents the outline of the tissue at its native state (before heating). In all of the simulations performed, it is observed that local heating by laser causes bending of the tissue. The bending angle is a function of exposure time and spot size (which is the Gaussian beam diameter). A similar response to laser heating was observed during experiments performed in our laboratory.
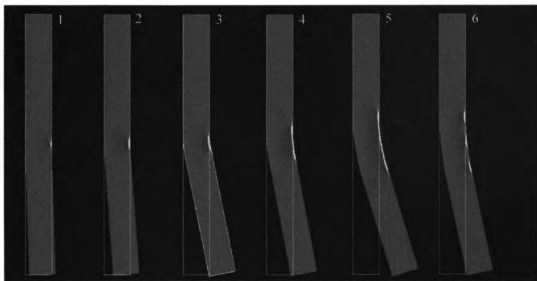
Figure 4.4: Results of the Heat-Induced Mechanical Response Simulations

As seen below in Figures 4.5 and 4.6, these simulations could be very useful tools in determining the stresses formed in the tissue after heating. In those figures a zoom view of the center of the tendon is presented. In Figure 4.5, the variation of the y-component of the normal stress (σ_{yy}) is shown. As expected, the initial compressive thermal stresses relax and cause the rest of the tissue to bend. The amount of bending is directly proportional to the laser spot diameter. This simulation tool is able to accommodate various heating modalities and effects like probe speed, the power deposited and other factors like heat transfer boundary conditions and tissue structure.
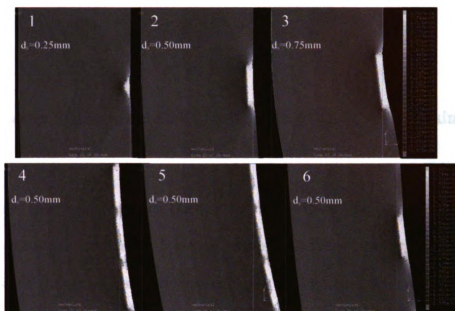
Figure 4.5: Variation of the Normal Stress in y-direction (σ_{yy}) (Range: White: 2.907 MPa compressive, Black: -1.975 MPa tensile). *(d_s: Laser spot size)*
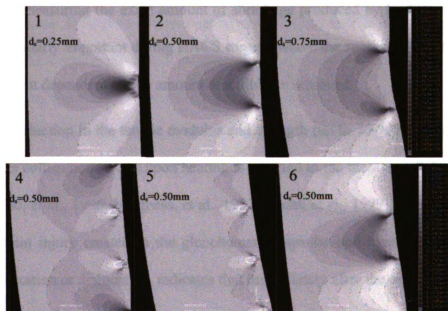
Figure 4.6: Variation of the Normal Stress in x-direction (σ_{xx}) (Range: White: 0.2589 MPa compressive, Black: -1.142 MPa tensile). *(d_s: Laser spot size)*

Chapter 5: Chemical Enhancement Methods (Cross-Linking)

There are two important factors that accompany the denaturation-induced shrinkage of collagenous tissues. These are: the mechanical property degradation and the partial loss of shrinkage (tissue elongation) upon cooling back to lower temperatures (defined here as recovery). Recovery is thought to be the result of re-naturation i.e., refolding of the partially unfolded tropocollagen molecules upon cessation of heating [Hormann & Schlebusch 1971; Watanabe, et al., 1997]. This may be the main cause of ambiguity in measuring the exact amount of shrinkage produced by heating. This factor may be particularly important during HACS surgery where the success of the operation is to a large extent dependent on the amount of shrinkage achieved.

The reduction in the tensile modulus and strength (up to 70-90% of the untreated tissue) of the collagenous tissue upon heating is reported in the literature [Schaefer, et al., 1997; Berend, et al., 1996; Vangness, et al., 1997; Hecht, et al., 1999]. This fact, coupled with the strain injury created in the glenohumeral capsular and ligamentous structures during subluxation or dislocation, indicates that immediately after the operation the tissue is excessively weak and vulnerable.

One possible solution to these problems is to apply a chemical method in conjunction with heating as a means of reducing the recovery of the tissue while

enhancing the mechanical properties. Examination of the feasibility of this idea was the motive for the preliminary research described here.

The ongoing search for a method to minimize the drawbacks (degradation of mechanical properties and recovery from the shrunken state) of the HACS procedures suggested the possibility of utilizing chemical cross-linking agents. The chemical modification of collagen films and collagenous tissues using cross-linking agents like glutaraldehyde (GTA), 1-ethyl-3-(3-dimethylaminopropyl)-carbodiimide (EDC), hexamethylene diisocyanate (HMDC) and diphenylphosphorylazide (DPPA) is a known procedure which induces inter/intramolecular bonds. These agents are generally used for fixation in histological examinations [Simionescu, et al., 1991], controlled drug release [Gohel & Amin, 1998], delaying the in-vivo degradation of [Lynn, et al., 1990] and suppressing the recipient immune response [Simionescu, et al., 1991; Gohel & Amin, 1998] to soft tissue xenografts like porcine heart valves and arteries. On the macro scale, the effects of these modifications are known to be pronounced with respect to mechanical properties like stiffness, strength and viscoelasticity [Finger, et al., 1987; Lee, et al., 1994; Davidson, 1989; Naimark, et al., 1998] as well as with respect to the denaturation temperature [Ruijgrok, et al., 1994; Horgan, et al., 1990; Moore, et al., 1996; Gavilanes, et al., 1984]. The most effective of these cross-linking agents is reported to be glutaraldehyde [Rault, et al., 1996; Jorge-Herrero, et al., 1999], which reacts with the ε-amine groups of lysine and hydroxylysine residues in the collagen. The chemical bonds induced by glutaraldehyde enhance the strength and stiffness of the collagenous tissues [Ruijgrok, et al., 1994; Rault, et al., 1996]. The penetration and reaction characteristics of glutaraldehyde are very much dependent on concentration and temperature. It is also

known that at high concentrations glutaraldehyde polymerizes on the tissue surface, forming a crust layer between the solution and the tissue [Nimni, et al., 1988]. This layer reduces further diffusion of the cross-linking agent into the tissue. In the glutaraldehyde penetration studies done in our laboratory, this fact has also been established as shown below in Figure 5.1. In these experiments, a fluorescent probe is utilized (Carboxyfluorescein Succinimidyl Ester, 5-FAM, SE: Molecular Probes, Eugene, OR), which binds to the sites within the tendon collagen (between the Lysine and Hydroxylysine residues) where glutaraldehyde molecules also attach. Therefore, the absence of fluorescence (the probe, 5-FAM, SE, is excited at 495 nm and its emission at 520nm is measured) in the tissue after exposure to a glutaraldehyde solution reveals the presence of glutaraldehyde bonding. The details of sample preparation, experimentation and sample results can be found in Appendix C. In Figure 5.1 below, the penetration characteristics of glutaraldehyde as a function of its concentration in saline and exposure time is presented. As seen in the figure, after 24 hours of exposure, the tendon is uniformly perfused with glutaraldehyde and all of the available sites are cross-linked. Therefore, there are no sites available for the fluorescent probe to attach and thus no fluorescence emission at 520 nm. On the other hand, after 15 minute exposure to 0.1% glutaraldehyde solution, there are very sharp intensity gradients at the boundaries of the tendon specimen indicating the cross-linking has not penetrated sufficiently into the tendon.

Glutaraldehyde was chosen as the strongest candidate for the preliminary studies performed to test the feasibility of using an adjuvant chemical treatment to thermotherapy. Considering the inherent cytotoxicity of this chemical at high concentrations (>5% w/v) [Nimni, et al., 1988], experiments are performed using very low concentrations (0.1-0.5%

w/v). Also a blocking agent solution (0.025M Glycine, 0.05M Sodium Borate, pH8.0) was applied after exposure to glutaraldehyde to neutralize the uncross-linked glutaraldehyde molecules during the test protocol.
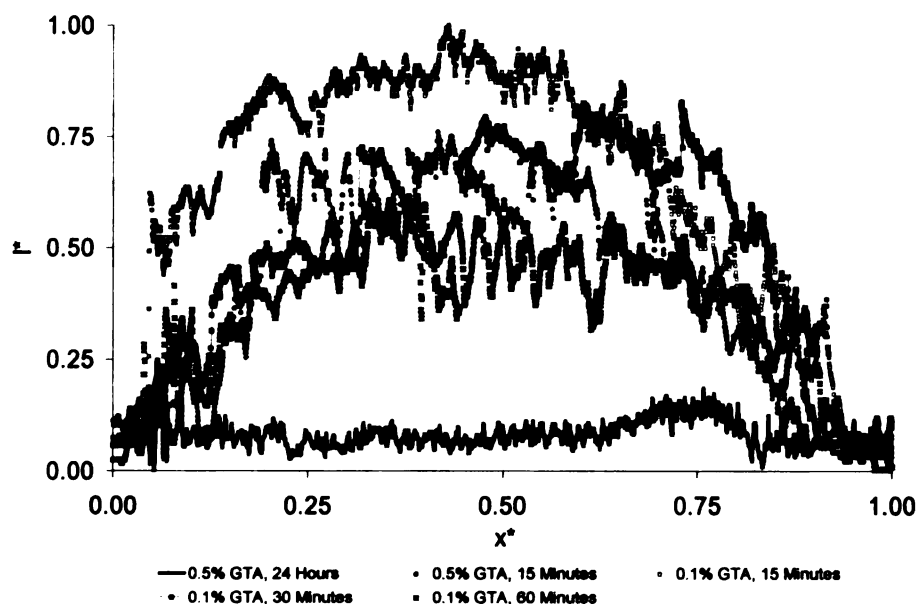
Figure 5.1: Normalized Fluorescence Intensity ($I^*=I/I_{max}$) at 520nm as a Function of Normalized Tendon Width ($x^*=x/x_{max}$).

5.1 Materials and Methods

In this section, the preliminary results of the in-vitro experiments performed to examine the feasibility of using a chemical cross-linking method in combination with thermotherapy are presented.

The experiments performed were mainly directed at quantifying the mechanical property enhancement achieved with the combined thermal-chemical treatment. After preparation and mechanical preconditioning, the specimens were heated, either immersed in a cross-linking solution or a saline solution and their responses were compared.

The specimens used were the patellar tendons of New Zealand white rabbits obtained from other researchers at MSU. A total of 30 specimens were collected from the hind legs of 30 animals. None of the animals had undergone experimentation that would affect their musculoskeletal tissues. The experimental specimens were prepared following the same protocol described in Section 2.4.1 of this thesis. The experimental setup was the same as the one described in Section 2.4.2.

The experimental procedure consisted of mechanical preconditioning which was aimed at minimizing the viscoelastic response of the tissue. The tissue was then loaded to test stress (~0.5MPa) and the testing protocol was initiated. The test stress was chosen in order to simulate physiological loading conditions and to limit the shrinkage of the specimen.

Testing consisted of three main steps. The first step was hydrothermal heating performed by circulating preheated cross-linking agent solution at a prescribed temperature in the range (65-85°C) around the specimen. In the control group however, heated phosphate buffered saline solution (PBS) instead of cross-linking agent solution was circulated. The second step was the circulation of a room temperature (24°C) cross-linking blocking agent. The cross-linking blocking agent was used to neutralize the unreacted cross-linking agent molecules therefore stopping the reaction and reducing

cytotoxicity. Temperature was monitored by three T-type thermocouples and sampled at 5Hz by a thermocouple board (DAS-TC/B, Keithey Instruments Inc., Cleveland, OH). Stress and strain data were collected at 10 Hz by an A/D board (DAS-1800-ST/DA, Keithey Instruments Inc., Cleveland, OH).

A representative temperature history of the specimen and the shrinkage response obtained is presented below in Figure 5.2. At the end of the testing protocol, a tensile test was applied on the specimen until failure. The specimens were then flash frozen and saved until fluorescence testing was performed to determine the extent of penetration of cross-linking agent.
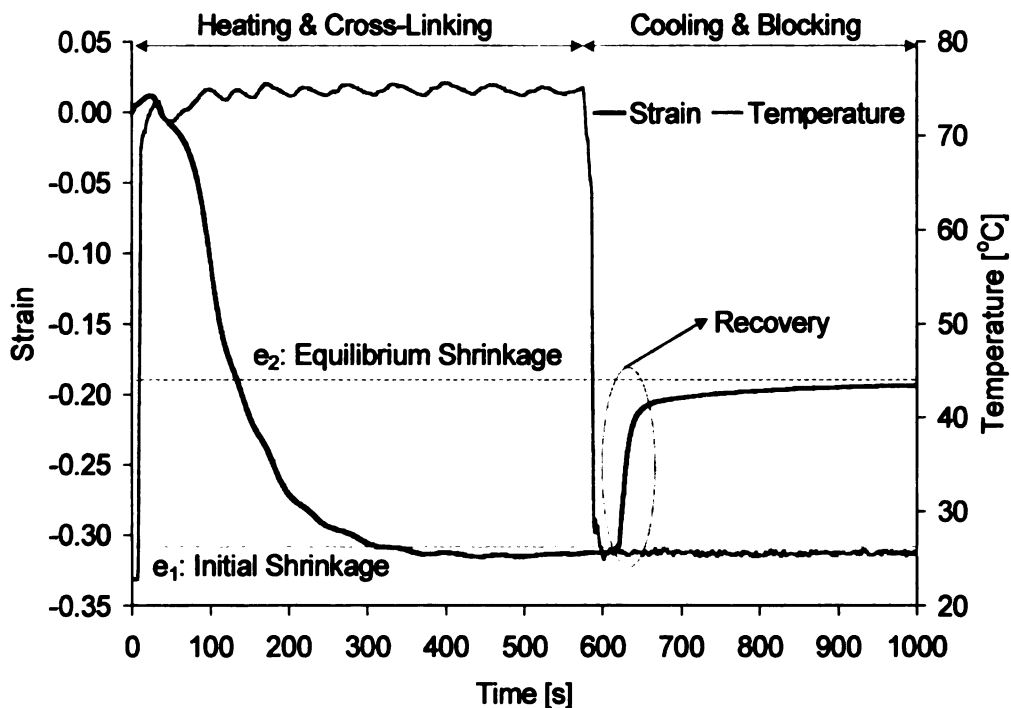
Figure 5.2: Characteristic Heat-Induced Response of Rabbit Patellar Tendon Specimen

5.2 Results

For each specimen tested, the variation of strain with respect to temperature was recorded and the initial, e_1, and equilibrium shrinkage values, e_2, as well as the recovery ratio, R, were calculated. The post-treatment tensile modulus, E, was calculated from the slope of the stress-strain data obtained during the tensile tests. The experimental groups and their respective controls completed are presented in Table 5.1 on page 112.

Table 5.1: Experimental Groups

Group	Exposure Time [s]	Treatment Tempearture [°C]	Heating Solution	Blocking Solution
1 (n=5)	600	75	0.5% GTA †	0.025M Gly ‡
2 (n=5)	600	80	0.5% GTA	0.025M Gly
3 (n=5)	600	85	0.5% GTA	0.025M Gly
4 (n=5)	1200	75	0.5% GTA	0.025M Gly
5 (n=5)	1200	80	0.5% GTA	0.025M Gly
6 (n=5)	1200	85	0.5% GTA	0.025M Gly

† 0.5% [w/v] Phosphate Buffered Glutaraldehyde Solution, pH7.4

‡ 0.025M Glycine, 0.05M Sodium Borate, pH8.0

5.2.1 Equilibrium Shrinkage, e_2

Equilibrium shrinkage, e_2, is the value of final shrinkage reached after cooling the tissue back to room temperature (Figure 5.3). For both groups (cross-linked and control),

there was an apparent exponential relation between the temperature of the treatment and the resulting strain (Figure 5.3). This agrees with the literature [Chen & Humphrey, 1998a]. The results also showed that except the 85°C treated group, there was not a significant difference between the glutaraldehyde treated and control groups in terms of the equilibrium shrinkage achieved. This implied that the glutaraldehyde treatment did not have a detrimental effect on the final shrinkage achieved (even yielded higher values for the 85°C group).
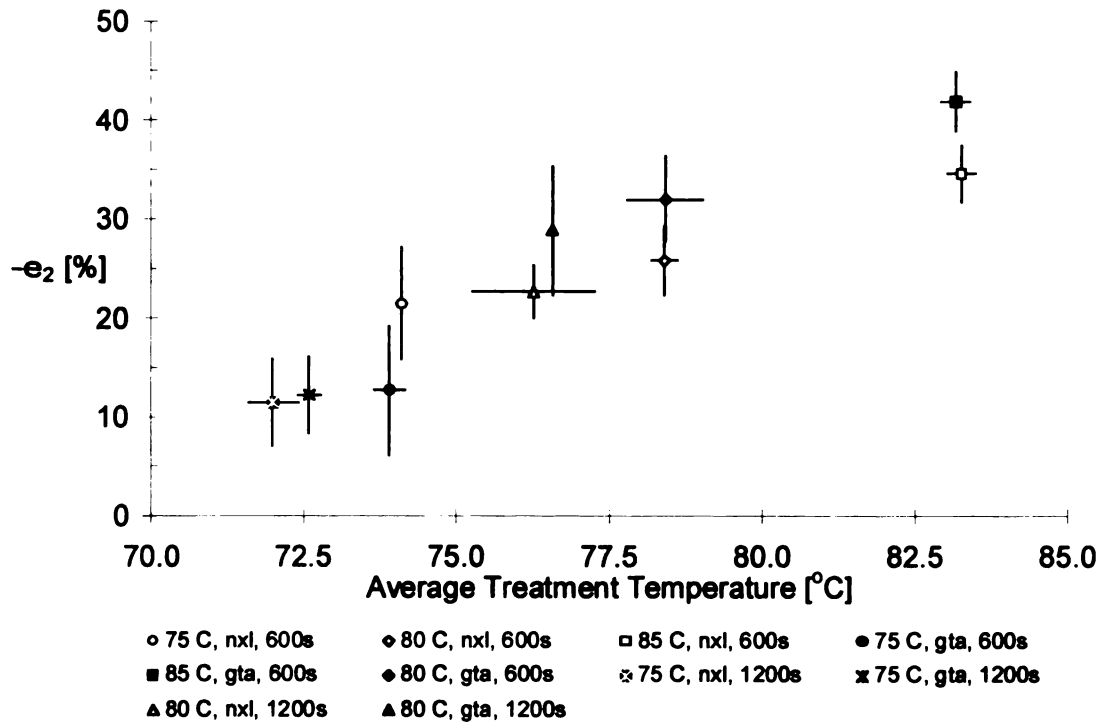
Figure 5.3: Variation of Equilibrium Shrinkage, e_2 with Treatment Temperature and Exposure Time

5.2.2 Recovery Ratio, *R*

As explained in detail above, following heating, when the tissue was cooled back to a lower temperature some of the initial shrinkage, e_1, recovered and the tissue slowly converged to its equilibrium shrinkage value, e_2 (Figure 5.2). This is due to re-naturation, the basic mechanism of which is the refolding of the partially unfolded tropocollagen helices.
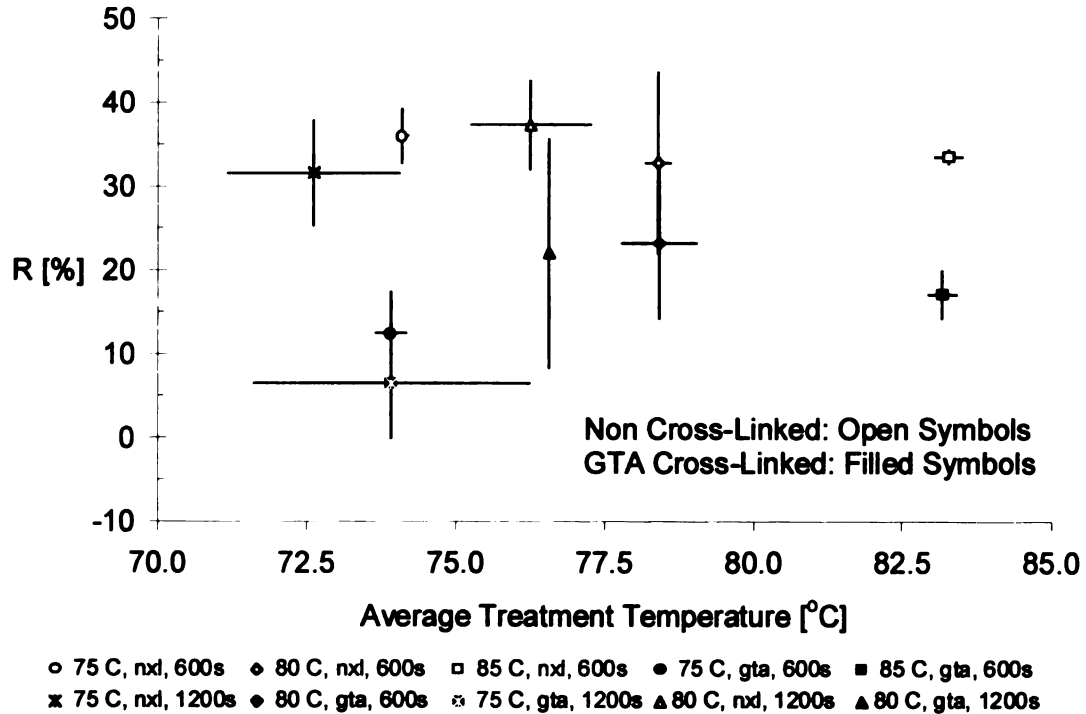
Figure 5.4: Variation of Recovery Ratio, *R,* with Treatment Temperature and Exposure Time

The ratio of the amount of tissue expansion observed at room temperature to the initial shrinkage observed at high temperature is defined here as the recovery ratio, *R.* The

results of the preliminary studies indicated that for all of the experimental groups, the recovery of glutaraldehyde cross-linked tissues were less than their controls by ~50% (Figure 5.4). This novel finding has very important implications for HACS procedures. To a great extent, the tissue will be fixed at its initial shrunken state. Therefore it will be easier for the surgeon to assess the amount of irreversible shrinkage achieved.

5.2.3 Tensile Modulus, E

Figure 5.5 summarizes the results of the tensile tests applied to the specimens after the completion of thermal-chemical treatment. For all of the experimental groups examined ($75^{\circ}C \leq T_{treatment} \leq 85^{\circ}C$, $600 \leq t_{treatment} \leq 1200s$), the glutaraldehyde treated specimens were stiffer than their controls ($E_{GTA}/E_{NXL} > 1$). The increase in tensile modulus ranged from 20% to 200% depending on the thermal treatment applied. This important finding established the fact that the application of cross-linking agents in conjunction with heating can be used to counteract the degradation of mechanical properties caused by heating.

It is reported that after subfailure levels of strain damage, the stiffness of the tissues drops significantly [Panjabi, et al., 1996]. The detrimental effects of thermotherapy on mechanical properties is well-established and is a function of the severity of the treatment [Panjabi, et al., 1996; Schaefer, et al., 1997; Berend, et al., 1996; Vangness, et al., 1997; Hecht, et al., 1999]. The combined effect of strain damage and thermotherapy reduce the stiffness to approximately 10-15% of its normal value. This combination of strain damage and heating is identical to the conditions that exist at the time of the

application of thermotherapy to a dislocation injured shoulder capsule. The stiffness increase achieved by chemical therapy as shown here is therefore very important for the efficacy of HACS procedures. These results prove the feasibility of utilizing chemical therapy as an adjuvant therapy to thermotherapy.
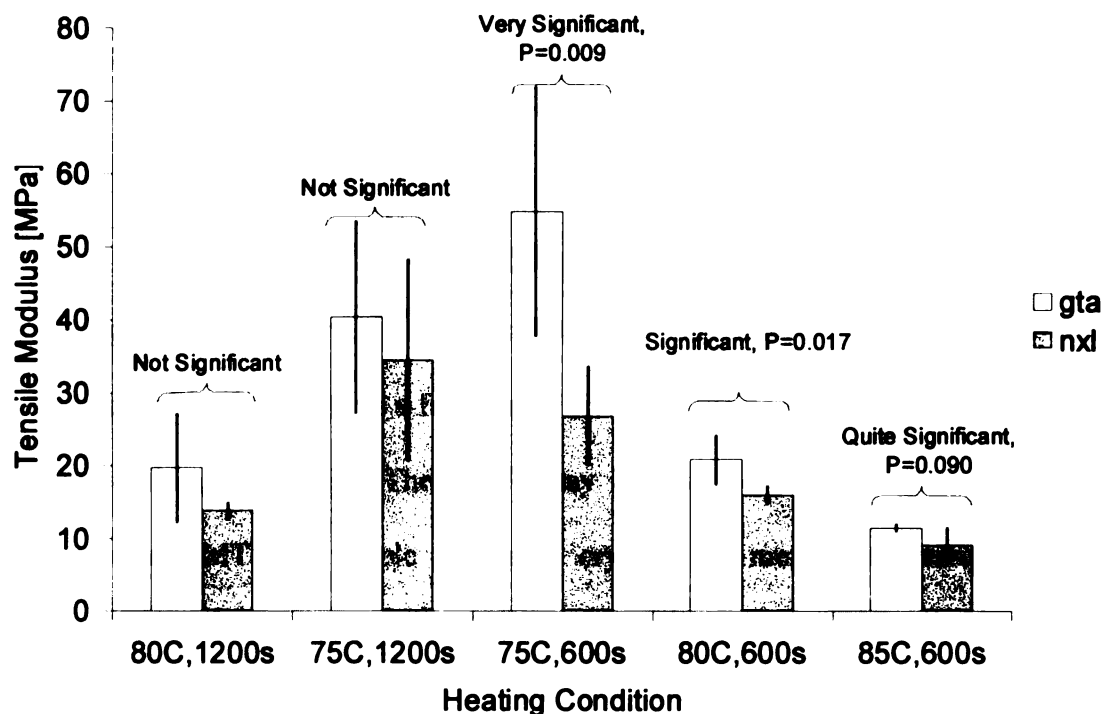
Figure 5.5: Variation of Modulus Ratio, E with Treatment Temperature and Exposure Time

5.3 Cytotoxicity

The results of the preliminary in-vitro experiments showed that the proposed combined thermal-chemical treatment was superior to thermotherapy alone. Using this method, 50% reduction in recovery and up to 200% increase in tensile modulus were

achieved. The next step was to confirm these findings in a living system to address the issues such as cytotoxicity and long term efficacy of the suggested cross-linking protocol. These studies were performed in collaboration with Dr. Steven Arnoczky of the College of Veterinary Medicine at MSU.

The first step of the cytotoxicity studies was the tissue culture tests performed with patellar tendon fibroblast cells. The control groups of these cells were exposed to culture media and PBS only. The experimental cell populations were subjected to different concentrations of glutaraldehyde for different exposure times. Some groups underwent blocking agent treatment after glutaraldehyde exposure. Then an MTT assay (Product No. M5655, Sigma Chemical Co., Saint Louis, MO) was used to determine the changes in the metabolic activity of the cells as a function of cross-linking agent concentration, exposure time and blocking agent type. The MTT assay is based on the cleavage of the yellow tetrazolium salt MTT to purple formazan crystals by metabolic active cells. The solubilized formazan product is quantified using standard microplate absorbance readers.

Six to seven tissue culture wells were used for each experimental group and 50,000 fibroblast cells were used in each well. All of the chemicals and the PBS used in the experiments were filtered (filter pore size = 0.2μm) for sterilization and heated to 37°C to eliminate heat shock on the cells. Through an automatic optical density reader opearated at 540 nm, the emission from the formazan crystals at each well (which is a measure of metabolic activity of the cells) was measured and the resuls are presented below in Figure 5.6. Unfortunately, these results indicated that even at these low concentrations, the cytotoxic effects of glutaraldehyde was very significant and that in order to apply chemical enhancement methods as an adjuvant therapy, a better approach would be to

examine the feasibility of using (mechanically less effective) non-cytotoxic agents. However, one important point that should not be disregarded is that even 20 minutes exposure to saline solution killed 45% of the cells.
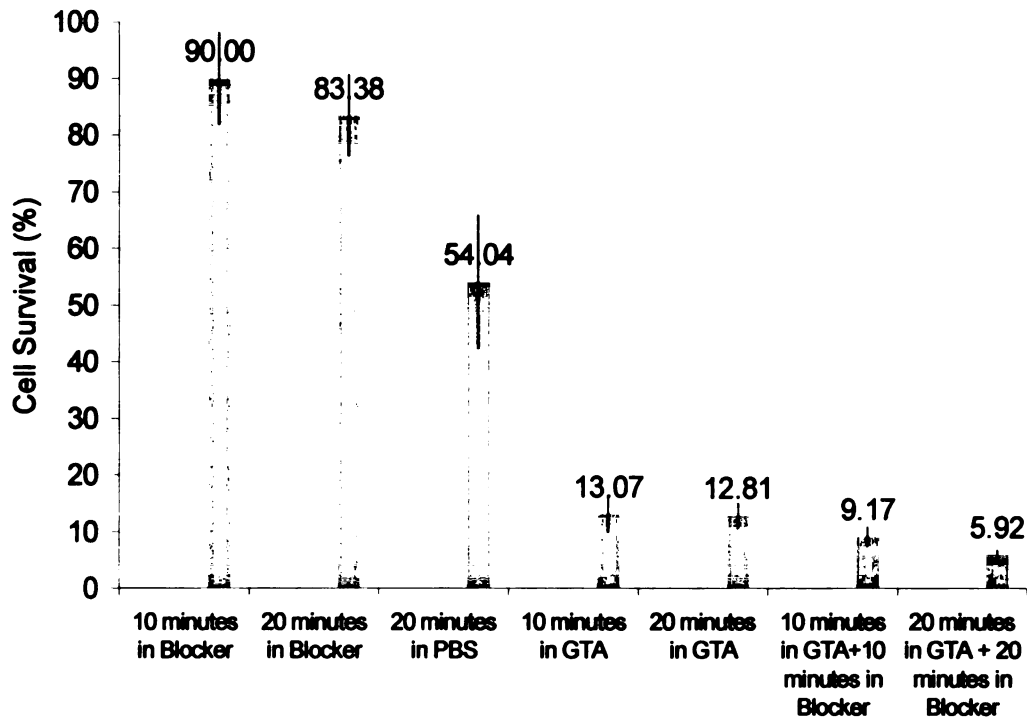
Figure 5.6: Results of Cytotoxicity Tests with Rabbit Patellar Tendon Fibroblasts

5.4 Other Studies

Similar cross-linking experiments were performed (following the same experimental protocol described in Section 5.1) by replacing glutaraldehyde with either 1-ethyl-3-(3-dimethylaminopropyl)-carbodiimide (EDC) or hexamethylene diisocyanate (HMDC) in the saline solution but the resultant mechanical property enhancement was not significant. An alternative process; photo-crosslinking of the tendon specimens

preconditioned by immersion in a sucrose solution (90g/L) followed by methylene blue or

riboflavin solution immersion and exposure to UV light was also tried without success.

Chapter 6: Conclusions

Over the last decade, sub-ablative thermotherapy has found ever-increasing application in orthopedic and ophthalmologic surgery. The therapy aims at altering the configuration of the strain-damaged, pathological or congenitally anomalous soft tissue in order to re-establish stability and function. The basic mechanism of this therapy is the heat-induced denaturation of the underlying collagenous network of the soft tissues. Heat-induced denaturation causes microstructural transformation of the collagen molecule and produces a thermal stress field along the direction of the collagen fiber orientation. The thermal stress field formed changes the configuration of the tissue proper.

The initial wide-spread use and short-term clinical success of these therapies are being questioned by the recent availability of the long-term clinical results in the literature [Anderson, et al., 2002]. The reports reveal the unpredictability of the outcome of the therapy and suggest more careful patient selection (for instance, the direction of the instability -anterior, posterior or multidirectional- is thought to be an important factor in determining the outcome of thermotherapy applied for the treatment of shoulder instability). There are also other major factors that contribute to the phenomena; such as the non-standard, unoptimized clinical practice of using a variety of heating modalities, patterns and techniques.

A thorough and careful examination of the literature revealed that most of the seemingly contradicting results in the literature can be explained and the unpredictability of the clinical outcome can be minimized by understanding the macroscale tissue response to the heat-induced microstructural transformations and by developing models, and simulation tools to be used in the analysis of the clinically important parameters and the design of optimized heating protocols. Therefore, the research presented here was aimed at establishing the scientific basis and developing the tools to increase the safety and efficacy of the *Sub-Ablative Thermotherapy* procedures applied to treat instabilities of the knee, ankle and shoulder joints and in the elimination of discogenic pain in the spine.

Proceeding the Introduction Section, where the background was presented, this thesis was divided into four main parts. In the first part, constitutive equations describing the heat-induced mechanical response of collagenous tissues were established by means of in-vitro experimentation with a model soft tissue. In the second part, the sub-ablative thermal damage created in the soft tissue by clinically applied heating modalities was examined using numerical simulations (through finite element analysis). In a similar fashion, in the third part of the thesis the heat-induced mechanical response of collagenous tissues were simulated. In the last part, feasibility of applying adjuvant, chemical enhancement methods to thermotherapy were examined.

The clinical relevance of the study presented in this thesis was explained in the Introduction Section (Chapter 1). The advantages and disadvantages of Sub-Ablative Thermotherapy in treating joint instability were presented and it was concluded in this section that detailed basic science studies were required to increase the efficacy of this therapy.

In the first main part of the thesis (Chapter 2), heat-induced mechanical response of the collagenous tissues was characterized by means of in-vitro experimentation using a model soft tissue; New Zealand white rabbit patellar tendon. Through thermal (isothermal heating and DSC studies) and thermomechanical analyses, the resultant gross mechanical response of the tissue to thermal stimuli was examined. Three distinct heat-induced response regimes were identified. These regimes are:

1. Irreversible Elongation: Elongation up to 0.5% strain accompanied by an increase in tensile modulus ($E \sim 125\%$ of the native tendon calculated at the reference state).

2. Irreversible Shrinkage: Decrease in the overall length of the sample in the dominant direction of fiber orientation accompanied by an exponential decrease in tensile modulus (with respect to the native value) and disappearance of viscoelastic response.

3. Reversible Shrinkage: Defined by thermoelastic response where shrinkage was completely reversible. Upon returning to room temperature, the tissue regained its pre-heating length. In this regime, there was no decrease in tensile modulus with further heating.

The first regime in the heat-induced collagenous tissue response (Irreversible Elongation regime, which corresponds to a slight elongation of the sample with improving mechanical properties) may be useful in developing new soft tissue thermal treatments aimed at increasing the tissue mechanical properties with minimal thermal strain formation. It may also be used in designing curing protocols for artificial collagen scaffolds used either as drug carriers or tissue substitutes.

Independent of the stress state, for all of the experimental conditions examined, formation of thermal strain and the variation of the mechanical properties with accumulated thermal damage were shown to collapse on respective master curves. An Arrhenius damage integral representation of soft tissue thermal history was shown to be adequate even when mechanical stress was present. It was postulated that the effects of thermal and mechanical history (in the load and temperature ranges examined) could be separated and the constitutive equations describing the heat-induced tissue response could be derived. It was suggested that the *delay* seen in the denaturation response of the collagenous tissue with increasing mechanical load was caused by a decrease in the activation entropy of denaturation, but that the denaturation enthalpy remained unchanged.

It was shown that the *mechanical success* (restoring the function) of sub-ablative thermotherapy (in the treatment of joint instability) was dependent on two major parameters. These were: the kinematic stability achieved by re-establishing the kinematical equilibrium of the joint (in terms of the locations and directions of the forces carried) and the structural stability of the tissues comprising the joint (in terms of their strength and resistance to deformation). The results of this research suggested that even though kinematic stability might be restored by thermotherapy (and that the mechanically deformed, elongated tissue could be brought back to its pre-injury length by heating), structural stability of the tissue was compromised (due to degradation of mechanical properties). This finding has very important clinical implications (at least during the short post-operative period before the onset of the healing response); the existence of a trade-off between the kinematic and the mechanical stability of the joint. It was shown that

overheating can be as ineffective as underheating and that there existed an optimum point (from a mechanistic perspective) in between. For instance, upon heating, two distinctly different final states of a tendon tissue could be reached: 8% shrinkage (from its native length) of the tissue resulting in a state where the tissue exhibited 50% of its initial tensile modulus or 16% shrinkage with a tissue that retained only 25% of its initial tensile modulus (data taken from Figure 2.23). Here, the important questions to be answered are: "Is this (thermally treated) tissue going to be able to carry the same physiological forces it used to carry before the injury without rupturing or stretching beyond its physiological length?" and "In which one of those states presented above is the tissue more likely to be both stable and functional?". In terms of maximization of the thermal stress developed in the heat-treated tissue, the mechanical optimum was shown to correspond to 12% shrinkage in a uniformly heated, dense, oriented collagenous tissue (such as tendon and ligament). This result established the first step in answering the questions presented above.

The results presented here and the conclusions drawn are valid for a uniformly heated, dense, oriented collagenous soft tissue. In clinical application of thermotherapy however, there are additional factors to be considered. These are the thermal and thermomechanical strain gradients formed due to non-uniform heating of the tissue as well as due to the non-uniformity of the tissue structure (spatial variation of collagen fiber orientation and gross tissue geometry). Within a locally heated tissue, the thermal damage field is not uniform. There are also distinct differences among the thermal damage fields created by hydrothermal, radiofrequency or laser heating due to the differences in their modes of action. Hydrothermal heating is mainly a surface heat transfer phenomena; heat

penetrates into the tissue by convection due to the circulation of high temperature liquid at the tissue-liquid interface. The mechanism of radiofrequency heating, on the other hand, is based on increased mechanical friction (and therefore increased heat generation) among the polar molecules, which are forced to oscillate by the rapid changes in the magnetic field created by the high frequency alternative current passing through the medium. In the case of laser heating, the light energy absorbed by different chromophores (depending on the wavelength of light, starting with certain amino acids in the UV range, ~193nm, all the way to water absorption in the IR range, ~2.96μm) inside the tissue and released as heat. Additional factors affecting the thermal damage field within the tissue are related to the the applicator (probe) geometry design, power setting and application patterns.

Therefore, in the second part of the thesis, the sub-ablative thermal damage created in the tissue by different heating modalities was examined through finite element analysis and the effects of different parameters (such as power setting, probe sweep speed and surface convection) were examined. In the FEA of thermal damage penetration, it was assumed that all of the tissue properties except heat capacity was constant.

Through FEA it was shown that there were significant differences among the clinically applied heating modalities. Heating imposed by bipolar radiofrequency is mainly superficial (confined within the top layers of the tissue so long as the treatment temperatures are sub-ablative). However, in monopolar radiofrequency heating, the alternating current flows directly through the tissue between the active electrode (located at the tip of the radiofrequency probe) and the ground electrode (which is placed over the abdomen of the patient in the clinical setting and underneath the target tissue during in-vitro experimentation).

Other factors that can be examined using the simulation tool developed in Chapter 2 include the effects of the laser wavelength, beam diameter, power setting, pulse width and frequency and laser probe speed. In the clinical setting, lasers are usually pulsed in order to decrease the risk of creating hot spots in the target tissue. Due to this pulsating behavior, the thermal damage accumulated in the tissue is not uniform but rather in the form of high damage "islands" surrounded by low damage regions (as seen in Figure 7, Insert 6). The effect of this type of heating on the mechanical properties and the healing response of the tissue proper have not yet been examined.

In the third part of this thesis, a computer simulation tool for the heat-induced mechanical response of collagenous tissues was developed. In developing the algorithm for this simulation, it was postulated that the gross response of a multi-dimensional dense collagenous tissue could be predicted from the mechanical response of the representative elementary volumes of a lower dimension. For instance, the response of the tissue simulated in two-dimensions was a combined outcome of the representative elementary volumes whose characteristic responses were dominantly in one dimension (along their dominant collagen fiber orientation). By the use of this algorithm, the effects of thermal damage accumulation, the shape of the thermal lesion formed and the final mechanical configuration and the state of collagenous tissue could be modeled. This algorithm is the product of a novel approach and can be used to predict the heat induced responses of collagenous tissues having very complex geometries subjected to very complex heating conditions. Future studies should focus on quantifying the applicability range of this algorithm. The limited experiments performed indicated that the validity was confined to small displacements.

It is interesting that even though soft tissue thermal therapy is being applied rather widely to treat shoulder, knee and ankle instabilities and even discogenic pain, the real mechanism responsible for re-establishing joint stability is not fully understood. According to some researchers, collagen denaturation and the resultant mechanical tightening is the major factor, but others claim that it is the heat-stimulated biological repair mechanisms that "do the job". Additionally, it is stated as a major concern that the temperatures required to initiate collagen denaturation are fatal for the cells. It is obvious that the lack of viable cells at the site of thermal injury delays the healing response of the tissue. However, before reaching a verdict, the desirability of a fast healing response should also be questioned. A very fast healing response could render the heat-treatment ineffective if the heat-treated (and thus modified) tissue is immediately replaced with new tissue or remodeled. On the other hand, if an accelerated response is desired, pulsating lasers or radiofrequency heating applied in a grid pattern could serve this purpose by leaving safe zones for cells surrounded by thermally treated zones. These zones would serve as safe heavens for the cells to survive through the procedure and facilitate their migration to the "damaged" regions to start modeling immediately after thermotherapy.

Thermal therapy is currently applied to cause tissue shrinkage, thus producing joint stabilization. However, heating causes significant reduction in the mechanical properties of the tissue (tensile modulus and failure strength). Consequently, adjunct methods that could retain the benefits of thermal therapy while minimizing or eliminating the degradation of mechanical properties are of interest. In the last part of this thesis, the feasibility of adapting a thermal-chemical therapy protocol was examined. This combined method was offered as a means of maintaining optimum joint stability without

compromising mechanical integrity of the tissue. Results of in-vitro experiments performed on an animal model (New Zealand rabbit patellar tendon) demonstrated the positive impact of combining chemical treatment with thermotherapy. The contribution of the chemical treatment using glutaraldehyde as a cross-linking agent may be summarized briefly as a reduction of strain recovery by as much as 50% and an increase in the tensile modulus by as much as 100% when compared to thermotherapy alone. However, preliminary tissue culture tests performed on patellar tendon fibroblasts showed that with increasing glutaraldehyde concentration, the potential cytotoxicity of the chemical treatment increased. This indicated an apparent trade-off between the efficiency of the chemical treatment protocol applied and its cytotoxicity. Future research should focus on defining optimal thermo-chemical means to produce safe and efficacious HACS procedures that produce the desired tissue shrinkage with enhanced mechanical properties through sub-ablative thermotherapy with non-cytotoxic cross-linking agents.

Application of heat and cold for treatment purposes is not novel, but developing the means of controlling and localizing its effects is. In summary, through the research presented in this thesis:

1. Constitutive equations governing the heat-induced mechanical response of dense, oriented, uniformly heated collagenous tissues were defined.

2. An Arrhenius damage integral representation of thermal damage was shown to be adequate irrespective of the stress-state of the collagenous tissue.

3. Through experimental analysis, it was shown for the collagenous tissues that there are three distinct heat-induced mechanical response regimes.

4. It was shown that irrespective of the stress-state, heat-induced shrinkage response and tensile modulus variation follow universal curves.

5. It was concluded that for sub-ablative thermotherapy procedures aimed at treating joint instability, there is a trade-off between the kinematic stability of the joint established by shrinking the lax capsuloligamentous tissues and the mechanical stability of the joint tissue compromised by the degradation of the mechanical properties.

6. Existance of a mechanical optimum for thermal treatment corresponding to the maximum thermal stress created in the uniformly denatured, dense collagenous tissue was demonstrated and was shown to correspond to an equilibrium shrinkage of approximately 12%.

7. Clinically applied heating modalities used in sub-ablative thermotherapy were shown to create distinctly different thermal damage fields within the target tissue.

8. Discrepansies and contradictions among the in-vitro experimental results and the clinical reports in the literature were shown to be caused mostly by different heating modalities used and different levels of denaturation reached in the target tissue.

9. Non-uniform thermal damage fields created by low frequency pulsed lasers could prove useful in accelerating the repair of the treated tissue by leaving low damage zones between high damage zones (where fibroblasts may survive), if such a response is desired.

10. A hybrid simulation algorithm comprised of in-vitro experimentation and finite element analysis was developed to simulate the heat-induced responses of collagenous

tissues in multi-dimensions. This simulation tool is believed to be very useful in pre-treatment therapy planning and optimization of therapies.

11. It was shown that chemical enhancement techniques are feasible candidates for developing adjuvant therapies for sub-ablative thermotherapy in minimizing the adverse mechanical effects of the said therapies.

12. The thermal and chemical treatment protocols developed here have the potential to be applied to the manufacture of artificial tissues and protein based drug carriers.

This thesis laid the foundation for modeling the heat-induced mechanical responses of collagenous tissues through development of novel in-vitro experimentation and simulation techniques. It also reached out to explore different avenues in adapting engineering techniques to medical problems, however it should be regarded as a beginning rather than an end.

Chapter 7: Directions for Future Research

The thermomechanical response simulation algorithm developed in this thesis was based on the correlations derived from the results of one-dimensional, in-vitro mechanical experimentation with rabbit patellar tendon tissues. In order to be able to accurately simulate the heat-induced mechanical response of a collagenous tissue, the analyses established here should be extended to multi-dimensions and should take into consideration the non-homogeneous nature of the tissues. This requires multi-dimensional mechanical testing combined with real-time strain measurement and structural information. The strain measurement may be performed using optical methods (such as particle tracing) which trace the displacements of predetermined points on the tissue surface while the tissue is heated in a controlled fashion. Coupled to this system, optical (birefringence and/or optical coherence tomography (OCT)) or magnetic resonance imaging techniques can also be utilized to collect structural information (before the experiment in order to determine the collagen fiber orientations as well as the heat-induced structural variations during the experiment). Data collected from these thermomechanical experiments may then be used to determine the anisotropic constitutive relationships in multi dimensions as a function of the thermal damage accumulated. These experiments can also be modified to examine the effects of various factors on the heat-

induced response characteristics of collagenous tissues (which are not examined in the research presented here) such as the tissue hydration level, adjuvant chemical cross-linking and permanent mechanical damage (microstructural mechanical damage induced prior to experimentation in order to simulate a mechanical injury). It is believed that both tissue hydration level and pre-existing microstructural mechanical damage affect the heat-induced response of the collagenous tissues.

The same setup mentioned above, may also be modified for experimentation with clinically applied heating modalities (such as monopolar/bipolar radiofrequency and Ho:YAG laser). A setup involving multiple CCD cameras may be utilized to determine the configuration change of the sample tissue specimen when it is subjected to localized heating. OCT, birefringence or MRI data collected during experiments can also be used to verify the thermal damage penetration values predicted by the FEA software developed as a part of this thesis.

After these studies are completed, the next challenge would be to apply the technology developed to the clinical setting.

Appendix A: Eshelby's Method

In Eshelby's Method [Eshelby, 1957], it is assumed that the stresses created in a continuum (Figure A.1), $\mathcal{R}$, due to a phase transformation (in this case denaturation) in a subregion, $\mathcal{N}$ can be calculated using the stress-free transformation strains, ε_{kl}^{T}, formed in $\mathcal{N}$ when $\mathcal{N}$ is isolated from $\mathcal{R}$.
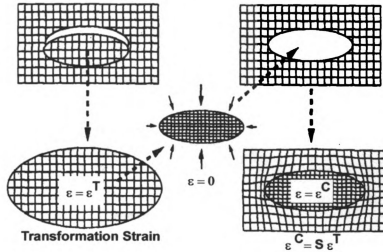
Figure A.1: Eshelby's Method for Stress-free Transformation of an Ellipsoidal Region
[Clyne & Withers, 1993]

These transformation strains are related to the resultant potential stress field, σ_{kl}^{T}, by:

$$\sigma_{ij}^{T} = C_{ijkl}^{T} \cdot \varepsilon_{kl}^{T} \qquad \qquad \text{A.1}$$

where the material constants, c_{ijkl}^{T}, are those of the transformed state (in this case the denatured tissue). In Eshelby's Method this stress field is relaxed later combining the regions $\mathcal{R}$ and $\mathcal{N}$ and letting them assume their final stress states.

R

Original (Reference) Configuration
Configuration "i"

$S_i . V_i$ R*

Stress-free Transformation

R*

Deformed (Present) Configuration
Configuration "j"

$S_j . V_j$

Transformation to
Original Configuration

R*

Original (Reference) Configuration
with Surface Tractions
Configuration "i"

$S_i . V_i$

Assembly

R

Configuration at t=0
Configuration "i"

$S_i . V_i$ R*

Relaxation

R

Configuration as t→∞
Configuration "k"

R*

$S_k . V_k$

Figure A.2: Transformation Stresses and Determination of the Final Configuration

In Chapter 4 of this thesis, following the same rationale used to develop Eshelby's Method [Eshelby, 1957], it is assumed that the global effects of the transformation stresses created in a sub-region, R^*, enclosed by a region R can be calculated from the stress-free transformations of the sub-region R^* when it is completely isolated (Figure A.2). According to this algorithm, if a stress field is formed in subregion R^*, (defined by a surface, S_i, and volume, V_i, in its reference configuration) possibly due to structural transformations (such as denaturation), one way to solve the resultant stress field is to start by completely isolating the subregion R^* from region R and allowing it to undergo stress-free transformations. In this isolated, transformed state (configuration "j"), the sub-region R^* is assumed to be defined by the surface S_j and the volume V_j which are different from those at the reference configuration (configurat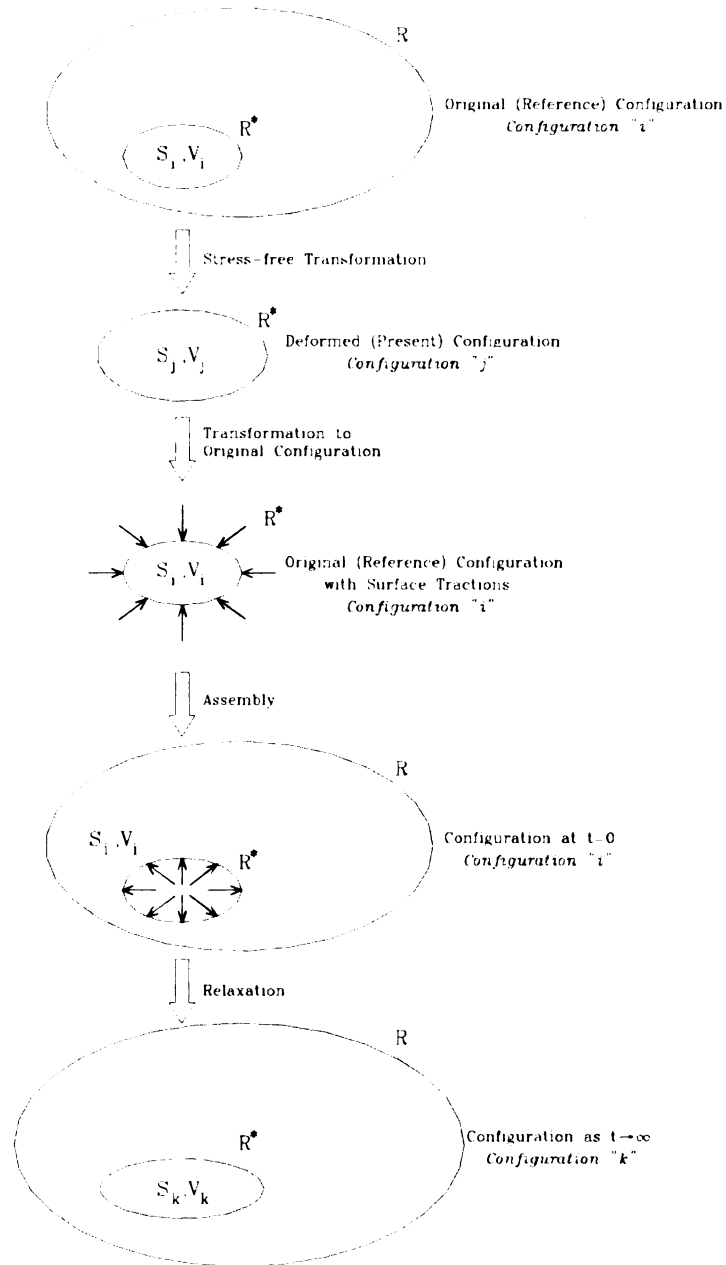ion "i"). Later, surface tractions are applied to bring the subregion R^* back to its original configuration defined by the surface, S_i, and volume, V_i. Note that the surface tractions applied are functions of the stress-free deformation sub-region R^* undergoes and the material properties of sub-region R^* in the transformed state. Next step is the assembly step where the subregion R^* and the region R are united again and equal and opposite traction forces are applied on the surface S_i, causing deformation of region R. This step corresponds to a new reference state (where t=0) since the shape of the subregion R^* has not been allowed to change yet. In order to determine the final configuration of the region R (which now completely encloses the sub-region, R^*) the constraints on the surface between R and R^* are removed and the steady state (equilibrium) solution to the equations of elasticity infinity is sought through transient analysis.

Appendix B: User Subroutines

Below a typical user subroutine coupled to the main body of the MARC FEA code is presented. The first subroutine (plotv) is used to calculate the Arrhenius Damage Integral for each node in the mesh during transient analysis. The second subroutine (flux) is used to define a moving Gaussian heat source.

B.1 Subroutine Plotv:

```
        subroutine plotv(v,s,sp,etot,eplas,ecreep,t,m,nn,layer,ndi,

    *   nshear,jpltcd,vhistory)

        implicit real*8 (a-h,o-z)

        save incort,v1,dt

        dimension s(*),etot(*),eplas(*),ecreep(*),sp(*),v1(100000,8),

    *   dt(100000,8),incort(100000,8)

        include '/home/uz/aksanalp/marc/creeps'

        include '/home/uz/aksanalp/marc/concom'

        real*8 incort,v1,dt,damagep,tempal

        save incort,v1,dt
```

```
tempal=t

if (inc.eq.0) then

  v=0.0

  v1(m,nn)=v

  incort(m,nn)=0

  return

endif

if (tempal.lt.311) then

  v1(m,nn)=0

  v=v1(m,nn)

  return

else

 damagep=(198.1498-67584.0/tempal)

  if (damagep.gt.0) then

    v1(m,nn)=v1(m,nn)+ABS(timinc)*EXP(ABS(1.0*damagep))

  else if (damagep.lt.0) then

    v1(m,nn)=v1(m,nn)+ABS(timinc)/EXP(ABS(1.0*damagep))

  else if (damagep.eq.0) then

    v1(m,nn)=v1(m,nn)+ABS(timinc)
```

```
        endif

        v=v1(m,nn)

        return

        endif

        end
```

B.2 Subroutine Flux:

```
        subroutine flux(f,temflu,mibody,time)

        implicit real*8 (a-h,o-z)

        save maxtemprt,incrementinfo

        dimension mibody(1),temflu(6),maxtemprt(10000,10),

      * incrementinfo(10000)

        include '/home/uz/aksanalp/marc/creeps'

        include '/home/uz/aksanalp/marc/concom'

        settemperature=75.0+273.15

        settemperaturehys=2.5

        waittime=1.0
```

```fortran
      if (time.le.waittime) then

       vel=0.0

      else

       vel=0.002

      endif

      EMAX=40.0

      ro=1.17E-3

      if (inc.eq.0) then

        do 2 J=0,10

         do 1 I=0,10000

           maxtemprt(I,J)=0.0

           incrementinfo(I)=0.0

1     continue

2     continue

      endif

      incrementinfo(inc)=ncycle

      if (ABS(temflu(5)).lt.1.22E-3) then

      if (time.le.waittime) then

      if (temflu(4).ge.0.0) then
```

```fortran
if (ABS(temflu(4)).lt.50.0E-6) then

maxtemprt(inc,ncycle)=temflu(3)

      endif

      endif

      else

   if (temflu(4).ge.0.0) then

   if (ABS(temflu(4)-vel*(time-waittime)).lt.50.0E-6) then

   maxtemprt(inc,ncycle)=temflu(3)

   endif

   endif

   endif

   endif

   if (inc.gt.0) then

   if (ncycle.eq.1) then

   temperaturediff=settemperature-maxtemprt((inc-1),

*  incrementinfo(inc-1))

   else

   temperaturediff=settemperature-maxtemprt(inc,(ncycle-1))

   endif
```

```
      endif

      if (temperaturediff.gt.settemperaturehys) then

       coordx=temflu(4)-vel*(time-waittime)

        coord=coordx**2+temflu(5)**2+temflu(6)**2

         f=EMAX*ro/(12.57*(coord**2))

        else

         f=0.0

      endif

      return

      end
```

Appendix C: Determination of Glutaraldehyde Penetration

C.1: Experimental Protocol

The samples are flash frozen in liquid nitrogen and cross-sectional samples at thicknesses of 25, 50, 100, 150 μm are cut using a cryotome.

The samples are kept hydrated by placing them in tissue culture wells that are filled with saline solution.

The wells are drained and filled with 1.5 ml of 0.25 mg/ml 5-FAM, SE and 1.5 ml of 0.15M sodium bicarbonate solution.

After 1 hour, the reaction is terminated by draining the wells and filling them with 3ml of 1.5M Hydroxylamine hydrochloride.

After 1 hour, the samples are washed twice with saline solution and mounted on microslides using a non-fluorescing mounting medium.

The tissue sample mounted on a microslide is excited at 495 nm and the emission at 520nm is captured by a high sensitivity CCD camera.

At 35 times magnification the tissue is scanned along the axis of cross-linking agent penetration and successive fluorescence and normal transmitted light images are collected at 0.5mm increments.

The images are merged and the fluorescence intensity variation along the width of the tendon is measured using the ImagePro software. The background emission is

suntracted and the intensity is normalized with respect to maximum fluorescence measured.
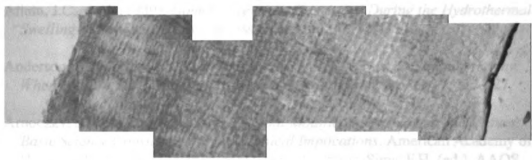
C.2: Sample Merged Images

Figure C.1: Transmitted Light Microscopy Across the Width of the Tendon Specimen
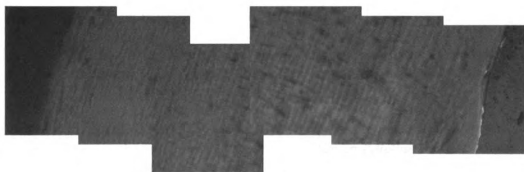

Figure C.2: Fluorescent Light Microscopy (520nm) Across the Width of the Same Tendon Specimen

BIBLIOGRAPHY

Aksan, A. & McGrath, J.J. (2002). *Thermomechanical Analysis of Soft Tissue Thermotherapy.* Journal of Biomechanical Engineering (*in review*).

Aksan, A., Nielubowicz, D.S., McGrath, J.J. (2001). *Modeling the Thermal Histories of Collagenous Tissues Subjected to Different Heating Modalities.* HTD-24433, Proceedings of 2001 ASME Winter Annual Meeting.

Allain, J.C., et al. (1980). *Isometric Tensions Developed During the Hydrothermal Swelling of Rat Skin.* Conective Tissue Research, 7, 127-133.

Anderson, K., McCarty, E.C., & Warren, R.F. (1999). *Thermal Capsulorrhaphy: Where Are We Today.* Sports Medicine and Arthroscopy Review, 7, 117-127.

Arnoczky, S.P., Aksan, A. (2001). *Thermal Modification of Connective Tissues: Basic Science Considerations and Clinical Implications.* American Academy of Orthopaedic Surgeons Instructional Course Lectures, Sims, F.H. (ed.), AAOS, Chicago, IL, 50, 3-11.

Baeyens, J-P., et al. (2001). *Glenohumeral Joint Kinematics Related to Minor Anterior Instability of the Shoulder at the End of the Late Preparatory Phase of Throwing.* Clinical Biomechanics, 16, 752-757.

Banas, M.P., et.al. (1993). *The Allman Modification of the Bristow Procedure for Recurrent Anterior Glenohumeral Instability.* Sports Medicine and Arthroscopy Review, 1, 242-248.

Bechtold, J.E., et al. (1994). *The Effects Of Freeze-Drying and Ethylene Oxide Sterilization on the Mechanical Properties of Human Patellar Tendon.* American Journal of Sports Medicine, 22, 4, 562-566.

Berend, M.E., et al. (1996). *Soft Tissue Shortening with the Ho:YAG Laser: Experimental Model and Structural Effects.* Transactions of Orthopaedic Research Society, 21, 1, 50.

Bigliani, J.U. (1989). *Anterior and Posterior Capsular Shift for Multidirectional Instability.* Techniques in Orthopaedics, 3, 36-45.

Burkhead, W.Z., et al. (1992). *Treatment of the Instability of the Shoulder with an Exercise Program.* Journal of Boneand Joint Surgery, 74A, 890-896.

Chen, S.S. and Humphrey, J.D. (1998*a*). *Heat-Induced Changes in the Mechanics of a Collagenous Tissue: Pseudoelastic Behavior at 37°C.* Journal of Biomechanics, 31, 211-216.

Chen, S.S., Wright, N.T. and Humphrey, J.D. (1997). *Heat-Induced Changes in the Mechanics of a Collagenous Tissue: Isothermal Free Shrinkage.* Journal of Biomechanical Engineering, 119, 372-378.

Chen, S.S., Wright, N.T. and Humphrey, J.D. (1998*b*). *Phenomenological Evolution Equation for Heat-Induced Shrinkage of Collagenous Tissue.* IEEE Transactions on Biomedical Engineering, 45, 10, 1234-1240.

Chen, S.S., Wright, N.T. and Humphrey, J.D. (1998*c*). *Heat-Induced Changes in the Mechanics of a Collagenous Tissue: Isothermal, Isotonic Shrinkage,* Journal of Biomechanical Engineering, 120, 382-388.

Chvapil, M. and Jensovsky, L. (1963). *The Shrinkage Temperature of Collagen Fibres Isolated from the Tail Tendons of Rats of Various Ages and from Different Places of the Same Tendon.* Gerontologia, 1, 18-29.

Cilesiz, I., et al. (1997). *Controlled Temperature Tissue Fusion: Argon Laser Welding of Rat Intestine In Vivo, Part One.* Lasers in Surgery and Medicine, 21, 269-277.

Clyne, T.W. & Withers, P.J. (1993). An Introduction to Metal Matrix Composites. Cambridge University Press, Cambridge, UK.

Eshelby, J.D. (1957). *The Determination of the Elastic Field of an Ellipsoidal Inclusion, and Related Problems.* Proceedings of the Royal Society, A241, 376-396.

Hayashi, K., et al. (1995). *The Effect of Nonablative Laser Energy on Joint Capsular Collagen.* American Journal of Sports Medicine, 23, 4, 482-487.

Hayashi, K., et al. (1996). *The Effect of Nonablative Laser Energy on the Ultrastructure of Joint Capsular Collagen.* Arthroscopy, 12, 4, 474-481.

Hayashi, K., et al. (1997). *The Effect of Thermal Heating on the Length and Histologic Properties of the Glenohumeral Joint Capsule.* Ameican Journal of Sports Medicine, 25, 1, 107-112.

Horgan, D.J., et al. (1990). *Collagen Crosslinks and Their Relationship to the Thermal Properties of Calf Tendons.* Archives of Biochemistry and Biophysics, 281, 1, 21-26.

Hormann, H. and Schlebusch, H. (1971). *Reversible and Irreversible Denaturation of Collagen Fibers.* Biochemistry, 10, 6, 932-937.

Hubbard, R.P., Chun, K.J. (1988). *Mechanical Reponses of Tendons to Repeated Extensions and Wait Periods.* Journal of Biomedical Engineering, 110, 11-19.

Jobe, F.W. (1989). *Anterior Capsulolabral Reconstruction.* Techniques in Orthopaedics, 3, 29-35.

Jobe, F.W., et al. (1991). *Anterior Capsulolabral Reconstruction of the Shoulder in Athletes in Overhead Sports.* American Journal of Sports Medicine, 19, 5, 428-434.

Kang, T., et al. (1995). *Heat-Induced Changes in the Mechanical Properties of Passive Coronary Arteries.* Journal of Biomechanical Engineering, 117, 86-93.

Le Lous, M., et al. (1983). *Hydrothermal Isometric Tension Curves from Different Connective Tissues. Role of Collagen Genetic Types and Noncollagenous Components.* Connective Tissue Research, 11, 199-206.

Le Lous, M., et al. (1985). *Age Related Evolution of Stable Collagen Reticulation in Human Skin.* Connective Tissue Research, 13, 145-155.

LeCarpentier, G.L. (1993). *Continuous Wave Laser Ablation of Tissue: Analysis of Thermal and Mechanical Events.* IEEE Transactions on Biomedical Engineering, 40, 2, 188-199.

Luo, Z.P., Bolander, M.E., An, K.N. (1997). *A Method For Determination Of Stiffness Of Collagen Molecules.* Biochemical And Biophysical Research Communications, 232, 1, 251-254.

Maitland, D.J. & Walsh, J.T. (1997). *Quantitative Measurements of Linear Birefringence During Heating of Native Collagen.* Lasers in Surgery and Medicine, 20, 310-318.

Manta, J.P., et al. (1997). *Arthroscopic Transglenoid Suture Capsulolabral Repair.* American Journal of Sports Medicine, 25, 5, 614-618.

Miles, C.A. and Ghelashvili, M. (1999). *Polymer-in-a-Box Mechanism for the Thermal Stabilization of Collagen Molecules in Fibers.* Biophysical Journal, 76, 3243-3252.

Miles, C.A., Burjanadze, T.V., Bailey, A.J. (1995). *The Kinetics of the Thermal Denaturation of Collagen in Unrestrained Rat Tail Tendon Determined by Differential Scanning Calorimetry.* Journal of Molecular Biology, 245, 437-446.

Naseef III, G.S., et al. (1997). *The thermal properties of Bovine Joint Capsule.* American Journal of Sports Medicine, 25, 5, 670-674.

Nath, S., et al. (1994). *Basic Aspects of Radiofrequency Catheter Ablation.* Journal of Cardiovascular Electrophysiology, 2, 10, 863-876.

Neer, C.S. II. (1990). Shoulder Reconstruction, WB Saunders, Philadelphia, PA.

Nemethy, G. (1998). *Energetics and Thermodynamics of Collagen Self Assembly.* Collagen: Volume1, Biochemistry, Nimni, M.E. (ed.). CRC Press, Boca Raton, FL, 79-94.

Nowacki, W. (1986). Thermoelasticity. Polish Scientific Publishers, Warszawa.

O'Brien, S.J., et al. (1990). *The Anatomy and Histology of the Inferior Glenohumeral Ligament Complex of the Shoulder.* American Journal of Sports Medicine, 18, 5, 449-456.

Obrien, S.J., et al. (1990). *The Anatomy and Histology of the Inferior Glenohumeral Ligament Complex of the Shoulder.* American Journal of Sports Medicine, 18, 5, 449-456.

Olde Damink, L.H.H., et al. (1995). *Glutaraldehyde as a Crosslinking agent for Collagen-Based Biomaterials.* Journal of Materials Science: Materials in Medicine, 6, 460-472.

Panjabi, M.M., et al. (1996). *Subfailure Injury of the Rabbit Anterior Cruciate Ligament.* Journal of Orthopaedic Research, 14, 216-222.

Panjabi, M.M., Moy, P., Oxland, T.R., Cholewicki, J. (1999). *Subfailure Injury Affects the Behavior of Rabbit ACL.* Clinical Biomechanics, 14, 24-31.

Pearce, J., Thomsen, S. (1995). *Rate Process Analysis of Thermal Damage.* Optical-Thermal Response of Laser-Irradiated Tissue, Welch, A.J., van Gemert, M.J.C. (eds.), Plenum Press, New York, 561-606.

Pearce, J.A., et al. (1993). *Kinetics for Birefringence Changes in Thermally Coagulated Rat Skin Collagen.* Proceedings of SPIE, 1876, 180-186.

Pearce, J.A., et al. (1993). *Quantitative Measures of Thermal Damage: Birefringence Changes in Thermally Coagulated Collagen.* HTD-Vol.268, Advances in Bioheat and Mass Transfer, 141-144.

Penascu, D., et al. (1995). *Three-Dimensional Finite Element Analysis of Current Density and Temperature Distributions During Radio-Frequency Ablation.* IEEE Transactions on Biomedical Engineering, 42, 9, 879-889.

Perry, J.J., Higgins, L.D. (2000). *Anterior and Posterior Cruciate Ligament Rupture After Thermal Treatment*. Arthroscopy, 16, 7, 732-736.

Praemer, M.A., Furner, S., Rice, P.R. (1999). Musculoskeletal Conditions in the United States, American Academy of Orthopaedic Surgeons, Rosemont, IL.

Privalov, P.L. (1982). Advances in Protein Chemistry, 35, 1-104.

Privalov, P.L. (1989). *Thermodynamic Problems of Protein Structure*. Annual Reviews in Biophysics and Chemistry, 18, 47-69.

Rosenthal, D. (1946). *The Theory of Moving Sources of Heat and Its Application to Metal Treatments*. Transactions of the ASME, 68, 849-866.

Ruijgrok, J.M., et al. (1994). *Optimizing Glutaraldehyde Cross-Linking of Collagen - Effects of Time, Temperature and Concentration as Measured by Shrinkage Temperature*. Journal of Materials Science: Materials in Medicine, 5, 2, 80-87.

Sankaran, V. & Walsh, J.T. (1998). *Birefringence Measurement of Rapid Structural Changes during Collagen Denaturation*. Photochemistry and Photobiology, 68, 6, 846-851.

Savoie III, F.H. & Field, L.D. (2000). *Thermal versus Suture Treatment of Symptomatic Capsular Laxity*. Clinics in Sports Medicine, 19, 1, 63-75.

Schaefer, S. L., et al. (1997). *Tissue Shrinkage with the Holmium:Yttrium Aluminum Garnet Laser*. American Journal of Sports Medicine, 25, 6, 841-848.

Shitzer, A. (1985). *Temperature Fields and Lesion Sizes in Electrosurgery and Induction Thermocoagulation*. Heat Transfer in Medicine and Biology. Shitzer, A. and Eberhart, R.C., eds. New York, NY: Plenum Press, 2, 55-84.

Svendsen, K.H. & Thomson, G.A. (1984). *A New Clamping And Stretching Procedure For Determination Of Collagen Fiber Stiffness And Strength Relations Upon Maturation*. Journal Of Biomechanics, 17, 3, 225-229.

Tang, J., et al. (1997). *Morphologic Changes in Collagen Fibers After 830 nm Diode Laser Welding*. Lasers in Surgery and Medicine, 21, 438-443.

Thabit, G. (1994). *Treatment of Unidirectional and Multidirectional Glenohumeral Instability by an Arthoscopic holmium:YAG Laser-Assisted Capsular Shift Procedure-A Pilot Study*, Laser Application in Arthroscopy. Neuchatel, Switzerland.

Tyler, F.T., et al. (2000). *Electrothermally-Assisted Capsulorraphy (ETAC): A New Surgical Method for Glenohumeral Instability and Its Rehabilitation Considerations*. Journal of Orthopaedic & Sports Physical Therapy, 30, 7, 390-400.

Usha, R., Ramasami, T. (1999). *Influence of Hydrogen Bond, Hydrophobic and Electrovalent Salt Linkages on the Transition Temperature, Enthalpy and Activation Energy in Rat Tail Tendon (RTT) Collagen Fibre*. Thermochimica Acta, 338, 17-25.

Vangness, C.T., et al. (1997). *Collagen Shortening: An Experimental Approach with Heat*. Clinical Orthopedics and Related Research, 337, 267-271.

Wall, M.S., et al. (1999). *Thermal Modification of Collagen*. Journal of Shoulder and Elbow Surgery, 8, 4, 339-334.

Welch, A. J. (1985). *Laser Irradiation of Tissue*. Heat Transfer in Medicine and Biology. Shitzer, A. and Eberhart, R.C., eds. New York, NY: Plenum Press, 2, 135-184.

Wiederhorn, N.M. and Reardon, G.V. (1952). *Studies Concerned with the Sturcture of Collagen. II. Stress-Strain Behavior of Thermally Contracted Collagen*. Journal of Polymer Science, 9, 4, 315-325.

Wolf, E.M. (1998). *Capsular Shrinkage Technical Guide*. Arthrocare Corporation, 1, 1.

Woo, L-Y.S., Gomez, M.A., Akeson, W.H. (1981). *The Time and History Dependent Viscoelastic Properties of the Canine Medial Collateral Ligament*. Journal of Biomedical Engineering, 103, 293-298.

Woo, S.L.-Y., et al. (1986). *Effects of Postmortem Storage by Freezing on Ligament Tensile Behavior*. Journal of Biomechanics, 19, 5, 399-404.

Wren, T.A.L. & Carter, D.R. (1998). *A Microstructural Model for the Tensile Constitutive and Failure Behavior of Soft Skeletal Connective Tissues*. Journal of Biomechanical Engineering, 120, 55-61.

Zayne, L.Z., et al. (1995). *The Surgical Treatment of Anterior Shoulder Instability*. Clinical and Sports Medicine, 14, 4, 863-883.